Contrib Mineral Petrol (1988) 98:455–489

Contributions to Mineralogy and Petrology

Crustal contributions to arc magmatism in the Andes of Central Chile

Wes Hildreth[1] **and Stephen Moorbath**[2]
[1] USGS, Menlo Park, California 94025, USA
[2] Department of Earth Sciences, University of Oxford, OX1 3PR, UK

Abstract. Fifteen andesite-dacite stratovolcanoes on the volcanic front of a single segment of the Andean arc show along-arc changes in isotopic and elemental ratios that demonstrate large crustal contributions to magma genesis. All 15 centers lie 90 km above the Benioff zone and 280 ± 20 km from the trench axis. Rate and geometry of subduction and composition and age of subducted sediments and seafloor are nearly constant along the segment. Nonetheless, from S to N along the volcanic front (at 57.5% SiO_2) K_2O rises from 1.1 to 2.4 wt %, Ba from 300 to 600 ppm, and Ce from 25 to 50 ppm, whereas FeO*/MgO declines from >2.5 to 1.4. Ce/Yb and Hf/Lu triple northward, in part reflecting suppression of HREE enrichment by deep-crustal garnet. Rb, Cs, Th, and U contents all rise markedly from S to N, but Rb/Cs values double northward – opposite to prediction were the regional alkali enrichment controlled by sediment subduction. K/Rb drops steeply and scatters greatly within many (biotite-free) andesitic suites. Wide diversity in Zr/Hf, Zr/Rb, Ba/Ta, and Ba/La within and among neighboring suites (which lack zircon and alkali feldspar) largely reflects local variability of intracrustal (not slab or mantle) contributions. Pb-isotope data define a limited range that straddles the Stacey-Kramers line, is bracketed by values of local basement rocks, in part plots above the field of Nazca plate sediment, and shows no indication of a steep (mantle + sedimentary) Pb mixing trend. $^{87}Sr/^{86}Sr$ values rise northward from 0.7036 to 0.7057, and $^{143}Nd/^{144}Nd$ values drop from 0.5129 to 0.5125. A northward climb in basal elevation of volcanic-front edifices from 1350 m to 4500 m elevation coincides with a Bouguer-anomaly gradient from −95 to −295 mgal, interpreted to indicate thickening of the crust from 30–35 km to 50–60 km. Complementary to the thickening crust, the mantle wedge beneath the front thins northward from about 60 km to 30–40 km (as slab depth is constant). The thick northern crust contains an abundance of Paleozoic and Triassic rocks, whereas the proportion of younger arc-intrusive basement increases southward. Primitive basalts are unknown anywhere along the arc. Base-level isotopic and chemical values for each volcano are established by blending of subcrustal and deep-crustal magmas in zones of melting, assimilation, storage and homogenization (MASH) at the mantle-crust transition. Scavenging of mid- to upper-crustal silicic-alkalic melts and intracrustal AFC (prominent at the largest center) can subsequently modify ascending magmas, but the base-level geochemical signature at each center reflects the depth of its MASH zone and the age, composition, and proportional contribution of the lowermost crust.

Offprint requests to: W. Hildreth

Introduction

Despite growing acceptance that several mantle, crustal, and subducted reservoirs contribute to arc magmas along continental margins, there is still no real consensus concerning the proportions of the various contributions nor concerning the loci and mechanisms of mixing among source components or among variably evolved magma batches. The present study was designed, therefore, to introduce a new perspective – illuminated by a unique set of *geological* constraints – to what has been largely a geochemical debate cast in terms of chemical and isotopic models and their ambiguities. The experiment undertaken was a comparative geochemical analysis of 15 Quaternary volcanoes, equidistant from the Chile Trench along the volcanic front of a single arc segment, beneath which the nature and age of the downgoing plate and the rate and geometry of subduction all appear to be nearly constant. In contrast, the thickness and average age of the continental crust markedly increase northward along the segment. Although the principal magma source is presumed to lie within a mantle wedge fluxed by a slab-derived contribution, it is argued here that most of the extensive chemical and isotopic variability along the volcanic front developed as the magmas rose through the upper plate, largely while stalled at or near the base of the continental crust.

Some of the ambiguity and uncertainty in identifying source components of arc magmas has resulted from comparing apples and oranges, from expecting too much identity of path and process in generating magmas along tectonically and geologically contrasting arcs and arc segments. The variety is great, as emphasized by Arculus and Johnson (1978) and by Gill (1981). Quaternary volcanic suites of northern Chile, for example, are readily distinguishable in trace-element concentrations, isotopic ratios, and phenocryst assemblages from most suites of central Chile (Thorpe et al. 1982; Harmon et al. 1984). As segmentation of the Andean arc and its Wadati-Benioff zone is well established (Stauder 1973; Swift and Carr 1974; Barazangi and Isacks 1976), comparison of suites from different segments inevita-

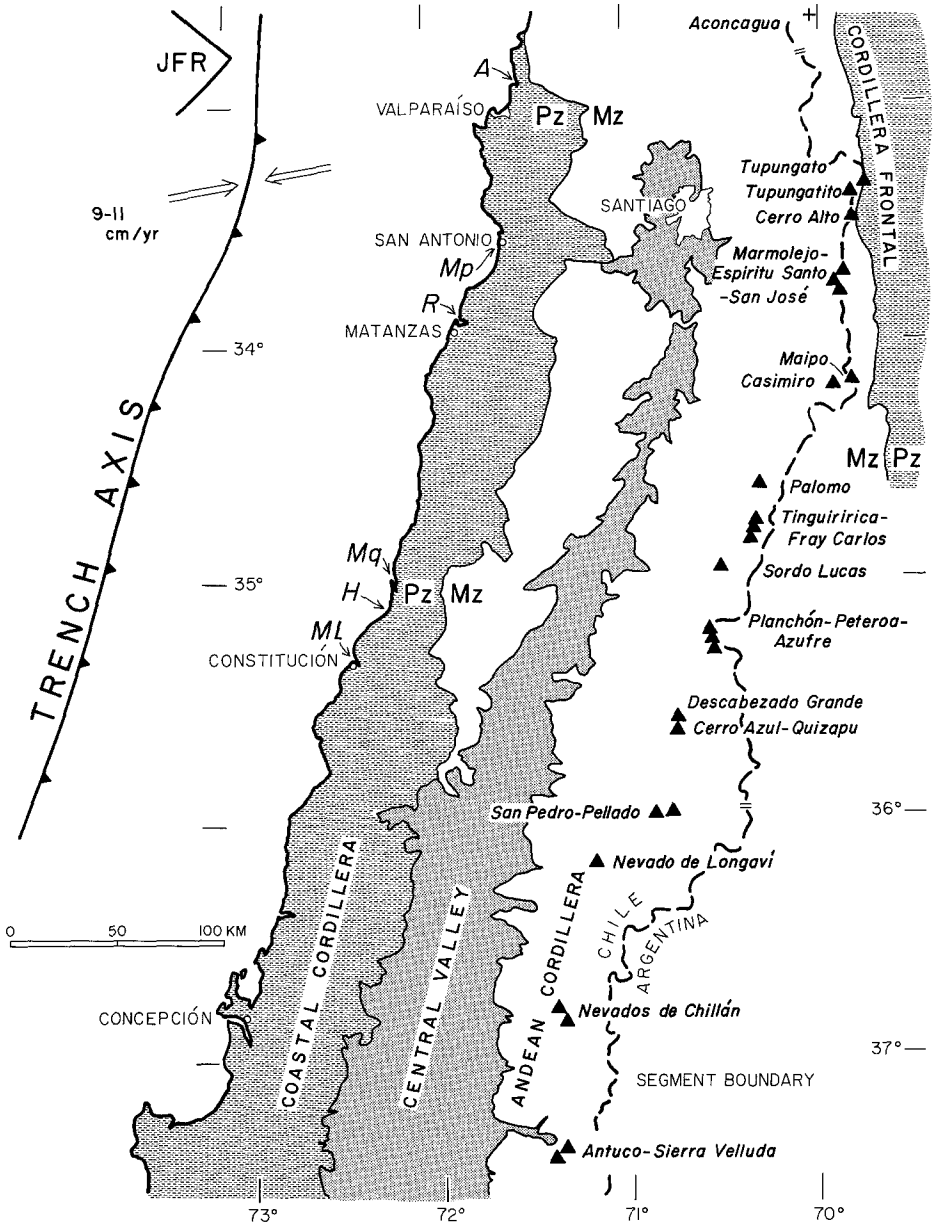

Fig. 1. Major late Quaternary volcanic centers along the volcanic front of the Southern Volcanic Zone (SVZ) in the Andes of central Chile. Triangles indicate the main edifices but several peripheral cones (notably around Cerro Azul) are not shown separately; centers behind the front, numerous south of 34.5°S, are omitted. Note that Maipo and its satellite Casimiro could be regarded as lying *behind* a gap in the volcanic front, rather than on it. *JFR* schematically indicates the zone of impingement of the Juan Fernandez Ridge on the Chile Trench adjacent to the northern termination of the Quaternary SVZ. A probable segment boundary is shown near 37°S. Plate-motion vector and convergence rate are shown across the trench axis, which lies at a constant distance from the volcanic front. In order to highlight the Mesozoic (*Mz*) and Paleozoic (*Pz*) basement belts, Tertiary volcanic and sedimentary rocks, widespread just east of the Central Valley, are omitted, as are 1.0-to-2.5-m.y.-old lavas that are extensive south of 35°S. Paleozoic plutonic, volcanic, and metamorphic basement rocks crop out widely in the Coastal Cordillera and in the Cordillera Frontal terrane on the eastern flank of the Andes. The international border (*dashed*) is the Pacific-Atlantic drainage divide. Sample locations for river-mouth sediments (*Table 2*) are indicated: Rio Aconcagua (*A*), Rio Maipo (*Mp*), Rio Rapel (*R*), Rio Mataquito (*Mq*), Rio Huenchullami (*H*), and Rio Maule (*Ml*)

bly introduces many uncertainties raised by the contrasts in rate and angle of subduction, materials subducted, stress regimes within different arc segments, and depths of the downgoing plate beneath them. The volcanic front in central Chile (33°–37°S), on the other hand, offers an unusual opportunity to investigate the importance of along-strike variations in the upper (South American) plate along a single arc segment, in a setting where lower-plate (subduction-related) variables are essentially constant.

The Central Chilean arc segment (33°–37°S)

The Quaternary volcanic chain forming the Southern Volcanic Zone (SVZ) of the Andes is virtually continuous for 1400 km south of Cerro Tupungato (33.3°S); only its northernmost 400-km-long segment, from Tupungato to the Nevados de Chillan (Fig. 1), is under direct discussion here. The northerly termination of the volcanically active segment at Tupungato (north of which Quaternary volcanic centers are absent for 650 km) coincides with abrupt shallowing of the inclined seismic zone (Barazangi and Isacks 1976;

Bevis and Isacks 1984), with the north end of the Chilean Central Valley, with impingement of the Juan Fernandez Ridge upon the Chile Trench (Fig. 1), and with the south end of the Sierras Pampeanas structural province of compressive crystalline-basement uplifts in the Argentine foreland (Jordan et al. 1983).

A less-well-defined southerly segment boundary at 37°S was proposed by Swift and Carr (1974), but no unambiguous Benioff-zone discontinuity was identified there by Barazangi and Isacks (1976), owing in part to a scarcity of deep and intermediate earthquakes. Herron (1981) suggested a boundary near 37°S, above a subcontinental projection of the Mocha Fracture Zone on the downgoing Nazca plate, and Stauder (1973) pointed out a coastward jump in the distribution of shallow seismicity near that latitude. Moreover, the 600-km-long north-south zone of aftershock epicenters that followed the M_w 9.5 Valdivia earthquake of 1960 ended sharply at 37°S (Lomnitz 1962; Plafker 1972). There is a marked decrease in seismicity deeper than 70 km near 37°S as well as a notable drop in average SiO_2 content of magmas erupted. Quaternary centers on the volcanic front north of 37°S consist predominantly of andesite and dacite, whereas from Volcan Antuco (37.4°S) southward most volcanic-front centers contain a high proportion of mafic andesite and basalt (Lopez-Escobar et al. 1981). The scarcity of silicic andesite south of 37°S has frequently been overstated, but mafic compositions (50–55% SiO_2) are indeed more abundant between 37° and 46°S than between 33° and 37°S (Moreno 1974, 1975; Stern et al. 1976; Lopez-Escobar et al. 1977, 1985; Lopez-Escobar 1984; Hickey et al. 1986). Finally, some kind of tectonic discontinuity is also suggested by the 20-km eastward jump in the volcanic front between the Nevados de Chillan and Antuco, a jump that contrasts with the 400-km-long southwest-stepping trend of the front within the segment under study (Fig. 1).

The volcanic front (33°–37°S)

The 15 volcanic-front edifices dealt with here (Fig. 1) are listed in Table 1, which gives some essential compositional and morphological data for each. All are andesite-dacite stratovolcanoes, simple or compound, except that Tupungato is dominated by a dacite dome cluster having an apron of derivative block-and-ash flows, and the Planchon and Antuco cones are basaltic components (51–53% SiO_2) of compositionally more variable compound edifices. Most centers are modest in volume (Table 1), by far the largest being the 95-km^3 compound edifice that consists of Cerro Marmolejo and overlapping younger cones called Espiritu Santo and San José. The most complex is probably the Descabezado Grande-Cerro Azul cluster, which includes a pair of adjacent stratocones, an older basaltic shield, and numerous peripheral cinder cones and silicic flank vents. Many of the late Quaternary centers overlie glaciated remnants of earlier Pleistocene volcanoes not dealt with here, as their ages and stratigraphy are virtually unknown. Twelve of the 15 have erupted in Holocene time, and only Tupungato, Cerro Alto, Cerro Sordo Lucas and (perhaps) Palomo are thought to be extinct.

At the north end of the segment, the volcanoes form a narrow chain along the Andean crest, attaining summit elevations of 5 to 6.5 km. From 34.5°S southward, the Quaternary volcanic zone broadens to >150 km, and the stratovolcanoes defining the volcanic front lie well west of the drainage divide. The oblique trend of the front away from the rangecrest reflects its southward transgression onto crust that is thinner and younger – as discussed below. The belt of contemporaneous magmatism behind the front south of 34.5°S includes calcalkaline and alkaline stratovolcanoes and shields (Llambias 1966; Llambias et al. 1982; Delpino and Bermudez 1985), widespread plateau basalts on the Argentine pampas (Fig. 1 of Stern et al. 1986), and several mafic-to-rhyolitic centers having large ash-flow calderas (Hildreth et al. 1984; Frey et al. 1984; Muñoz and Stern 1985; Llambias et al. 1978). None of these fall within the subject of the present discussion, which is restricted to the tectonically simpler array of volcanic-front centers that are equidistant from the Chile Trench and above the downgoing plate.

Spacing among the Holocene centers along the front ranges from 73 km to 21 km, or to 7 km if Cerro Azul and Descabezado Grande are considered as independent systems. Although 5 of the spacings are between 36 km and 46 km, the average is 58 km for centers having Holocene activity; this average drops to 38.5 km if we include the 3 extinct centers. The recurrent myth of uniform spacing between arc volcanoes cannot be evoked in the southern Andes.

A fiction that has propagated through the literature on the SVZ is that the arc segment 33°–37°S consists principally of hornblende- and biotite-bearing andesites. Table 1 indicates that some of the centers lack such phases altogether, that along the volcanic front hornblende occurs only in rocks having >57% SiO_2, and that biotite is quite uncommon. Overwhelmingly predominant are 2-pyroxene and olivine-clinopyroxene andesites, though biotite-hornblende dacite is dominant at Tupungato and olivine basalt at Planchon. Quartz and sanidine are absent as phenocrysts on the volcanic front and occur only sparingly in rhyolitic lavas and tuffs erupted behind the front.

The downgoing plate

Apparent constancy within the segment in both Benioff-zone configuration and material subducted makes it very unlikely that large geochemical differences among volcanic-front centers could reflect the depth, conditions, processes, or compositions of the downgoing plate. It will be shown below that many of the along-arc geochemical trends are wholly inconsistent with regional patterns that would be predicted for lower-plate control.

All the volcanic-front centers lie 270–285 km from the trench axis (Fig. 1) except for Nevado de Longavi (260 km) and Volcan Maipo (which at 296 km might alternatively be considered to lie *behind* a gap in the volcanic front). Within the resolution of the seismic data, all are also essentially equidistant (90–100 km) above the top of the inclined seismic zone, which here dips only 18°–20° eastward (Stauder 1973; Barazangi and Isacks 1976; Bevis and Isacks 1984), not 30° as frequently stated. Hypocentral trend-surface analysis applied by Bevis and Isacks (1984) to intermediate-depth teleseismic data suggested a depth of about 115±15 km to the "middle" of the Benioff zone (or ~100 km to its upper surface) along most of the volcanic front. Their analysis would permit Benioff-zone depths to be 10–15 km shallower beneath Chillan, Antuco, and other volcanic-front centers south of 37°S, but the number of intermediate-depth hypocenters here is too small to provide adequate resolution.

The plate convergence rate has been calculated to be in the range 9.3–10.8 cm/a along a 77°–80° azimuth (Fig. 1) and is almost identical for the entire 33°–37°S segment (Minster and Jordan 1978; Chase 1978).

The oceanic crust now being subducted here formed in middle and late Eocene time, and adjacent to the segment its age increases northward only slightly (Herron 1981). Projection of the Nazca plate marine magnetic anomaly pattern beneath the continent suggests that oceanic crust as old as 48 Ma (chron #21) is now beneath the northernmost volcano (Tupungato) and that crust as young as 41 Ma (chron #17) is now beneath the southernmost (Chillan). Downdip transport time from trench to arc at the present convergence rate is only ~3 Ma. The slight age differences along the segment of the relatively young subducted lithosphere are unlikely to result in significant variations of thermal and mechanical properties within the downgoing plate (Wortel and Vlaar 1978). Neither are any aseismic ridges, oceanic plateaus, fracture zones, or other anomalies recognized on the Nazca plate seafloor opposite the segment under study.

Volume and provenance of sediments reaching the Chile Trench are also relatively constant within the 33°–37°S segment, in contrast with the sediment-starved and sediment-filled trench segments to the north and south, respectively (Scholl and Marlow 1974; Schweller et al. 1981; Thornburg and Kulm 1987a). From 33°S to 37°S the trench axis shallows only slightly from 5.5 km to 5 km depth, and the thickness of axial turbidites ranges between

Table 1. Principal Quaternary centers on the volcanic front 33°S to 37.5°S†

Code	Volcanic-front edifices	KM to trench axis	Elevation (m)		Volume erupted (km^3)	SiO_2 range	$(K_2O)_{60}$	Peacock index	Hb-in	Bi-in	Notes	Refs.
			base	summit								
CT	Tupungato	285	4500	6550	25	58–65	2.12	58	<58	60	Extinct central-vent complex of dacite lavas and lithic pyroclastic flows.	1, 2
TT	Tupungatito	280	4700	5933	6	56–65	2.82	57	–	–	Overlies eroded dacitic edifice of >10 km^3, undated but lithologically similar to Tupungato.	1
CA	Cerro Alto	282	4300	6111	40	56–64	2.35	57.5	57	–	Glaciated edifice includes Nevado de los Piuquenes and Cerro Trono. Extinct.	1
CM	Marmolejo-San Jose	281	4000	6110	95	55–67	2.21*	58.5	57	61	Holocene units are slightly more potassic: $(K_2O)_{60}=2.38$.	1, 3, 4
VM	Maipo-Casimiro	296	3600	5290	25*	(54–58)	~2.25	~58.5	~58	–	Stratocone only; does not include mid-Pleistocene rhyolites. Casimiro (VC) is a small eroded, peripheral cone of mafic andesite.	5, 6, 7
VP	Palomo	274	3400	4850	5	53–66	1.98	58.5	57	–	Small stratocone; probably extinct.	1, 5
VT	Tinguiririca-Fray Carlos	285	3300	4300	15	56–63	2.91	58	–	–	Mid-Pleistocene biotite dacite lavas lie 15 km southwest; no hb or bi in young cones.	1
SL	Sordo Lucas	276	2900	3540	>3	(59–63)	2.12	59.5	59	–	Extinct; highly eroded.	1
PPA	Planchon-Peteroa-Azufre	281	2600	4090	55	51–69	2.51	59	–	–	Possible phreatic eruptions in 1937, 1967.	1
DG	Descabezado Grande	274	2250	3953	30	53–71	2.09	58	–	–	Phreatic eruption in June 1932.	1
AZ	Cerro Azul-Quizapu	274	2200	3788	20*	51–70	2.11	58	67	–	Volume includes 11 km^3 cone; 4 km^3 1846-7 lava flows; 5 km^3 1932 ejecta.	1
SP	San Pedro-Tatara	276	1750	3621	>40	51–68	–	–	~68	–	Work in progress by M.A. Dungan et al. Older Pellado-Guadal edifice would double total volume.	8
NL	Nevado de Longavi	260	1500	3242	15	56–65	1.10	60.5	65	–	–	1, 9
NC	Nevados de Chillan	270	1500	3212	60*	55–69	1.64	59	–	–	Volume includes edifice beneath Holocene cones, thought by (10) to have a large caldera.	10, 13
VA	Antuco-Sierra Velluda	285	1350	2987	25*	50–60	1.59	59	–	–	Volume given is Antuco only; older Sierra Velluda may amount to ~40 km^3.	11, 12, 13

† Chemical data are based on USGS XRF major-element analyses (or data in cited sources) normalized to 99.6 wt% anhydrous (leaving 0.4 wt% for trace oxides and halogens). Parentheses in SiO_2 column indicate estimates based on sparse data; compositional ranges erupted could be wider. Volumes are subject to large errors owing to irregular basement, edifice shape, and erosion, but the estimates tend to be conservative. $(K_2O)_{60}$ is wt% K_2O in each suite at 60 wt% SiO_2; see Figure 2 for $(K_2O)_{57.5}$. *Hb-in* and *Bi-in* columns give wt% SiO_2 in suite at first appearance of hornblende and biotite, respectively; – in those columns signifies that the phase is not known to occur at the center in question. Arc-trench distances given would be ~10% greater if measured along the convergence azimuth

* See NOTES column

References: (1) This study, new data; (2) Gonzalez Diaz (1961); (3) Thiele and Katsui (1969); (4) Lopez-Escobar et al. (1986); (5) Charrier (1981); (6) Stern et al. (1984); (7) Hickey et al. (1986); (8) Davidson et al. (1987); (9) Gardeweg (1981); (10) Déruelle and Déruelle (1974); (11) Vergara and Katsui (1969); (12) Lopez-Escobar et al. (1981); (13) Déruelle (1979). In addition, Moreno (1974) is a general reference showing photographs of many of these centers

1.5 and 2 km. Pelagic and hemipelagic sediment just seaward of the trench is only ~200 m thick (Schweller et al. 1981). The terrigenous sediments are derived predominantly by erosion of Mesozoic and Cenozoic rocks in the Andes and are transported to the narrow continental shelf by a handful of major rivers. These rivers cut across the arid and subdued Coast Ranges, the Paleozoic crystalline rocks of which contribute only a small fraction of the total yield of continent-derived sediment along this segment (Thornburg and Kulm 1987b).

Absence of a major accretionary prism inboard of the trench, the apparent continuity of Paleozoic crystalline basement beneath the continental shelf and slope (Scholl et al. 1970; Mordojovich 1974), and the progressive eastward migration of successive Jurassic to Quaternary magmatic arcs (Drake et al. 1982) all indicate not only sediment subduction but tectonic erosion of the continent's leading edge (Plafker 1972; Hussong et al. 1976; Kulm et al. 1977; Scholl et al. 1977). Whether sediment subduction and tectonic erosion influence Quaternary magma generation or not, there is no evidence to suggest any latitudinal *variation* in their importance or effectiveness within the 33°–37°S segment. The rate and geometry of subduction, as well as the age and (as far as is known) composition of subducted lithosphere and sediment, appear to change little along strike. An enormous mass of Mesozoic and Cenozoic sediment is missing, presumably subducted, and this is true throughout the segment.

The continental plate

South of 33°S, central Chile is divided into three physiographic provinces, the Coastal Cordillera, the Andean Cordillera, and the longitudinal Central Valley between them (Fig. 1). At these latitudes, the Coastal Cordillera consists of Paleozoic metamorphic and plutonic rocks (Gonzalez-Bonorino 1971; Caminos et al. 1982), which are cut along their inboard margin by Mesozoic batholiths and overlapped by east-dipping homoclinal assemblages of marine sedimentary rocks, andesitic-dacitic arc rocks, and ignimbrite sheets, all of Mesozoic age (Coira et al. 1982). The Central Valley is a late Neogene and Quaternary structural downwarp, discontinuously faulted along its margins, that deepens and broadens southward (see Kausel and Lomnitz 1968; Marangunic et al. 1979). Between 33° and 37°S, the Andean Cordillera widens southward from ~115 to 140 km, decreases in average elevation (Fig. 2), and is physiographically sharply limited against the Central Valley and the Argentine pampas. The structurally complex foreland zone (Precordillera and Sierras Pampeanas) prominent on the Argentine flank of the Andes north of 33°S (Jordan et al. 1983; Ramos et al. 1986) apparently dies out where the Quaternary magmatic arc begins.

The Andean Cordillera consists here of two major tectonic elements, which together comprise a single, physiographically discrete range: (1) the Cordillera Frontal (Caminos 1979), a complex Paleozoic-to-Triassic orogen that crops out only east of the rangecrest, and (2) the Cordillera Principal (Yrigoyen 1979), consisting largely of the thick Jurassic-through-Cenozoic volcanic and sedimentary sequence that has accumulated during Andean plate convergence. These strata were deposited upon the Paleozoic basement, and their eastern margin has been thrust still farther eastward across that basement during late Cenozoic compression and uplift of the Andes. It needs to be emphasized that the Andean Cordillera is a tectonic range quite different from constructional volcanic arcs such as the Cascades and the Aleutians. Quaternary volcanic rocks make up no more than 5% of the outcrop area and <3% of the volume of this segment of the Andes above the level of the Chilean Central Valley.

All the Quaternary volcanic centers in central Chile (Fig. 1) lie on or west of the Andean crest (thus entirely within the Cordillera Principal), where the volumetrically dominant rocks exposed are strongly deformed clastic, carbonate, evaporitic, and subordinate volcanic strata of Jurassic and Cretaceous age, with or without a mantle of Neogene volcanic rocks. The northernmost volcanoes straddle the exposed contact (Fig. 1) between these Mesozoic strata and the subjacent basement of Paleozoic (and Triassic) rhyolitic, granitoid, and marine clastic rocks. It is not proven that the Paleozoic basement rocks of the Cordillera Frontal are continuous beneath the thick Mesozoic and Cenozoic cover with basement rocks of similar age in the Coastal Cordillera. The conventional interpretation postulates a broad synclinorium, but Drake et al. (1982) suggested extensive east-west necking or rifting of the basement beneath central Chile during the repeated post-Paleozoic episodes of emplacement of north-south linear batholiths. Levi and Aguirre (1981) and Coira et al. (1982) similarly proposed significant attenuation of the Chilean basement by ensialic back-arc extension east of the Jurassic to mid-Cretaceous magmatic belt, the plutonic elements of which today crop out largely (at these latitudes) in the Coastal Cordillera.

Although Mesozoic or younger rocks thus underlie the entire Quaternary volcanic front from 33° to 37°S, Paleozoic crystalline rocks are probably everywhere present at depth, dominantly so beneath the north end of the chain. No Precambrian crystalline basement, ultramafic or ophiolitic rocks, or thick flyschoid sequences crop out along this segment of the Chilean Andes (i.e., within the Cordillera Principal), though such rocks are present in adjacent Argentina (Caminos 1982; Ramos et al. 1986).

Elevation, gravity, and crustal thickness

From north to south, the late Quaternary volcanic chain can be conveniently subdivided according to the ages of the subjacent rocks: (1) From Tupungato to Maipo the volcanoes rest directly on the strongly folded Mesozoic strata; (2) from Palomo to Planchon hundreds to a few thousands of meters of Miocene andesitic and silicic volcanic rocks overlie the Mesozoic rocks; and (3) from Descabezado Grande southward, the Miocene veneer is further mantled by a few hundred meters of undeformed Pliocene and lower Pleistocene volcanic rocks, largely andesites (Drake 1976; Vergara and Muñoz 1982). This southward progression principally reflects the north-to-south drop in average elevation of the Andean crest, from 5–7 km at 33°S to 2–3 km at 37°S (Fig. 2), and the attendant effects of terrain and climate on the depth of erosion. Beneath and just west of the northernmost Quaternary volcanoes, for example, porphyry stocks and andesitic dikes of Miocene age are abundant (Thiele 1980, shows some), but only a few scraps of the associated volcanic rocks have escaped erosion.

The drastic southward decline in general elevation of the rangecrest is reflected in the basal and summit elevations of Quaternary centers along the volcanic front (Fig. 2). The steady drop in basal elevations levels out between 36° and 38°S, but with less regularity the trend continues to 42°S, where the volcanic front reaches sea level. This southward decline, notably the steep segment between 33° and 36°S, is likely to be principally an expression of diminishing thickness of the continental crust. There are three or four components to this thinning. First, the elevation of the rangecrest and the thickness of the crust beneath it decline smoothly southward without any obvious discontinuities in physiography or gravity profile (Fig. 2; Lomnitz 1962). Second, the S 20°W trend of the volcanic front takes it from the rangecrest at 33°–34°S to 20–40 km west of the crest at 36°–37°S. Third, structural trends in Paleozoic basement rocks at these latitudes in Argentina are S to SSE, suggesting that the modern volcanic arc angles obliquely (Fig. 1) toward the pre-Andean continental margin, presumably toward thinner crust. Fourth, if the crust beneath the axis of Chile indeed underwent back-arc or intra-arc attenuation during Mesozoic magmatism, then the S 20°W encroachment of the chain toward the Central Valley also takes it onto thinner (and younger) crust.

No trans-Andean seismic experiments have been conducted at these latitudes, but where such work has been undertaken in northern Chile and Peru (Aldrich et al. 1958; James 1971) across segments of the Andes having elevations and Bouguer gravity anomalies comparable to those at 33°–34°S, the crust is thought to be as thick as 60–70 km.

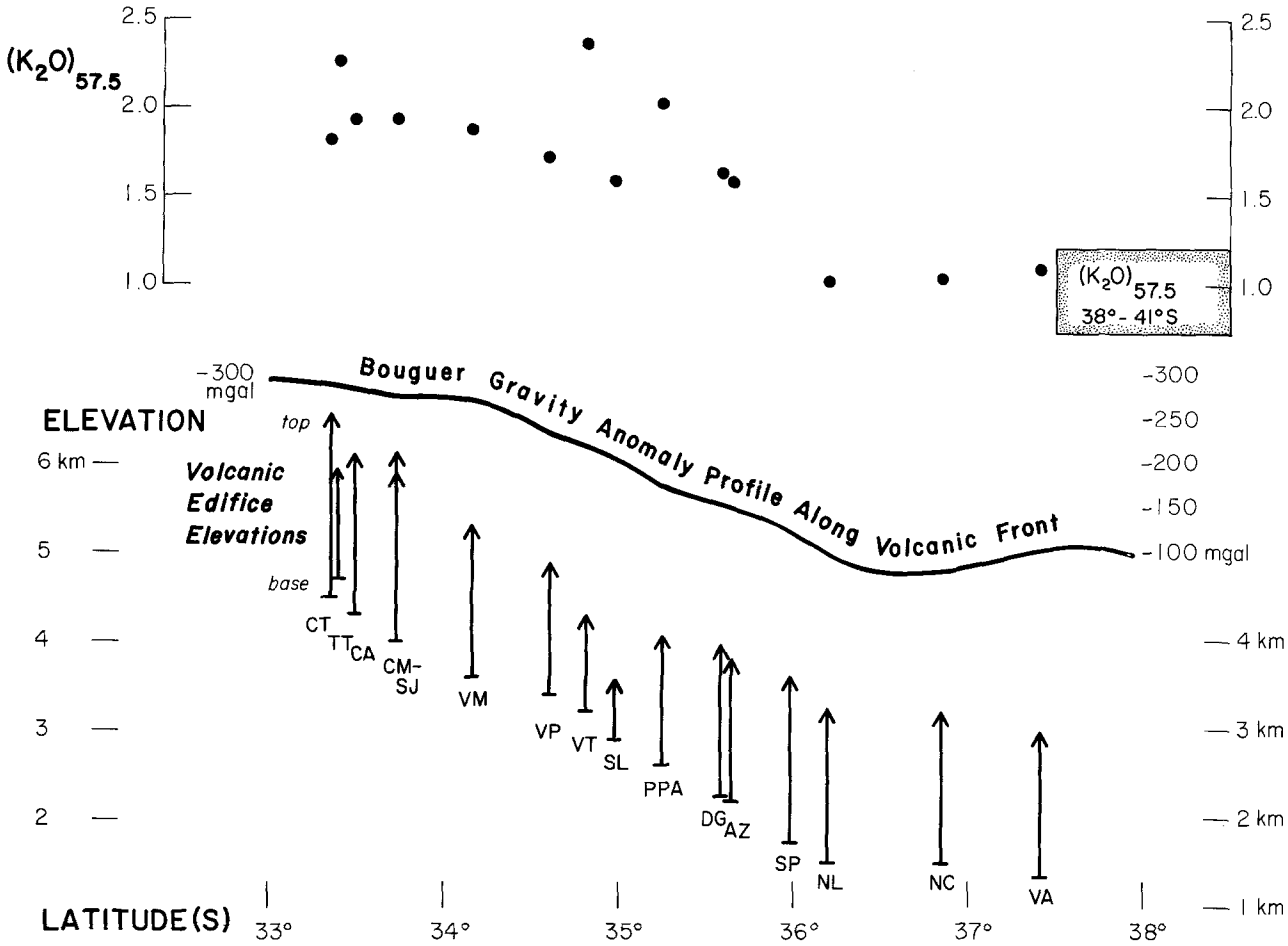

Fig. 2. Elevations relative to sea level and K_2O contents at 57.5% SiO_2 of centers on the volcanic front between latitudes 33°S and 37.5°S. Also shown is the Bouguer gravity-anomaly profile along the volcanic front, interpolated from the data of Dragicevic et al. (1961) and Lomnitz (1962). The northward increase in K_2O correlates with apparent crustal thickness, *not* with arc-trench distance or depth to the Benioff zone, both of which are essentially *constant* for all the volcanoes shown. The *shaded field* encloses the range of $(K_2O)_{57.5}$ values for rock suites from volcanic-front centers farther south (38°–41.5°S). Elevations are given for summits and approximate bases of edifices, excluding far-travelled intracanyon flows. Volcano names are abbreviated: Cerro Tupungato (*CT*); Volcan Tupungatito (*TT*); Cerro Alto (*CA*); Cerro Marmolejo-Volcan San Jose (*CM–SJ*, compound edifice); Volcan Maipo (*VM*); Volcan Palomo (*VP*); Volcan Tinguiririca (*VT*); Cerro Sordo Lucas (*SL*); Volcanes Planchon-Peteroa-Azufre (*PPA*); Volcan Descabezado Grande (*DG*); Cerro Azul (*AZ*); Volcan San Pedro (*SP*, no chemical data); Nevado de Longavi (*NL*); Nevados de Chillan (*NC*); Volcan Antuco (*VA*)

Several gravity profiles across the Andes between latitudes 32° and 39°S have been published by Dragicevic et al. (1961), Lomnitz (1962), Dragicevic (1970), Introcaso and Huerta (1972), Introcaso (1976), and Diez Rodriguez and Introcaso (1985). A trans-Andean profile 70 km north of Cerro Tupungato gave a maximum negative Bouguer anomaly of −295 mgal on the rangecrest. Various models yield apparent crustal thicknesses there of 55–75 km. The gravity network is linked to that of northern Chile, where James (1971) reported generally good correspondence between the regional Bouguer anomaly pattern and crustal thickness variations inferred from seismic studies. Anomalies in the range −250 to −300 mgal in northern Chile occur in areas where seismic data suggest that the crust is 55±5 km thick.

The Bouguer anomaly diminishes southward along the rangecrest to −220 mgal near Volcan Tinguiririca and −175 mgal at Planchon (Fig. 2). A trans-Andean profile at 36°S gave an anomaly of −170 mgal at Laguna del Maule on the crest and −95 mgal on the volcanic front, values that yield model crustal thicknesses of 45–50 km and 35–40 km, respectively. Another trans-Andean profile at 38°40′S yielded −110 mgal on the crest and −95 mgal on the volcanic front 70 km farther west (Diez Rodriguez and Introcaso 1986). South of 36°S (Fig. 2), both elevation and Bouguer anomalies decline more gradually than in the steep segment between 34° and 36°S, where geochemical gradients are also greatest.

Although seismic refraction studies are needed to refine our knowledge of crustal structure and thickness in this part of the Andes, the gravity data, elevation gradient, and regional geology all indicate a marked southward thinning of the crust. Along the volcanic front, the gravity models suggest that the crust thins from 55–65 km beneath Tupungato to 35–40 km at the south end of the segment studied and to 30–35 km south of 37°S. Along the steepest part of this crustal gradient, the K_2O content of Quaternary magmas drops southward by a factor of two (Fig. 2) – even though the volcanoes maintain almost constant vertical and horizontal separations from the subducted plate.

Geochemical variations along the volcanic front (33°–37°S)

Many other geochemical concentrations and ratios display similarly impressive latitudinal changes along the volcanic front. For sample suites from each center, $^{143}Nd/^{144}Nd$, Lu/Hf, and FeO*/MgO increase southward, whereas $^{87}Sr/^{86}Sr$, Ce/Yb, Rb/Cs and abundances of K, Rb, Cs, Ba,

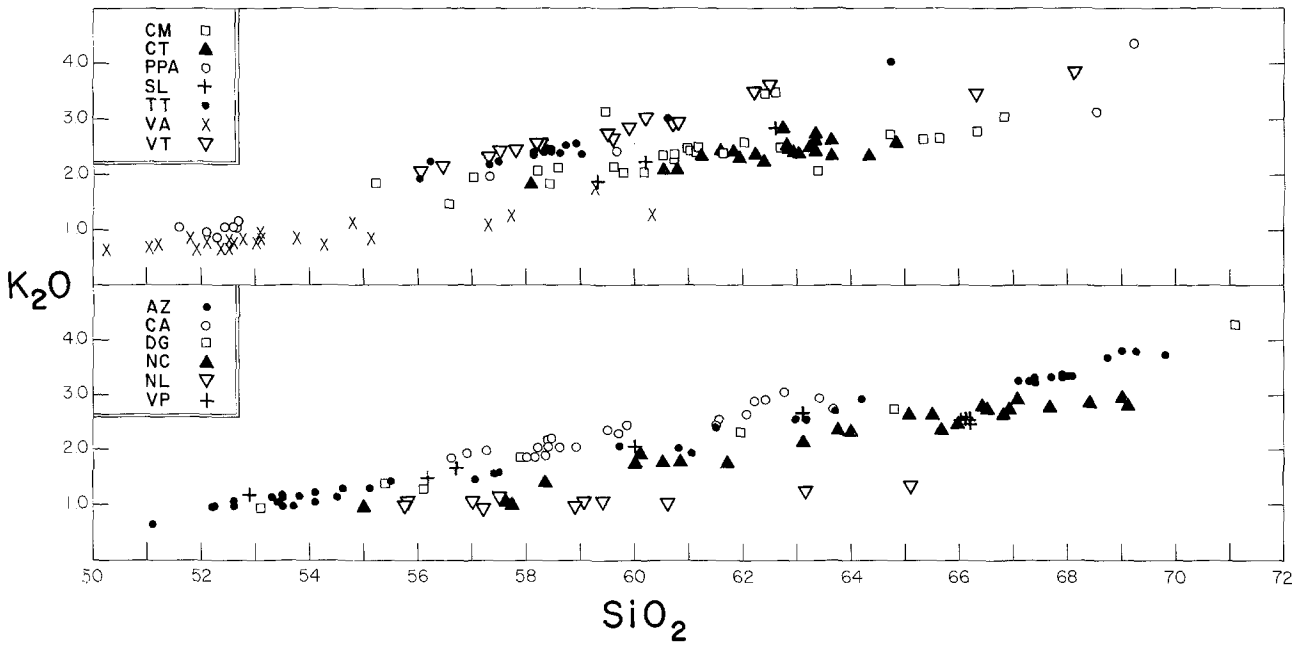

Fig. 3. K_2O-SiO_2 variation (in wt%) in suites of volcanic rocks from centers along the volcanic front, 33°–37°S. Separate panels, employed to reduce clutter, have no other significance. Abbreviations as in *Fig. 2*. Longavi data from Gardeweg (1981); Chillan and Antuco data from Déruelle (1979; 1982) and Lopez-Escobar et al. (1981)

Th, and LREE increase northward. Though not by any means amounting to a simple center-by-center gradient, the overall north-to-south compositional change is large and unequivocal. For simplicity of presentation, major-element, isotopic, and trace-element data will be dealt with sequentially. The isotopic data are given in Tables 2 and 3, and the chemical data will be available as a U.S. Geological Survey Open-File Report. Analytical methods are given in an appendix, below.

Major elements

As true basalts are scarce in this segment and even mafic andesites are absent at a few centers, comparison of relatively primitive members of the various suites is impossible. For systematic comparison of these variably fractionated suites, therefore, we employ several geochemical values taken at 57.5% SiO_2, calculated by least-squares regression of data normalized anhydrous. Reasonably linear trends for each volcano on certain SiO_2-variation diagrams (Fig. 3) and large differences in the slopes of such trends for different volcanoes (Fig. 4) make such comparisons especially informative. Most of the edifices sampled are relatively simple, and only at Marmolejo, a long-lived compound center having strong evidence for an upper-crustal contribution, do subordinate major-element trends plot significantly off the main regressions (Figs. 3, 4).

K_2O concentration is highlighted here because of its widely asserted relationship to the depth of the inclined seismic zone beneath arc volcanoes. The increases in K_2O contents across many magmatic arcs, although apparently related to distance from a trench, need have no genetic linkage whatsoever either with the downgoing plate or with the asthenospheric mantle. Irrespective of the depths to which partial melting might extend in the mantle, increasing K_2O values across and along arcs may in large part be caused by progressively greater contributions from the crust and subcrustal lithosphere. Such a hypothesis is strongly sustained by the data displayed in Fig. 2, wherein K_2O values are shown to increase more than twofold along a volcanic front that strikes onto thicker and more mature continental crust (above a complementarily thinning mantle wedge) while remaining parallel to the trench and to a Benioff zone of essentially constant depth. Circumstantial evidence that the regional K_2O trends across and along certain arcs principally reflect upper-plate processes and compositions has been noted widely (Hamilton 1979; Gill 1981; Coulon and Thorpe 1981), but the present tightly constrained data set is virtually unequivocal.

Figure 4 shows K_2O-SiO_2 regression lines for the volcanic-front centers of Figures 1 and 2, as well as for several in the next arc segment south. Not only does K_2O content generally increase northward, but its rate of increase with SiO_2 also steepens northward. This is in spite of the more widespread and earlier crystallization of hornblende (and biotite) in northerly suites (Table 1) and the correspondingly greater role of pyroxenes and olivines in southerly suites. The progression is far from latitudinally systematic, as Volcan Tinguiririca at 34.8°S has the most potassic suite of all, yet the general correspondence with the gravity and elevation profiles is excellent; no volcanic-front center north of 36°S has a $(K_2O)_{57.5}$ value lower than 1.6, whereas for the next several hundred km south of 36°S, almost all have values <1.3 and several have values <1.0 (Fig. 2).

A marked latitudinal shift, again irregular but impressive overall, also characterizes the Fe/Mg values of the centers along the volcanic front (Fig. 4). By Miyashiro's (1974) criterion, the volcanoes become generally more calcalkaline, less tholeiitic, northward; at the south end of this segment and especially in the next segment south, many suites plot as tholeiitic on such diagrams (Lopez-Escobar 1984). The northerly centers not only have lower Fe/Mg ratios overall but have smaller *rates* of relative Fe-enrichment with progressive differentiation; each of the most strongly calcalkaline suites also extends into the high-K field of Fig. 4.

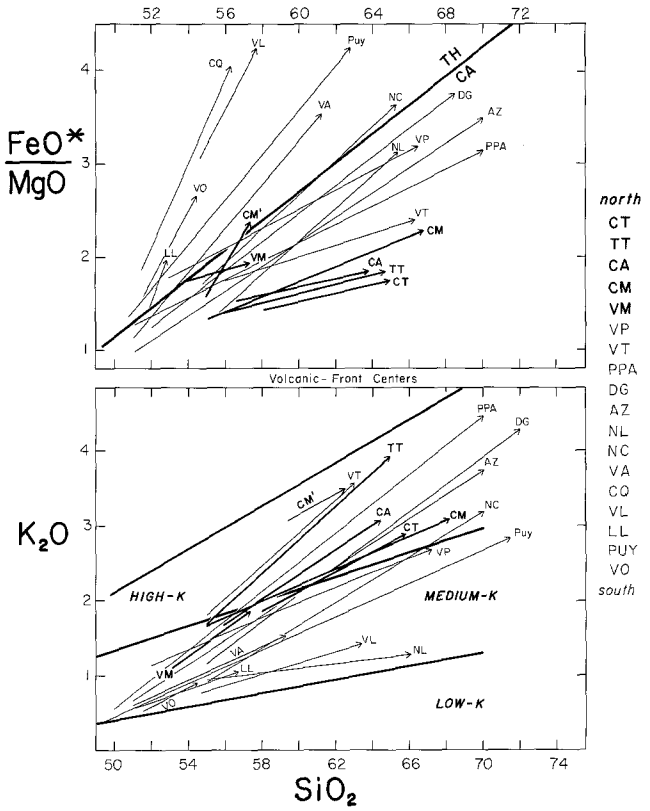

Fig. 4. Least-squares regression lines for K_2O vs. SiO_2 and FeO*/MgO vs. SiO_2 for volcanic-front centers in central Chile. K_2O fields after Gill (1981); tholeiitic (*TH*)-calcalkaline (*CA*) boundary after Miyashiro (1974). Abbreviations of volcano names as in *Fig. 2*, listed in north-to-south order at right margin. Five northernmost centers are shown by bolder lines. Also shown are trends for 5 volcanic-front centers south of Antuco, at 38°–41°S: Volcan Callaqui (*CQ*), Volcan Lonquimay (*VL*), Volcan Llaima (*LL*), Volcan Puyehue (*PUY*), and Volcan Osorno (*VO*). Data for these centers from Déruelle (1979, 1982) and Gerlach et al. (1987). *CM'* indicates subordinate suites at Cerro Marmolejo of very high-K andesites and of tholeiitic mafic blobs common in many flows of calc-alkaline andesite

All suites considered here are "calc-alkalic" in the original sense of Peacock (1931), having alkali-lime indices between 57 and 60.5 (Table 1), the values tending irregularly to decrease northward. By a more restrictive definition of "tholeiitic" based on the (AFM) criterion of Irvine and Baragar (1971), suites from most centers south of 37°S remain tholeiitic, but all of those in the segment under study are calcalkaline. No volcano in central Chile, on or behind the front, on thick crust or on crust as thin as 30 km, is known to have erupted a low-K (island-arc) tholeiitic suite.

Because between-suite differences are much less pronounced for other major-element trends, it is doubtful whether additional along-arc comparisons can be meaningfully extracted from the overlapping sets of major-element data. The northernmost centers tend to show slightly lower TiO_2 and higher MgO contents than southerly ones, in keeping with the regional Fe/Mg trend (Fig. 4), but values of CaO, Al_2O_3, Na_2O, and P_2O_5 overlap extensively along the entire segment. At 57.5% SiO_2, the Tupungato and Tupungatito suites have ~0.93% TiO_2 and ~4.1% MgO, whereas the corresponding values for southerly centers are mostly near 1.1% and 3.5–3.8%, respectively. TiO_2 contents are even greater and MgO values still lower in suites from tholeiitic centers in the segment south of 37°S.

Alumina values are characteristically high, 16.5 to 19 wt% throughout the basalt-andesite compositional spectrum at all volcanic-front centers, and $(CaO)_{57.5}$ is consistently between 6.3 and 7.1%, showing no latitudinal pattern. For nine volcanoes between 34° and 41°S, Hickey et al. (1986) noted that Al_2O_3/CaO ratios of mafic lavas are generally higher north of 38°S, and they suggested that this might reflect larger amounts of crustal assimilation and/or clinopyroxene fractionation beneath northerly centers. Mafic members of suites studied here are similar to their high-Al_2O_3/CaO group, and the ratio rises steeply with fractionation in all suites, but no along-arc trend has been discerned *within* the 33–37°S segment.

In a general way, average SiO_2 contents of volcanic-front centers appear to increase northward along the segment (Table 1), although this is a difficult point to quantify volumetrically and is not without exceptions. The general trend partly reflects the absence of basalt north of Planchon, the northernmost Quaternary center known to have products with <53% SiO_2. Lavas and ejecta having as little as 51% SiO_2 are present at Planchon, Azul, San Pedro, and Antuco, and they are abundant at many centers between 37° and 41°S (Lopez-Escobar et al. 1977; Hickey et al. 1986). Primitive basalts (e.g., Nye and Reid 1986) are essentially absent from the segment under study and from the segment southward as well. A few satellites of Volcan Osorno, 850 km south of Tupungato, have the only noncumulate basalts on or near the volcanic front of central Chile that are known to contain more than 7% MgO or less than 50% SiO_2 (Moreno et al. 1979); almost none have Ni >75 ppm nor Cr >200 ppm.

Sr and Nd Isotopes

Sr and Nd isotopic results for volcanic-front centers as far south as 38.5°S are displayed in Figure 5; most of the data from 33°–37°S are new (Tables 2 and 3). Along the segment south of 37°S, Déruelle et al. (1983) identified a modest northward decline in $^{87}Sr/^{86}Sr$, the values dropping gradually from near 0.7043 at Calbuco (41.3°S) to as low as 0.7037 at Antuco (37.4°S). Our data indicate a marked reversal of that trend north of Antuco, as ratios in the segment under study increase northward to values as high as 0.7057 at Cerro Marmolejo (33.7°S). The progressive climb in $^{87}Sr/^{86}Sr$ ratios of Quaternary volcanic rocks coincides closely with the regional gradients in K_2O, gravity, and elevation shown in Fig. 2. Moreover, the pronounced increase in Sr-isotopic ratios near 34.5°S (Fig. 5) takes place precisely where the gravity-anomaly profile flattens out on approaching its most negative values. It also coincides with a physiographic singularity, as all centers from Volcan Maipo northward lie on the rangecrest and all centers farther south (except Planchon) lie west of it. Fundamentally, all of these relations are thought to reflect the oblique SSW trend of the volcanic chain across the concealed transition from tectonically thickened to normal or attenuated Paleozoic basement.

Figure 5 additionally illustrates that $^{87}Sr/^{86}Sr$ ratios for the large compound Marmolejo edifice extend to values considerably more radiogenic than those of other northerly centers. The good inverse correlation between Sr concentra-

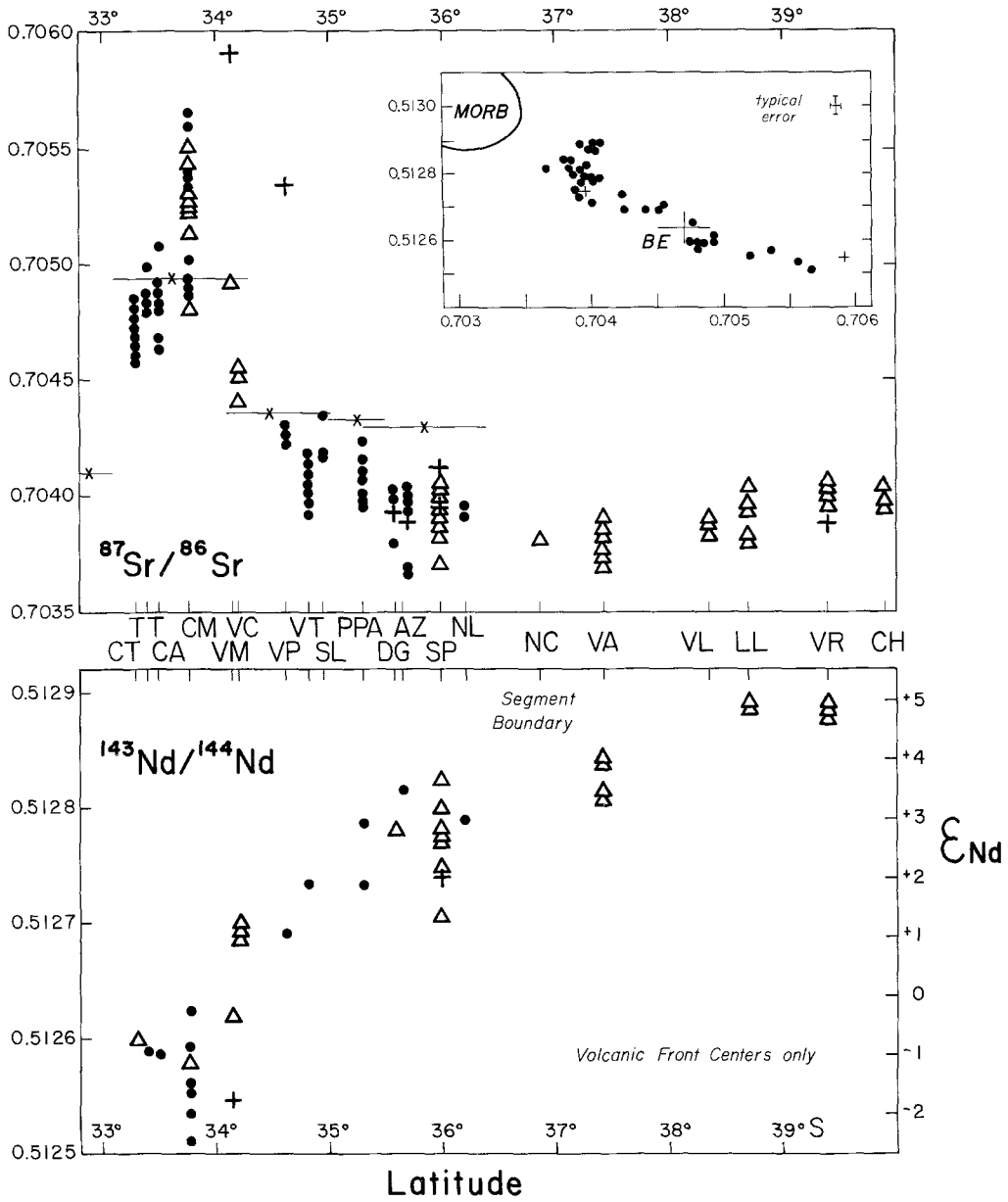

Fig. 5. Sr and Nd isotopic ratios vs. latitude for central Chilean volcanic-front centers. Inset shows distribution of these data relative to MORB and bulk-earth (BE) values. *Solid dots* represents data from this study (*Tables 2* and *3*); *triangles* show data from Déruelle et al. 1983, Stern et al. 1984, Lopez-Escobar et al. 1985, Hickey et al. 1986, and Davidson et al. 1987. Upright crosses are rhyolites. X's in *upper panel* represent Sr-isotopic values of river-mouth sediments from 5 major river systems that drain parts of the Andes indicated by the latitudinal lengths of the horizontal bars. Abbreviations of volcano names as in *Figs. 2* and *4*; also shown are data for Volcan Villarrica (*VR*), Volcan Choshuenco (*CH*), and Volcan Casimiro (*VC*), a small satellite of Volcan Maipo

tions and $^{87}Sr/^{86}Sr$ values of the Marmolejo suite contrasts clearly with other suites plotted in Fig. 6 and is readily interpretable in terms of concurrent assimilation and fractional crystallization (AFC; De Paolo 1981). The array of Marmolejo data in Fig. 6 suggests heterogeneous assimilation of relatively radiogenic crustal components having an integrated Sr content lower than ~300 ppm, probably partial melts of various mid-to-upper-crustal crystalline rocks. Selected AFC and simple-mixing models illustrate how different modes of assimilation and 10–40% of various assimilants could yield the array. By far the most voluminous center in the segment and certainly one of the longest lived, Marmolejo may well have evolved a larger and/or more complex mid- and upper-crustal magma reservoir than any other volcano under discussion. The Marmolejo magmas arriving from the deep crust and initiating AFC processes in shallower reservoirs apparently contained $<55\%$ SiO_2, had >650 ppm Sr, and had $^{87}Sr/^{86}Sr < 0.7048$.

Such "base-level" magma, as will be elaborated below, is thought to ascend from zones of profound melting, mixing, and homogenization near the mantle-crust transition beneath each center. Because of contrasts in depth, mineralogy, average age, and (possibly) bulk composition of the deep crust north and south along the segment, lower-crustal contributions are more easily recognizable (and probably greater) where the crust is thicker. Accordingly, base-level Sr-isotopic values, from which subsequent mid- to upper-crustal fractionation or AFC sequences evolve, are charac-

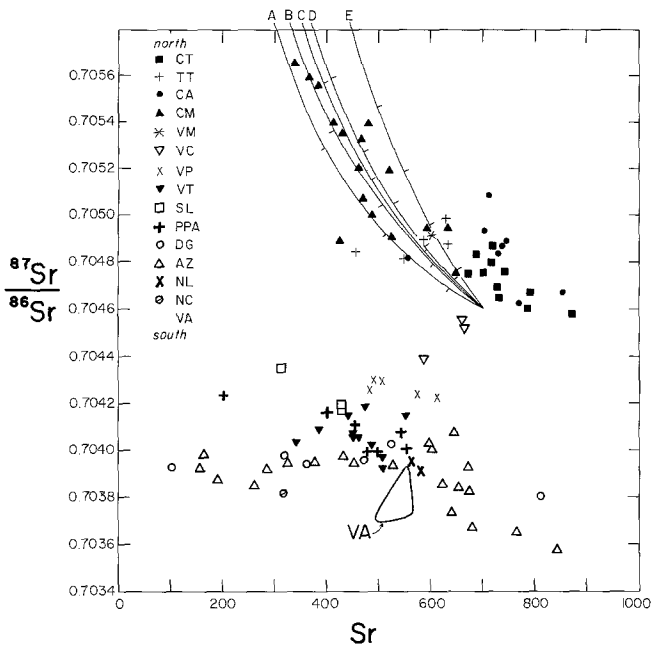

Fig. 6. Sr content (ppm) vs $^{87}Sr/^{86}Sr$ for volcanic-front centers 33°–37°S. Data from *Table 2* or published sources cited in *Fig. 5*; abbreviations as in *Table 1*. Only the Marmolejo suite (CM) shows an extended correlation, interpreted as a result of mid- to upper-crustal AFC and illustrated by *Curves* A–E, all of which employ 700 ppm Sr and 0.7046 as deep-crustally established base-level values of ascending magma. *Curve A* represents simple mixing with a contaminant that averages 100 ppm Sr at 0.710. AFC *Curves B–E* (De Paolo 1981) reflect the following parameters: Sr content and $^{87}Sr/^{86}Sr$ of average contaminant, bulk D_{Sr}, and r = mass assimilation rate/crystallization rate. *Curve B* (100, 0.750, 2.0, 0.2) models assimilation of an upper-crustal Permian granite. *Curve C* (200, 0.712, 1.5, 0.5), *Curve D* (200, 0.720, 1.5, 0.2), and *Curve E* (200, 0.710, 1.0, 0.5) model assimilation of Paleozoic mid-crustal intermediate rocks, illustrating effects of various values of D and r. *Ticks on curves* are in 10% increments of wt% contaminant for *A*, and of fraction of the initial magma remaining for *B–E*. Tupungato (*CT*), Alto (*CA*), Planchon (*PPA*), and the high-Sr part of the Azul (*AZ*) suite may also reflect less pronounced AFC arrays

teristically 0.7045–0.7048 at northerly centers (33°–34°S) but as low as 0.7037 at 36°–37°S where the crust is thinner and less mature.

Although the Marmolejo suite alone exhibits a range of $^{87}Sr/^{86}Sr$ values sufficient to demonstrate mid- or upper-crustal AFC, similar behavior is suggested by the Tupungato, Cerro Alto, and Planchon suites and the Sr-rich part of the Cerro Azul array in Fig. 6. Far from ruling out crustal assimilation, intrasuite scatter on such a plot can merely reflect a variety of assimilants and/or signify a multicompartmental reservoir in which batches of magma evolve independently in time and depth. Moreover, even a sub-horizontal trend like the Sr-poorer part of the Cerro Azul array in Fig. 6 could simply mean that young gabbroic to tonalitic crust provided partial melts that lacked much isotopic contrast with the Quaternary magma.

Nd-isotopic ratios exhibit a regional trend complementary to that of $^{87}Sr/^{86}Sr$ (Fig. 5), ε_{Nd} values decreasing northward from +5 to about −1. The patterns with latitude are notably similar in showing marked gradients north of 36°S and lower Nd-isotopic values for Cerro Marmolejo than for the 3 centers north of it.

Sr in sediments

Figure 5 also shows Sr-isotopic ratios for samples of present-day sediment (fine to medium sand) collected at the mouths of the 5 major river systems (Table 2; Fig. 1; Rios Aconcagua, Maipo, Rapel, Mataquito, and Maule) that together drain ~90% of this segment of Chile and probably supply (as turbidites) >95% of the detritus entering this part of the Chile Trench. The isotopic data clearly reflect the Andean provenance of the sediments, which are derived predominantly from Cenozoic volcanogenic and plutonic rocks, except in the Rio Maipo system where Mesozoic sedimentary and volcanic strata having $^{87}Sr/^{86}Sr$ values of 0.7045–0.7086 (Table 2) also make a major contribution. Paleozoic rocks exposed in the Andes (Fig. 1) are drained exclusively to the Atlantic, and those in the Coastal Cordillera are drained by very few streams (mostly ephemeral) other than tributaries to the 5 rivers sampled.

Sediment reaching the trench from sources other than these 5 river systems probably amounts to no more than ten percent of the total subducted sediment budget. The thin seafloor accumulation of post-middle Eocene pelagic clays, chalks, and cherts (Schweller et al. 1981), considerably diluted by fine continent-derived detritus, apparently contributes <5%. Sediment contributed directly to the sea by small streams heading in the Coastal Cordillera probably amounts to much less than 1%. The tiny Rio Huenchullami (35.2°S, Fig. 1), for example, which drains only the Coastal Cordillera, transports detritus having relatively radiogenic Sr (0.7113; Table 2), but such contributions are not quantitatively important nor likely to vary much along the segment. Finally, an unknown fraction of the sediment is channeled northward along the trench axis from sources in the next segment south (Thornburg and Kulm 1987a). Compositional studies show that those sediments are derived predominantly from arc volcanic rocks (Thornburg and Kulm 1987b), which in the 37°S–41°S segment contain Sr even less radiogenic (0.7037–0.7041) than in our river-mouth samples (Déruelle et al. 1983). The 0.7041–0.7049 ratios of the river sediments (Fig. 5) are therefore thought to provide a reasonable indication of the $^{87}Sr/^{86}Sr$ values of sediment subducted beneath this part of Chile, although the range observed is likely to be reduced by mixing during northward sediment transport along the trench floor. Such low values provide insufficient isotopic leverage to account for the northward increase in $^{87}Sr/^{86}Sr$ along the Quaternary volcanic front by subductive recycling of sedimentary Sr. Diagenetic or connate seawater Sr (0.709) would be insufficient to change the isotopic budget significantly and would not in any case affect the along-arc isotopic gradient. Preferential subduction of *pelagic* sediment, sometimes postulated as a mechanism to enrich sources of arc magmas in radiogenic Pb and Sr, is not a defensible hypothesis in central Chile; the absence of an accretionary prism against the Paleozoic continental margin demonstrates that both pelagic sediment and the much greater mass of the trench-filling terrigenous sediment shed during 200 m.y. of Andean convergence have been subducted.

Though Chilean sediments are clearly subducted, their limited along-trench variability, modest Sr contents (127–432 ppm; Table 2), and low isotopic contrast with the magmas make it quite unlikely that they control the along-arc isotopic gradients illustrated in Fig. 5. Advocates of subducted-plate control would have to appeal to a N-S

gradient in the amount of hydrothermally altered seafloor basalt; but there is no evidence for this, and, in any event, it could not explain the along-arc Nd-isotopic gradient. As with the major-element trends along the volcanic front, the isotopic differences have to reflect processes and compositional variations within the upper plate.

Table 2 additionally gives $^{87}Sr/^{86}Sr$ values for partially molten granitoid xenoliths ejected in recent eruptions of Tupungatito and Cerro Azul and for late Paleozoic basement rocks from the Cordillera Frontal terrane that strikes beneath the northerly volcanoes. Several of the basement rocks and Tupungatito xenoliths have high $^{87}Sr/^{86}Sr$ values (0.75–0.77), whereas xenoliths from Cerro Azul (0.7039–0.7046) have far less Sr-isotopic contrast with the host magmas. Although we do not suggest that such *upper*-crustal rocks provide the principal crustal contribution, these north-south relations nonetheless underscore the contrasting assimilation potential of the Paleozoic vis-a-vis the younger basement rocks. In the case of Marmolejo, 2–10 wt% assimilation of the radiogenic Cordillera Frontal rocks could yield the Sr array of Fig. 6 by AFC in an upper-crustal reservoir (e.g., Curve B; $F=0.95$–0.60).

Figure 5 (inset) also shows the Nd-Sr data plotted on an isotope correlation diagram. All data plot close to the conventional "mantle array." The dominance of post-Carboniferous basement and the apparent absence of Precambrian crust (or lithosphere) beneath this part of the Andes make it far more reasonable, however, that evolved geochemical reservoirs capable of providing differential isotopic leverage sufficient to promote the along-arc $^{87}Sr/^{86}Sr$ gradient and the remarkable, latitudinally systematic, $^{143}Nd/^{144}Nd$ gradient (six ε-units) reside not in the mantle but in the continental crust. Furthermore, because the sub-Andean mantle must have been extensively modified during voluminous Permo-Triassic magmatism and because it has been subjected to sporadic arc magmatism throughout post-Triassic time, it appears quite unlikely that subcrustal lithospheric reservoirs of Phanerozoic age could have differentially evolved in sufficient isolation to provide partial melts or assimilants now capable of imparting such a wide range of ε_{Nd} values to Quaternary magmas. Since there are no such leverage problems with typical crustal reservoirs (richer in LREE, lower and more variable Sm/Nd), the regional evidence therefore strongly favors intracrustal control of the isotopic variability.

Pb isotopes

Pb-isotopic data are given in Table 2 and are plotted in Figs. 7 and 8. Within the segment, values of $^{206}Pb/^{204}Pb$ show limited variation, from 18.49 to 18.69, a range of about one percent (where typical analytical error is $\pm 0.1\%$). This range is nonetheless considerably greater than that of all the volcanic-front centers taken together in the next arc segment south (37°–41° S; Fig. 7). There is no simple trend with latitude, as the least radiogenic Pb occurs in products of the northernmost volcanoes and the most radiogenic Pb tends to occur at centers in the middle of the segment (VT, VP; Fig. 7). Samples from a single center, the Marmolejo complex (CM), span most of the $^{206}Pb/^{204}Pb$ range established. As Marmolejo is the one center where mid- or upper-crustal AFC processes have been positively established on the basis of Sr-isotope data (Fig. 6), the atypical spread in $^{206}Pb/^{204}Pb$ values (and in $^{208}Pb/^{204}Pb$ values; Table 2) may also have resulted from variable amounts of assimilation (and/or a range of assimilants) in complex magma reservoirs.

Several noteworthy relationships are illustrated in Figs. 7 and 8.

(1) Relative to the limited Pb-isotopic range of the 37°–41°S centers, those in the segment under study exhibit shifts to both higher *and* lower values of $^{206}Pb/^{204}Pb$ but only to *higher* values of $^{207}Pb/^{204}Pb$ and $^{208}Pb/^{204}Pb$. This can be explained most simply by intracrustal Pb contributions.

(2) The volcanic Pb data plot in the upper part of the field of Nazca plate sedimentary Pb or, in the case of the northerly centers, mostly above it (Fig. 7). In other words, the northernmost centers are more enriched in $^{207}Pb/^{204}Pb$ than are pelagic sediments on the downgoing plate. It is therefore unlikely that the arc Pb is dominated by a contribution from a subducted sedimentary reservoir. There is no evidence (or reason to expect) that Nazca plate sediments adjacent to the 37°–41°S and 33°–37°S arc segments, respectively, differ significantly in their Pb-isotope ratios, casting further doubt on the proposition that the along-arc differences in Pb-isotope signature are controlled by input of pelagic sedimentary Pb. Because of the youth of the Eocene seafloor being subducted here, any isotopic shift due to aging of subducted Pb would be too small to modify this line of reasoning. In any event, the downgoing sediments here are strongly dominated by trench-filling terrigenous turbidites largely of Andean provenance. The river-mouth sediments that supply such turbidites have Pb-isotope ratios (Table 2) that would plot well *inside* the fields of arc data in Figures 7 and 8, showing that such material provides no Pb-isotopic leverage.

(3) All of the volcanic Pb data plot far above the main trend of Pb-isotope values for oceanic basalts (ORL; Fig. 7) and well above the field of analyzed Nazca plate seafloor basalts. In contrast with sets of Pb-isotope data published for the Aleutian, Cascades, and Mariana arcs, there is no evidence here for a steep mixing trend between MORB-type Pb and that of a ^{207}Pb-rich reservoir. If Pb derived from the subducted oceanic lithosphere makes any contribution at all to the arc Pb here, it can only be a small one relative to contributions from reservoirs having elevated values of $^{207}Pb/^{204}Pb$ and $^{208}Pb/^{204}Pb$.

(4) The volcanic Pb data, especially for those centers lying along the northern half of the segment under consideration (Fig. 7; CA, CM, CT, TT, SL, VT, VP), plot close to the Stacey-Kramers (1975) average crustal Pb-evolution curve and between the upper-crust and orogene fields of Zartman and Doe (1981). In light of the strong case against lower-plate control of many other along-arc geochemical variations, it therefore appears that the reservoir dominating the Pb-isotope variability here is likely to be the continental crust – which is older and thicker beneath the 33°–35°S volcanoes having the relatively elevated $^{207}Pb/^{204}Pb$ and $^{208}Pb/^{204}Pb$ values. The main Pb-isotopic control may simply be the swamping of subcrustally derived Pb by magmatic assimilation of crustal fluids and leucomelts, which could contain 10–50 times the concentration of Pb held by a truly primitive basalt.

(5) The volcanic Pb data are nearly bracketed (Fig. 7) by the isotopic values (Table 2) of a Permian granite north of Tupungato and partially molten granitic xenoliths (having Paleozoic Rb-Sr model ages) ejected by Tupungatito. These basement samples represent the extremes of the pres-

Table 2. Sr and Pb isotope data

Center	*SiO_2*	*Rb*	*Sr*	Rb/Sr	$^{87}Rb/^{86}Sr$	$^{87}Sr/^{86}Sr$	$^{206}Pb/^{204}Pb$	$^{207}Pb/^{204}Pb$	$^{208}Pb/^{204}Pb$
Tupungato									
T5	64.3	57	733	0.078	0.226	0.70466±3			
T12	60.5	54	872	0.062	0.179	0.70458±4	18.518	15.614	38.471
T15	58.0	40	719	0.056	0.162	0.70480±3			
T17	62.3	59	788	0.075	0.217	0.70461±4			
T20	63.3	60	793	0.076	0.220	0.70468±3			
T41	61.8	67	723	0.093	0.269	0.70487±3			
T49	62.2	61	692	0.088	0.255	0.70483±4			
T53	63.3	72	702	0.103	0.298	0.70475±3	18.502	15.600	38.429
T55	62.8	72	673	0.107	0.310	0.70474±3			
T57	61.5	63	732	0.086	0.249	0.70470±3			
T65	63.0	64	741	0.086	0.249	0.70476±3	18.496	15.581	38.391
Tupungatito									
T6	62.3	122	549	0.222	0.642	0.70481±3	18.571	15.609	38.514
T29	58.3	86	589	0.146	0.422	0.70489±3			
T32	56.0	62	634	0.098	0.284	0.70488±3			
T33	57.3	62	630	0.098	0.284	0.70499±3	18.602	15.595	38.508
T48	64.7	163	457	0.357	1.033	0.70484±3	18.559	15.612	38.499
T27*	76.3	119	37	3.22	9.35	0.75556±4	18.497	15.561	38.380
T31*	78.0	247	40	6.18	17.97	0.76353±4	18.518	15.579	38.354
T38*	75.9	134	194	0.691	2.00	0.72501±6			
Cerro Alto									
T84	58.6	50	739	0.068	0.197	0.70487±5			
T85	56.9	42	747	0.056	0.162	0.70488±5	18.529	15.618	38.494
T88	61.6	61	712	0.086	0.249	0.70508±5	18.496	15.595	38.430
T95	61.5	68	771	0.088	0.255	0.70463±4			
T99	58.4	46	727	0.063	0.182	0.70484±3			
T100	58.3	46	856	0.054	0.161	0.70468±3	18.552	15.618	38.490
T109	56.6	50	705	0.071	0.205	0.70492±3			
T110	62.8	95	554	0.171	0.495	0.70481±3	18.561	15.617	38.531
Marmolejo									
CM1	60.2	55	647	0.085	0.246	0.70476±5	18.547	15.603	38.467
CM2	62.6	166	425	0.391	1.13	0.70488±3	18.547	15.624	38.532
CM3	58.4	51	596	0.086	0.249	0.70494±5			
CM5	66.3	109	469	0.232	0.671	0.70533±5			
CM7	64.7	94	460	0.204	0.590	0.70520±5	18.569	15.588	38.473
CM7A	57.3	12	627	0.019	0.055	0.70494±3	18.575	15.597	38.499
CM11	65.3	102	368	0.277	0.802	0.70560±6	18.695	15.613	38.618
CM11A	59.7	67	488	0.137	0.396	0.70502±5	18.693	15.624	38.663
CM12	61.6	82	413	0.199	0.576	0.70541±5			
CM16	65.6	106	383	0.277	0.802	0.70556±4	18.689	15.604	38.589
CM16A	56.5	57	516	0.110	0.318	0.70520±3	18.709	15.624	38.657
CM18	66.8	109	339	0.322	0.932	0.70566±7	18.577	15.610	38.543
CM19	60.5	82	426	0.192	0.556	0.70536±5	18.524	15.588	38.431
CM19A	55.2	61	473	0.129	0.373	0.70508±6	18.511	15.578	38.401
CM22	58.2	65	528	0.123	0.356	0.70489±6	18.573	15.624	38.570
CM27	59.6	66	481	0.137	0.396	0.70540±4			
Palomo									
VP1	56.2	37	614	0.060	0.174	0.70423±5	18.660	15.632	38.634
VP2	60.0	68	575	0.118	0.341	0.70424±5	18.663	15.635	38.621
VP4	66.1	71	484	0.147	0.425	0.70426±3			
VP5	66.2	70	491	0.143	0.414	0.70430±6	18.663	15.630	38.619
VP8	63.1	89	508	0.175	0.506	0.70429±4			
older units									
VP10	52.9	34	512	0.066	0.191	0.70514±5			
VP11	75.7	122	156	0.782	2.26	0.70534±3	18.697	15.613	38.594
Tinguiririca									
VT9	59.9	127	443	0.287	0.830	0.70415±3			
VT10	60.2	132	453	0.291	0.842	0.70408±3			
VT11	56.5	87	553	0.157	0.454	0.70414±3	18.649	15.641	38.631
VT12	68.1	161	343	0.469	1.36	0.70404±3			
VT13	60.8	122	452	0.270	0.781	0.70406±5	18.627	15.617	38.552
VT15	57.8	99	505	0.196	0.567	0.70397±6			
VT20	62.5	168	385	0.436	1.26	0.70410±5	18.643	15.644	38.622

Table 2 (continued)

Center	*SiO_2*	*Rb*	*Sr*	Rb/Sr	$^{87}Rb/^{86}Sr$	$^{87}Sr/^{86}Sr$	$^{206}Pb/^{204}Pb$	$^{207}Pb/^{204}Pb$	$^{208}Pb/^{204}Pb$
Fray Carlos									
VT1	58.2	115	509	0.225	0.651	0.70392±5			
VT2	57.5	93	487	0.191	0.553	0.70402±4			
VT3	58.2	100	474	0.211	0.610	0.70418±5			
VT6	59.5	111	459	0.242	0.700	0.70406±5			
VT7	60.8	125	451	0.277	0.801	0.70407±4	18.641	15.636	38.549
Sordo Lucas									
AP3	60.2	61	429	0.142	0.411	0.70419±5			
AP4	62.6	98	313	0.313	0.906	0.70435±5	18.619	15.640	38.561
AP5	59.3	57	429	0.133	0.385	0.70417±4	18.575	15.629	38.468
Planchon-Peteroa									
PP1	51.6	17	556	0.031	0.090	0.70400±4	18.594	15.622	38.532
PP2	52.6	26	545	0.048	0.139	0.70407±3			
PP6	57.3	67	456	0.147	0.425	0.70411±4			
PP7	59.7	85	402	0.211	0.610	0.70416±4	18.603	15.594	38.485
PP8	69.2	167	202	0.827	2.39	0.70424±4	18.626	15.603	38.538
PP10	52.3	19	500	0.038	0.110	0.70399±4			
PP13	52.1	22	478	0.046	0.113	0.70399±4	18.616	15.607	38.609
Descabezado Grande									
D2-1-24F	56.1	34	811	0.042	0.122	0.70380±5			
D2-1-25A	71.1	138	103	1.34	3.88	0.70393±6	18.580	15.598	38.475
Q60	55.4	33	525	0.063	0.182	0.70403±4	18.590	15.611	38.505
Q62	57.9	49	474	0.103	0.298	0.70396±4			
Q63	64.8	81	320	0.253	0.732	0.70399±4			
Q64	61.9	61	383	0.159	0.460	0.70393±4	18.588	15.608	38.481
Cerro Azul									
main cone									
Q45	53.5	27	602	0.045	0.130	0.70401±3	18.604	15.604	38.494
Q47	64.2	87	326	0.267	0.773	0.70396±4	18.598	15.623	38.541
Q47A	52.6	28	673	0.042	0.122	0.70393±4			
Q53	61.5	70	377	0.186	0.538	0.70396±5			
Q55	69.2	115	155	0.742	2.15	0.70393±5	18.587	15.603	38.482
Q58	57.0	38	513	0.074	0.214	0.70393±5	18.586	15.607	38.491
Q66	61.1	45	457	0.098	0.284	0.70394±4	18.593	15.609	38.492
old shield									
Q32	51.1	15	622	0.024	0.069	0.70388±4	18.626	15.613	38.532
Q42	52.2	21	642	0.033	0.095	0.70408±7	18.601	15.606	38.493
Q44	53.4	23	766	0.030	0.087	0.70367±4	18.567	15.606	38.466
C85-2	53.2	28	849	0.033	0.095	0.70357±4	18.604	15.615	38.497
peripheral cones									
Q27	53.5	26	653	0.040	0.166	0.70385±4			
Q28	54.1	33	680	0.049	0.142	0.70368±5			
Q29	54.1	24	639	0.038	0.110	0.70372±3	18.596	15.595	38.430
Q29A*	70.5	135	261	0.517	1.50	0.70394±4	18.569	15.595	38.462
Q30	53.8	31	683	0.045	0.130	0.70382±7	18.589	15.590	38.493
Quizapu vent									
Q2	69.8	128	190	0.674	1.95	0.70389±4	18.568	15.584	38.431
Q5	67.9	108	262	0.412	1.19	0.70387±4			
Q9	59.7	62	434	0.143	0.414	0.70398±3	18.579	15.593	38.458
Q17	52.6	24	599	0.040	0.116	0.70404±5			
Q19*	75.5	221	85	2.60	7.52	0.70460±4			
Q22	68.0	103	285	0.361	1.04	0.70393±4	18.580	15.597	38.461
Q36	69.0	116	165	0.703	2.03	0.70399±4			
Nevado de Longavi									
MG9	56.9	28	584	0.048	0.139	0.70391±4	18.590	15.617	38.516
MG181	57.1	28	565	0.050	0.145	0.70396±3	18.584	15.619	38.512

* Asterisks identify partially melted granitoid xenoliths included in juvenile ejecta of Tupungatito and Cerro Azul. Rb and Sr values are given in ppm; SiO_2 in wt%, normalized H_2O-free. Marmolejo suite includes San José and Espiritu Santo cones of a compound edifice. Undated older units 8–10 km NE of Palomo are apparently unrelated. Fray Carlos is a discrete cone directly adjacent to Tinguiririca. First 5 samples from Quizapu were all erupted in 1932; Q-22 in 1846; Q-36 is prehistoric

Table 2 (continued)

		Rb	Sr	Rb/Sr	$^{87}Rb/^{86}Sr$	$^{87}Sr/^{86}Sr$	$^{206}Pb/^{204}Pb$	$^{207}Pb/^{204}Pb$	$^{208}Pb/^{204}Pb$
Paleozoic-Triassic basement									
AB-1	greywacke, Villavicenzio	59	65	0.908	2.64	0.73746±7			
AB-2	phyllitic shale, Villavicenzio	155	65	2.38	6.93	0.76647±6			
AB-4	granite, Polvaredas	174	38	4.58	13.34	~0.7695	18.978	15.628	39.063
AB-5	rhyolite ignimbrite, Polvaredas	190	47	4.04	11.76	~0.7617			
AB-6	rhyolite lava, Polvaredas	211	44	4.80	13.97	~0.7608			
AB-7	greywacke, Rio Mendoza	96	61	1.57	4.56	0.73609±6			
AB-8	phyllitic shale, Rio Mendoza	68	96	0.708	2.05	0.72747±7			
Mesozoic basement rocks									
MB-1	J black shale	70	203	0.345	0.999	0.70860±5			
MB-2	K limestone	40	328	0.122	0.353	0.70766±6			
MB-3	J gypsum	13	1342	0.010	0.029	0.70686±5			
MB-4	J andesite	11	515	0.021	0.061	0.70453±4			
MB-5	K volcanic sandstone	43	445	0.097	0.281	0.70452±6			
MB-6	K red shale	59	343	0.172	0.498	0.70644±4			
River-mouth sediments									
SED-1	Rio Aconcagua	57	396	0.144	0.417	0.70410±5	18.535	15.594	38.404
SED-3	Rio Maipo	54	432	0.125	0.362	0.70494±5	18.587	15.609	38.478
SED-5	Rio Rapel	59	432	0.137	0.396	0.70436±4	18.567	15.591	38.421
SED-7	Rio Mataquito	61	390	0.156	0.451	0.70433±7	18.564	15.599	38.459
SED-9	Rio Huenchullami	78	127	0.614	1.78	0.71128±4	18.678	15.620	38.588
SED-10	Rio Maule	46	363	0.127	0.367	0.70430±5	18.561	15.606	38.462

Paleozoic-Triassic terrane strikes from Rio Mendoza area southward under Tupungato and other northerly volcanoes. Jurassic and Cretaceous rocks were collected from deformed belt under and adjacent to Marmolejo in Estero del Plomo and Rio Yeso. For locations of river mouths, see Fig. 1.

See Appendix for analytical methods

Table 3. Nd isotope data

Center	#	SiO_2	$^{143}Nd/^{144}Nd$	εNd
Tupungatito	T48	64.7	0.512589±20	−0.96±0.39
Cerro Alto	T110	62.8	0.512587±27	−0.99±0.52
Marmolejo	CM1	60.2	0.512622±20	−0.31±0.39
	CM3	58.4	0.512591±19	−0.92±0.37
	CM7	64.7	0.512552±25	−1.68±0.50
	CM16	65.6	0.512534±18	−2.03±0.35
	CM19	60.5	0.512553±20	−1.66±0.39
	CM18	66.8	0.512510±20	−2.50±0.39
Palomo	VP4	66.1	0.512691±26	+1.03±0.50
Tinguiririca	VT1	58.2	0.512735±28	+1.89±0.54
Planchón	PP1	51.6	0.512787±20	+2.91±0.39
	PP8	69.2	0.512733±25	+1.85±0.48
Cerro Azul	Q44	53.4	0.512816±20	+3.47±0.39
Nevado de Longaví	MG181	57.1	0.512789±23	+2.95±0.43

See Appendix for analytical methods

ently known range of Pb-isotope values along the segment. Values for Tertiary quartz diorite and ore Pb from a mine northwest of Tupungato (Tilton 1979) would plot right in the middle of the main data clusters in Figures 7 and 8. A partially melted xenolith of Tertiary granodiorite ejected by a Holocene scoria cone adjacent to Cerro Azul is isotopically similar in both Pb and Sr to the Azul suite itself (Table 2; Fig. 7), illustrating the low level of isotopic contrast where the basement is younger than Paleozoic. All available Pb-isotope data for rhyolites in this part of Chile (Table 2; Barreiro et al. 1982; Frey et al. 1984; authors' unpubl. data) also fall within the range defined by the less silicic volcanic rocks (Fig. 7), in spite of the general tendency for many rhyolites to exhibit more "crustal" Nd- and Sr-isotope ratios (Fig. 5). Hence, the lack of a latitudinally systematic pattern in $^{206}Pb/^{204}Pb$ comparable to those of Nd- and Sr-isotope ratios (Fig. 5) probably reflects in general the limited Pb-isotopic variability of crustal rocks in this province and in detail the dependence of crustal Pb contamination on a magma's ascent path. The contrasting Pb-isotope ranges of the adjacent arc segments, much more restricted at 37°–41°S than at 33°–35°S, may reflect the dominance of Mesozoic and Cenozoic crust south of the 35th parallel and of slightly more evolved, isotopically more heterogeneous, Paleozoic crust north of there.

(6) The $^{207}Pb/^{204}Pb$ vs $^{208}Pb/^{204}Pb$ relationships plotted in Figure 8 illustrate the characteristic deviation of arc suites from the fields of MORB and OIB toward Pb-isotopic values typical of upper continental crust. In this instance, the diagram illustrates further that Pb-isotope compositions of the Chilean arc suites are not dominated by contributions from MORB- or OIB-type sources. Compared to the restricted field for centers at 37°–41°S, data for the centers under study extend to considerably more radiogenic values, apparently along a variety of trends. As emphasized by Hickey et al. (1986), the divergence of many (but not all) arc suites from the oceanic Pb fields on such a diagram requires a continentally derived component. Since the relationship shown in the previous diagram (Fig. 7) and our Pb-isotopic data for river-mouth sediments (Table 2) both suggest that Nazca plate sedimentary Pb fails to provide adequate isotopic leverage, and because sub-

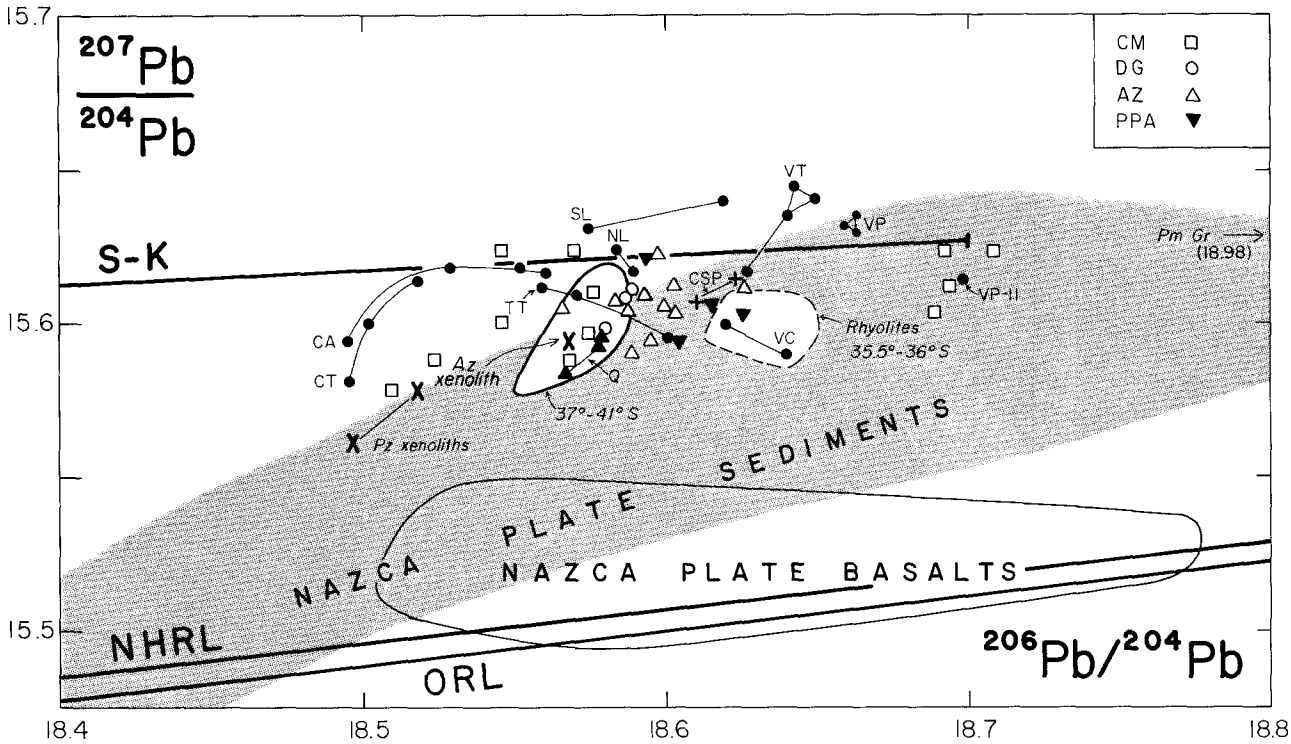

Fig. 7. Pb-isotope values for volcanic-front centers between 33° and 36°S; data from *Table 2*. Abbreviations as in *Table 1* and previous diagrams. Data for individual centers are connected by *tie lines*, except for Cerro Marmolejo (□), which shows a wide range, and for three others (*inset*) to reduce clutter. *Q* indicates 3 samples of historic eruptive products from Volcan Quizapu, a satellitic vent of Cerro Azul, and *VP-11* represents a Tertiary rhyolitic intrusion near Volcan Palomo. Data for Cerro San Pedro (*CSP;* 36°S) are from Tilton (1979). Field for *37°–41° S* encloses unpublished Oxford data and published data for Antuco, Llaima, Villarrica, Puyehue, and Osorno, volcanic-front centers in the next segment south (Hickey et al. 1986). Also shown are data for a Permian granite (Pm Gr) north of Tupungato, for Paleozoic (Pz) granitoid xenoliths in Tupungatito ejecta, and for a Tertiary granitoid xenolith in Azul (Az) ejecta. Field for *Rhyolites 35.5°–36° S* encloses 8 data for Laguna del Maule, Rio Puelche, and Loma Seca Tuff rhyolites, all behind the front (authors' unpubl. data; Barreiro et al. 1982). For comparison, oceanic regression line (ORL) is that of Tilton (1983); northern hemisphere Pb reference line (NHRL) is that of Hart (1984); S–K is the average crustal Pb-evolution curve of Stacey and Kramers (1975); field of Nazca plate basalts is from Unruh and Tatsumoto (1976); and field of Nazca plate sediments is constructed from Unruh and Tatsumoto (1976), Dasch (1981), and Tilton (1983)

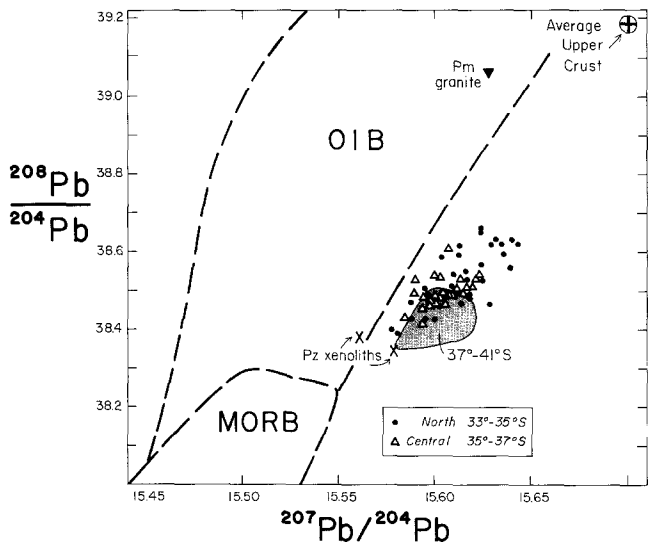

Fig. 8. $^{208}Pb/^{204}Pb$ vs. $^{207}Pb/^{204}Pb$ for volcanic-front centers 33°–41°S. Data from *Table 2* and from Harmon et al. (1984) and Hickey et al. (1986); OIB and MORB fields from the latter. Average upper crustal value is from Zartman and Doe (1981). Permian (Pm) granite and Paleozoic (Pz) granitic xenoliths as in *Fig. 7* and *Table 2*

duction of neither terrigenous nor pelagic sedimentary Pb explains the differences between the adjacent arc segments, derivation of the continental component must be predominantly intracrustal.

The restricted Pb-isotope variability of volcanic rocks within the thin-crust segment at 37°–41° S (Figs. 7 and 8) is thought by some investigators to reflect the subcrustal mixture of slab- and mantle-derived Pb brought up by primitive basalts; more likely it reflects an overprint by Pb assimilated from the Mesozoic and Cenozoic crust of that segment. The late Paleozoic crustal rocks beneath the 33°–35° S volcanoes, on the other hand, are both old enough and lithologically variable enough (including a major upper-crustal fraction of granite and rhyolite) to provide a range of potential assimilants having isotopic leverage sufficient to promote modest elevation of $^{207}Pb/^{204}Pb$ and $^{208}Pb/^{204}Pb$ and *either* increases or decreases (both modest) in $^{206}Pb/^{204}Pb$ relative to baseline values of subcrustal basalt. The granite and xenoliths effectively bracketing most of the data of Figs. 7 and 8 provide convenient and appropriate illustrations of these possibilities. The tendency apparent in Fig. 8 toward $^{207}Pb/^{208}Pb$ values a bit higher than those of the granite and upper-crustal average suggests Pb contributions from Pre-Mesozoic deep-crustal rocks having slightly lower Th/Pb ratios.

These interpretations should not be construed as a rejection of the hypothesis that subducted Pb can find its way into arc magmas. For some arcs on immature crust, a small sedimentary contribution may well dominate the arc Pb budget (Meijer 1976; Kay et al. 1978; Barreiro 1983; White and Dupré 1986); but the along-arc geologic and geochemical context in Chile indicates a predominantly upper-plate control.

Similarly, we do not wish to dismiss entirely a potential Pb contribution from the subcrustal lithosphere, however elusive a concept such lithosphere may be for a dynamic sub-arc mantle that has experienced magmatism quasi-continuously since Permian time. Pb-poor basalt that rises from asthenospheric depths is less likely, however, to undergo recognizable Pb contamination in the mantle lithosphere than within the continental crust which is far richer in both Pb and fluids and includes feldspar-rich rocks having generally lower solidi. In parallel with the Nd-isotopic variability discussed earlier, the Pb-isotopic leverage of potential assimilants is likely to be much greater in Paleozoic crust, on grounds of both Pb concentration and a wider probable range of U/Pb values, than in lithospheric mantle of presumably equivalent (or, owing to secular additions, younger) average age. Moreover, as the top of the Benioff zone is only 90–100 km deep here, mantle lithosphere (if it exists at all) must be much thinner than the 60-km-thick Paleozoic crust beneath the northerly volcanoes. We conclude that the arc Pb is largely controlled by intracrustal contributions.

Ba enrichment

The characteristically great enrichments of arc basalts (relative to MORB) in Ba, Sr, Pb, and alkalies have been widely attributed, following Kay (1977, 1980), to an easily mobilized, subducted sedimentary component. A dominantly lower-plate source of these enrichments is unlikely, however, for the continental-arc suites under consideration here for several reasons. We have already discussed the along-arc Sr- and Pb-isotopic variations and will turn to Rb/Cs relations below; here we emphasize the regional variations in Ba contents, which are much less subject than Sr contents to the vagaries of plagioclase fractionation. Like K_2O, Ba rises markedly along the volcanic front, from characteristic values at 57.5% SiO_2 of about 300 ppm at Antuco to 500–600 ppm at the northernmost centers (Fig. 9).

The ratio Ba/La is commonly taken as a measure of the excess of LIL to LRE elements in arc rocks, relative to MORB or chondritic values (Fig. 10). Ba/La ranges greatly among arc suites, tending to be greatest in LREE-poor low-K island-arc tholeiites and highly variable in medium- and high-K arc suites like those in Chile (Gill 1981; Arculus and Johnson 1981). At the centers studied here, there is little intra-suite change in Ba/La with progressive fractionation, as both elements are strongly excluded from the fractionating phenocryst phases. Excluding the high Ba/La values of Tupungato and Cerro Alto, there is a fairly consistent, modest decline in $(Ba/La)_{57.5}$ northward along the arc (Fig. 9), a trend that would conventionally be interpreted to signify a relatively *smaller* contribution from the subducted plate toward the north end of the segment. This interpretation, however, would conflict with the northward alkali enrichment (Figs. 2, 9) and with the regional Sr-isotopic gradient (Fig. 5), all of which would conventionally suggest a greater lower-plate contribution to the northerly centers were subducted components indeed dominant. Figures 9 and 10 indicate that they are not.

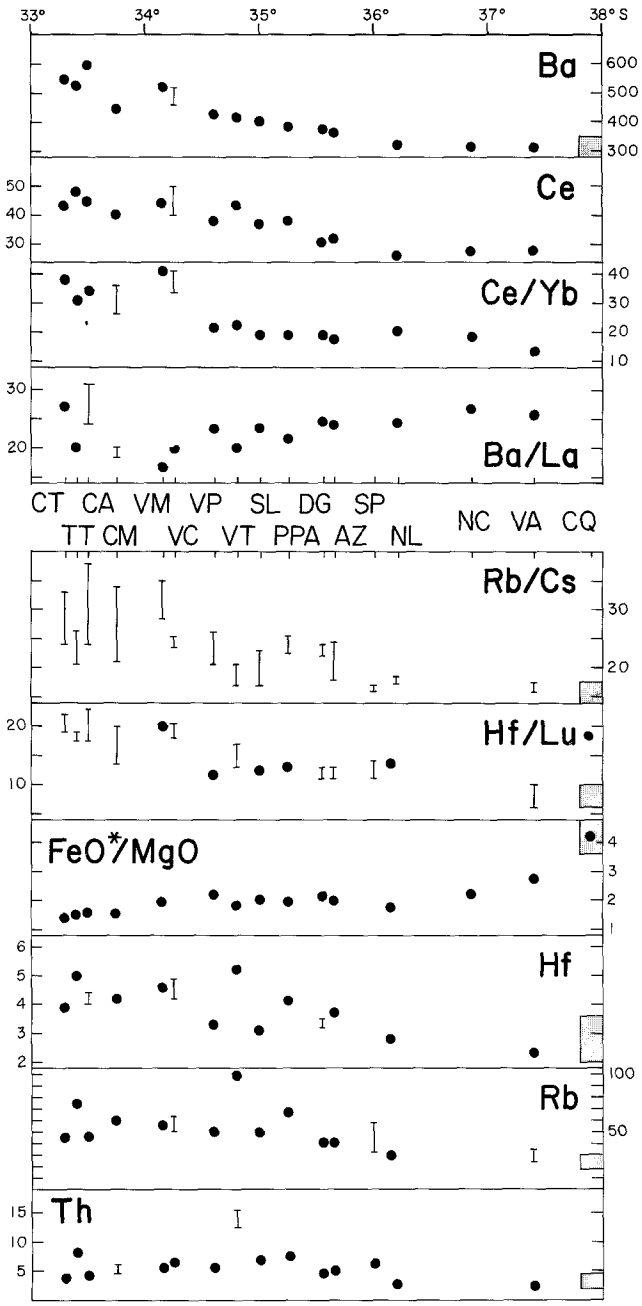

Fig. 9. Latitudinal variations of selected concentrations and ratios of elements taken at 57.5% SiO_2 in volcanic-front suites. *Vertical bars* represent approximations or extrapolations of sparse data or ranges of data not coherent enough to fix a 57.5 value. Rb/Cs does not change systematically with SiO_2; *bars* show complete ranges of ratios, for glassy samples only. *Shaded boxes* at right indicate ranges of available values for basalts and andesites of volcanic-front centers at 38°–41°S. Sources of data other than our own: Lopez-Escobar et al. (1981), Charrier (1981), Harmon et al. (1984), Déruelle (1979, 1982), Stern et al. (1984), Hickey et al. (1986)

Figure 9 shows that, at equivalent SiO_2 contents, both Ba and LREE concentrations increase strongly from south to north along the front, the LREE at a slightly greater rate than Ba. The general northward decline in Ba/La there-

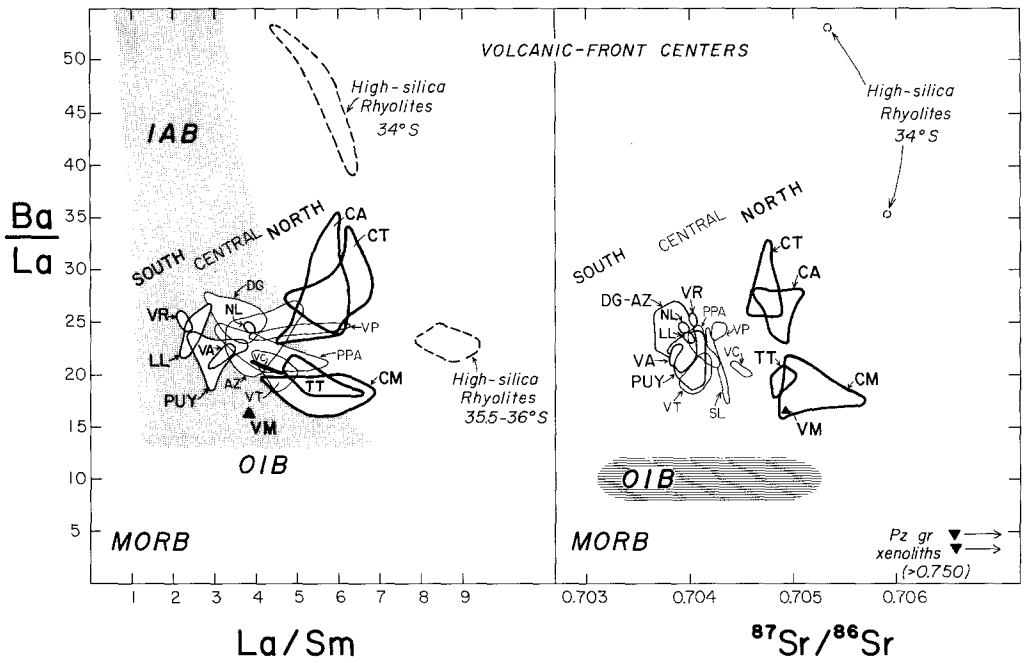

Fig. 10. Ratios of Ba/La vs. La/Sm and $^{87}Sr/^{86}Sr$ for volcanic-front centers 33°–40.5°S. Ba/La is a measure of the excess enrichment of alkaline-earth elements relative to LREE, a feature distinguishing arc suites from MORB and most OIB. Overlapping fields of individual centers are grouped according to three line-weights: North 33°–34°S; Central 34.5°–35.5°S; and South 36°–40.5°S. Abbreviations of volcano names as in *Fig. 2*. Island-arc basalt (IAB) field from Arculus and Johnson (1981). Data from Stern et al. (1984), Hickey et al. (1986), and the present work. Chondritic values of Ba/La and La/Sm are about 10 and 1.65, respectively

fore principally reflects greater northerly LREE enrichment, *relative* contributions that few would attribute to the subducted plate.

Figure 10 further illustrates that the marked enrichment of Ba (and by implication Sr and Pb) compared to oceanic basalts is not caused by subduction alone but is in large part a result of upper-plate processes. Of the four northernmost suites, all of which are relatively (and similarly) enriched in LREE (La/Sm), two have high ratios of Ba/La and two have low ratios. Because phenocryst assemblages of the two pairs are equivalent (plag + oxides ± hb ± px ± bi), this strong divergence is unlikely to reflect high-level crystal fractionation; in any event, although La/Sm increases with progressive fractionation *within* the suites, Ba/La scatters. The Ba contents and Ba/La ratios of the four suites thus exhibit rather unexpected contrasts for centers so closely and similarly situated. The four centers are equidistant from the trench and the Benioff zone, and taken together they span less than 50 km of arc length; accordingly, they are hardly likely to have received drastically different slab-derived contributions. Moreover, the apparent along-trench uniformity of the downgoing sediments gives no indication that variability in such a contribution should exist, let alone be capable of controlling the large along-arc differences displayed in Figs. 5, 9, and 10.

Figure 10 additionally shows that the south-to-north divergence in Ba/La values persists when plotted against $^{87}Sr/^{86}Sr$ ratios. This signifies that no correlation exists between enrichment in radiogenic Sr and the magnitude of the excess relative enrichment of alkaline-earth elements over LREE; if the slab-derived contribution were dominant, there should be such a correlation (Arculus and Johnson 1981).

The south-to-north compositional variation patterns summarized in Figs. 5, 9, and 10 are more readily explained by upper-plate, largely intracrustal, processes. The divergence of Ba/La ratios toward both higher and lower values (Fig. 10) involves only those centers north of 35.5°S where the crust starts to thicken appreciably (Fig. 2), and it develops just where these continental-arc data start to trend out of the island-arc field (Fig. 10); the greatest spread is among the four neighboring centers where the crust is thickest and the mantle wedge thinnest. The variable Ba/La patterns probably result from contrasting interactions with the thick heterogeneous crust beneath the different centers. Available data for various high-silica rhyolites and partially melted granitic xenoliths from this part of the Andes, plotted in Fig. 10, attest that different assimilants, depths, and styles of crustal contamination could result in drastically different degrees of enrichment or depletion in Ba and LREE in arc magmas. Just as crustal assimilation can shift the $^{206}Pb/^{204}Pb$ ratios of arc magmas to values either higher or lower than those of their mantle-derived parents, so can Ba and Sr concentrations be levered in either direction – owing to the extremely wide compositional ranges (10–1000 ppm) of the potential crustal assimilants.

In summary, scavenging by arc basalts of melts and fluids relatively rich in Ba, Sr, Pb, alkalies, and LREE from various rocks at various depths along a 60-km crustal column is a much more likely cause of the *local* variability of these elements and their isotopic ratios than is heterogeneity of mantle or slab contributions on so local a scale. The southward decrease in variability within and among volcanic-front centers implies either less effective or less recognizable crustal assimilation where the crust is thinner. This along-arc difference in variability could simply reflect less crustal assimilation in the south, where crustal ascent paths and average residence times would be shorter, or it may largely reflect the smaller compositional contrast of younger, less differentiated, more mafic crust assimilated in the south. We will return below to discussion of antici-

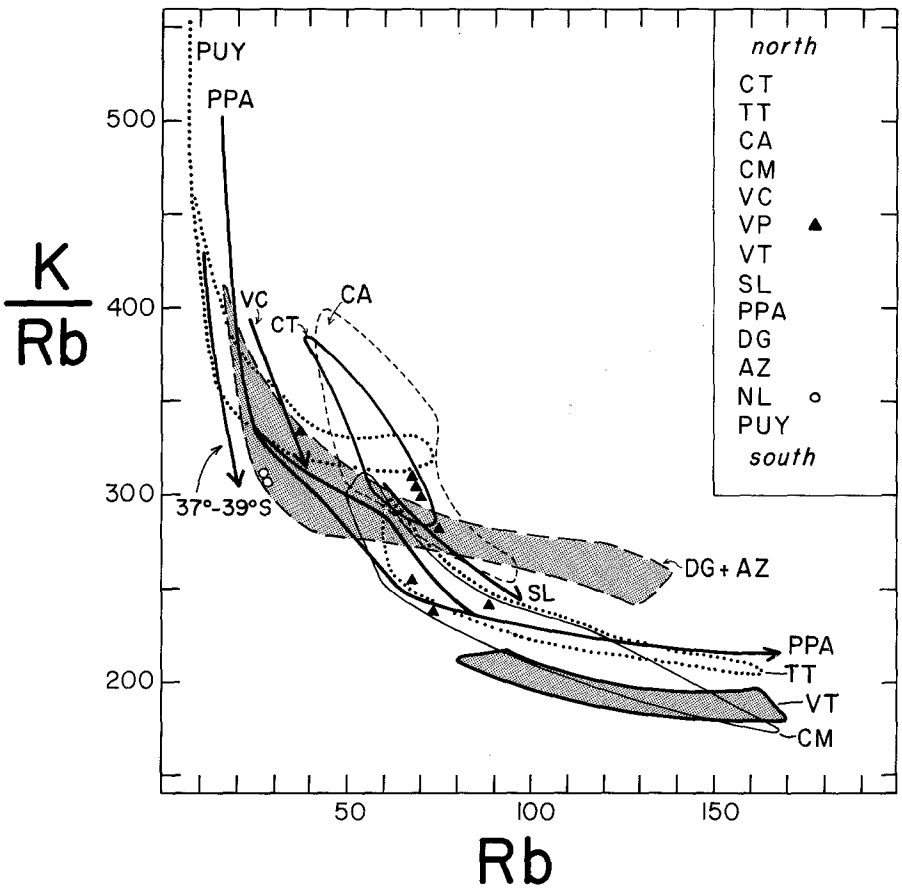

Fig. 11. Variation of K/Rb vs Rb for volcanic-front centers 33°–36°S. Abbreviations of volcano names as in *Figs. 2* and *4*. *Line* marked 37°–39°S indicates trend of data for basalts and andesites of Antuco, Llaima and Villarrica volcanoes (Hickey et al. 1986); Puyehue (PUY; 40.5°S) field is from Gerlach et al. (1987). Fields for Puyehue and Descabezado Grande + Cerro Azul DG + AZ) represent data extending to 71% SiO_2, Planchon (PPA) to 69% SiO_2, but no others to >68% SiO_2. Relative to southerly suites, more northerly suites exhibit much wider ranges of K/Rb at intermediate compositions and/or extend to much lower K/Rb at silicic ends of spectra

pated differences between deep- and upper-crustal assimilation.

Alkali enrichment

Rb variation parallels that of K rather closely, both elements being much more enriched in suites north of 36°S than farther south – though in detail the along-arc trend is not very systematic (Figs. 2, 9, 11, 13). Cs concentrations increase northward to a smaller extent and more erratically than those of Rb. No regional trend in Na has been discerned. K, Rb, and Cs are most abundant at Tupungatito, Planchon, and especially at Tinguiririca. Across the crustal transition zone near 36°S, SiO_2-normalized concentrations of K, Rb, and Cs double or triple relative to volcanic-front centers at 37°–41°S. Moreover, alkali concentrations are not simply greater but are much more *variable* at volcanoes built on the thicker crust north of 36°S – both within centers and in comparing neighboring ones (Figs. 2, 9, 11).

The alkali ratios K/Rb and Rb/Cs also exhibit considerably wider ranges in northerly centers than farther south (Figs. 9, 11). Although K/Rb values decline with progressive Rb enrichment in *all* suites, the northern suites at Tupungato, Alto, and Marmolejo show very extensive K/Rb variations over rather limited ranges of fractionation (Fig. 11): 345–295, 395–305, and 310–250, respectively, over Rb ranges of <10 ppm. Suites tend to have steeply coherent K/Rb trajectories up to about 20 ppm Rb (Fig. 11), but these broaden into wide fields in crossing the intermediate part of the compositional spectrum (20–80 ppm Rb, 55–63% SiO_2); the fractionation trajectories then narrow again in the dacite-rhyolite part of the range. Both the early steep drops and the broad intermediate patterns are likely to reflect the wide variety of crustal interactions (addition of various crustal partial melts, contrasting AFC paths, blending of variably evolved batches) that affect mafic magmas stalled in the lower crust or percolating upward through heterogeneous crust prior to aggregation in magma chambers. The more coherent dacite-rhyolite trends probably result from subsequent fractionation of plagioclase and hornblende within such chambers.

In accord with such a model, the northerly suites extend to much lower K/Rb values than do suites farther south (Fig. 11). For example, K/Rb values at Volcan Puyehue (Gerlach et al. 1987) in the thinner-crust segment to the south descend only to ~320 at 71% SiO_2 whereas (at identical maximum SiO_2 content) K/Rb at Descabezado Grande and Cerro Azul (35.5°S) drops to 250. Still farther north, K/Rb reaches 215 at 69% SiO_2 at Peteroa (35.2°S), 180 at 68% SiO_2 at Tinguiririca (34.8°S), and 175 at 66% SiO_2 at Marmolejo (33.7°S). In view of the apparent constancy of the subduction regime along the arc, the gradient in crustal thickness, and the northward trends in Nd and Sr isotopic signatures (Fig. 5), it is hard to escape the conclusion that the regional K/Rb pattern results from intracrustal additions to subcrustally derived magmas.

The along-arc change in average Rb/Cs ratios (Fig. 9) further supports the view that the northward alkali enrichment is controlled by intracrustal rather than slab-derived contributions. Overabundance of Cs relative to K and Rb in *island*-arc suites (compared to MORB and OIB suites) is a widespread attribute, commonly credited to involvement of Cs-enriched pelagic sediments in arc-magma genesis (Morris and Hart 1983; White and Patchett 1984). White

and Dupré (1986) give a Rb/Cs range of 11–20 for marine sediments, compared to a main range of 20–33 for *island*-arc volcanic rocks and a main range of 50–100 for MORB and OIB. As both elements are highly incompatible in reasonable phenocryst assemblages, Rb/Cs should not be significantly modified by crystal fractionation across the basalt-andesite spectrum of arc suites. Biotite fractionation might provide exceptions, but here biotite occurs at only two centers, only in rocks having >60% SiO_2, and does not bear upon the Rb/Cs relationships shown in Figure 9. Because Cs is readily lost during post-eruptive devitrification, only fresh glassy samples have been considered.

Figure 9 shows that Rb/Cs effectively doubles along the segment from south to north, opposite what would be predicted were a Cs-enriched sedimentary component responsible for the general northward alkali enrichment. It is actually several of the tholeiitic suites, having *lower* alkali contents, at several centers south of 37°S, that have the low ranges of Rb/Cs similar to those of marine sediments (Hickey et al. 1986).

The higher and more variable abundances and ratios of K, Rb, and Cs at northerly centers (Figs. 2, 9, 11, 13) are thus much more likely to result from deep-crustal melting *and* from subsequent scavenging of crustal melts and fluids along the percolation columns beneath long-lived centers (Hildreth 1981) than to reflect the slab-derived component. Indeed, the experimental data of Watson (1982) lead one to expect selective contamination in K (and presumably Rb and Cs) of virtually any mafic magmas that penetrate silicic-alkalic crustal rocks. Crustal scavenging should, in principle, be more important in the thicker, older, more differentiated crust north of 36°S. In addition to longer transit paths and interaction times in thicker crust, the northerly increase in alkali contents of Quaternary magmas may reflect in part the greater fraction of true granites in the Paleozoic-Triassic basement as compared to the younger basement farther south, where diorite to granodiorite dominate exposed plutonic suites. The northerly increase in Rb/Cs and K/Cs could result from the relatively greater mobility of Cs, its preferential extraction and upward transport in fluids and leucomelts, and a consequent depletion of Cs from the Paleozoic lower and middle crust during the repeated episodes of post-Paleozoic Andean magmatism. The compilation of Taylor and McLennan (1985) indeed yields a lower-crustal average Rb/Cs value of ~53 and an upper-crustal average of ~30, demonstrating exactly such a fractionation. The relative underabundance of Cs at northerly volcanoes, therefore, probably reflects a major deep-crustal contribution from the thick, secularly differentiated, continental basement. Where the crust is younger and thinner south of 36°S, however, the low Rb/Cs and K/Cs values of Quaternary magmas may indeed ultimately reflect the slab-derived flux of alkali-enriched fluids, both the Quaternary flux itself and a remobilized Cs-rich component scavenged from Andean arc-plutonic rocks of Mesozoic and Tertiary age.

Rare earth elements (REE)

LREE contents and slopes of REE patterns increase with SiO_2 in all suites studied. Farther south, however, the increases in slope with differentiation are less pronounced and even equivocal at some centers (Fig. 12). Within the segment investigated, above and beyond intrasuite REE fractionation, there is also a regional tendency for SiO_2-normalized values of LREE, La/Sm, and Ce/Yb all to increase northward; taken at 57.5% SiO_2, the characteristic value of each roughly doubles from south to north (Figs. 9, 10). For all seven centers north of 35°S, the most mafic rocks sampled (53–57% SiO_2) have Ce abundances in the range 36–50 ppm, approximately 3 to 10 times the Ce contents of intraoceanic-arc lavas with equivalent SiO_2 or MgO, suggesting a major LREE contribution from the continental crust.

Negative Eu anomalies are nearly ubiquitous in evolved rocks, but in the most mafic members of each suite they are either absent or too small to resolve by INAA. Positive Eu anomalies have not been discerned in any of the >140 rocks analyzed. Negative Ce anomalies, common features of *island*-arc volcanic rocks (White and Patchett 1984), have not been recognized here (but small ones might not be resolvable by INAA). The apparent absence of Eu- and Ce-anomalous mafic rocks here is thus thought to limit the contribution of pelagic sediment to the magma source region to no more than a few percent (McLennan and Taylor 1981; White and Dupré 1986), consistent with the general lack of evidence here for a major lower-plate contribution.

Although SiO_2-normalized LREE concentrations ($Ce_{57.5}$ in Fig. 9) double northward along the segment, Figure 12 illustrates that the northward rise in $(Ce/Yb)_{57.5}$ also reflects the relative constancy of HREE contents within and among the northerly suites. South of 36°S, Ce/Yb ratios are 10 to 15 and change little with progressive differentiation. Suites from the crustal transition zone at 35°–36°S (Cerro Azul, Descabezado Grande, and Planchon-Peteroa-Azufre) have Ce/Yb ratios in the range 14–23 and somewhat greater LREE/HREE relative enrichment with differentiation. From Tinguiririca (34.8°S) northward, on thicker older crust, all suites have restricted ranges and low contents of HREE (4–8 times chondrites), and the steeper slopes of their REE patterns owe as much to nonenrichment of HREE as to the progressive increases of LREE with SiO_2 and latitude (Figs. 9, 12).

Such nonenrichment of HREE (and Y) is relatively uncommon among arc volcanoes and is largely restricted to calcalkaline continental-margin suites, as pointed out by Gill (1981). In the SVZ, however, such HREE behavior characterizes all the centers north of 35°S (Fig. 12) but none yet studied on the thinner crust extending hundreds of kilometers southward along the volcanic front (Lopez-Escobar 1984). Because of the northward-thinning mantle wedge and the apparent constancy in the subduction regime, the north-south contrast in REE behavior must also be attributable to intracrustal processes.

Figure 12 shows that the most mafic members of all suites, north to south, have similar HREE contents (4–8× chondrites). The relative constancy of HREE during LREE enrichment in the northerly suites can in principle be explained by fractionation of a phenocryst assemblage in which garnet (or conceivably amphibole) plays an important role or by interaction with wall-rocks containing these minerals. Fractionation of the low-pressure plagioclase + olivine + pyroxenes ± titanomagnetite assemblage dominant at the southerly centers clearly fails to suppress HREE enrichment (Fig. 12).

As amphibole-melt partition coefficients for HREE in most andesites fall between 0.5 and 2 (Gill 1981), hornblende fractionation is seemingly a feasible HREE suppres-

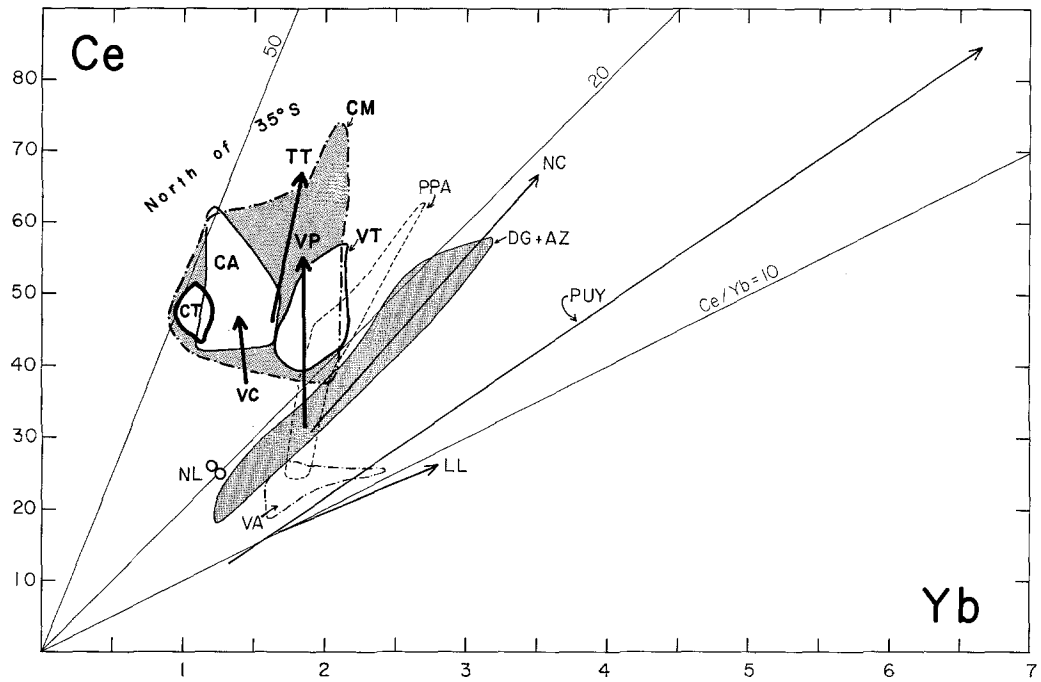

Fig. 12. Ranges of Ce vs Yb concentrations (in ppm) for volcanic-front centers. Abbreviations of volcano names as in Figs. 2–5. *Bolder symbols* distinguish 7 centers on thicker crust north of 35°S, where HREE remain quasi-constant during LREE-enrichment with progressive differentiation

sant; but, were this the dominant process, the still larger preference of amphibole for MREE (Gd to Er) would yield dish-shaped REE patterns that are not observed. Moreover, amphibole phenocrysts are not present here in rocks having less than 57% SiO_2, and at many centers (both north and south) the absence of amphibole extends to silicic andesites and even some dacites (Table 1). To be an effective influence on REE behavior, therefore, hornblende fractionation would have to be a deep-crustal process for which petrographic evience is lost during magma ascent. Interaction of primitive basalts with hornblende-rich lower-crustal rocks, either by assimilation and reaction with the enclosing wall rocks or by mixing with silicic partial melts thereof, could provide an alternative means of HREE suppression. The deep crust beneath the Andean arc is likely to be rich in gabbroic-to-tonalitic intrusions, their cumulates and fractionates, and their metamorphosed equivalents. Owing to persistent slab dehydration, mantle-generated basaltic magma may transfer sufficient water to the lower crust to offset upward losses and to stabilize plutonic and metamorphic amphibole (cf. Takahashi 1986). Interaction of rising batches of basalt with earlier-formed hornblende-rich mafic-to-intermediate plutons and amphibolite could conceivably provide a HREE-poor contribution. Because there is no ready basis for postulating a north-south difference in the effectiveness of such a process, however, amphibole control is not our favored hypothesis for the high-Ce/Yb northerly suites.

Deep-crustal garnet is more likely to play the key HREE-retaining role. In fact, Ce/Yb ratios as great as 52 (Fig. 12), HREE contents as low as 3.7 times chondritic, and the general absence of concave-up REE patterns in mafic samples are all features more likely to reflect the influence of garnet than of hornblende (Nicholls and Harris 1980). The steep REE pattern of a Tupungato silicic andesite has in fact been modeled as a product of 3% melting of garnet peridotite (Lopez-Escobar et al. 1977). There is no apparent reason, however, that garnet peridotite (or eclogite), if present at all, should be a more effective HREE sink in the mantle wedge (or slab) beneath thick crust than beneath thin crust. The sink is more likely to lie within the thick crust itself. Lopez-Escobar (1984) attributed the gentler REE slopes (Ce/Yb=9–20; Fig. 12) of the mafic members of suites south of 35°S to olivine+pyroxene fractionation of parental basalts derived from garnet-free peridotite in the mantle wedge – a reasonable hypothesis for primitive basalts along the whole volcanic front. The HREE contents of the most mafic members in each suite are everywhere similar, but the HREE suppression in andesites and dacites occurs uniquely where the crust is 45–60 km thick.

Garnet-bearing granulites, gabbros, and eclogites are expected to be stable in the lower crust here, and garnet could even be a phenocryst in basaltic and andesitic magmas (Wyllie 1977; Huang and Wyllie 1986) under the 12–17 kb pressures of the deep crust beneath the northerly volcanoes. The main role of garnet may lie in the environment of lower-crustal mixing and homogenization, where LREE-rich crustal partial melts strongly depleted in HREE are mixed with basaltic magmas evolving toward andesite. The arguments of Gill (1981, p. 284) against a role for garnet are less compelling if the garnet occurs in tonalites, gabbros, and granulites (rather than in eclogite or peridotite) or if it precipitates from mafic magma over a restricted ascent interval in the deep crust. For feldspar-rich garnet-bearing crustal rocks, *bulk D* for Y, Sc, and HREE should generally be lower than in garnet-peridotitic or eclogitic assemblages, mitigating Gill's prediction that melts in equilibrium with garnetiferous assemblages should be extremely depleted in all 3 elements. In particular, if garnet is viewed as promoting modifications of evolving magmas instead of being an essential phase in magma genesis, the much larger value of D^{gt}_{Yb} than of D^{gt}_{Y} and D^{gt}_{Sc} would permit coevolution

of very low Yb contents (1–2 ppm) along with the moderate contents of Y (15–25 ppm) and Sc (14–29 ppm) observed among the basalts and mafic andesites here.

In summary, then, partial melts of most crustal rocks would be rhyolitic to dacitic in composition (Wyllie et al. 1976; Wyllie 1977) and would normally raise LREE contents and Ce/Yb ratios of basaltic magmas assimilating them. Other factors being equal, thicker crust (presumably hotter at its base) should promote greater LREE enrichment of fractionating magmas, by means of diverse interactions with heterogeneous crustal rocks. On the other hand, the twofold northward enrichment in LREE ($Ce_{57.5}$ in Fig. 9) hardly seems likely to reflect a systematically changing contribution from the peridotitic mantle wedge, which itself *thins* northward. The extent to which high-pressure fractionation of hornblende or garnet phenocrysts might influence the low HREE contents of the northerly suites is uncertain, but low-pressure hornblende phenocrysts are present in silicic andesites at only a few centers (Table 1) and in mafic andesites at none; phenocrystic garnet is everywhere absent. If either is a fractionating phase in the deep crust, petrographic evidence is always lost by resorption, reaction, or physical separation prior to eruption; such loss is not unexpected if the 50-km crustal ascent is fitful, takes place by means of fracture propagation (Shaw 1980; Hildreth 1981), and in some cases involves mid-to-upper-crustal magma reservoirs (where additional crustal assimilation can also occur). Our favored interpretation is that the low HREE contents are attributable to lower-crustal contributions extracted from garnet-bearing residues. The regional contrast in REE patterns is consistent with large-scale mixing and homogenization of subcrustal and crustal contributions, and the trace-element and isotopic data suggest that this largely takes place within the *lower* crust, which extends beneath northern centers to depths where crustal garnet is stable. Near the base of a 60-km-thick crust, Andean basaltic-to-intermediate intrusions might crystallize garnet and during later episodes of partial re-melting yield HREE-poor melt contributions. It is also likely that the Permo-Triassic silicic magmatic belt beneath the northerly centers grades downward into a pre-Andean granulitic lower crust that has been partially rehydrated by intrusion of H_2O-bearing gabbros during 200 m.y. of Andean arc magmatism, producing a complex mixture of hornblende- and garnet-bearing lithologies, the spatial variations in which might account for some of the compositional heterogeneity among the northerly volcanoes today.

High-field-strength elements (HFSE)

As in most convergent-margin suites, TiO_2 concentrations are low throughout the segment. Values decline slightly but steadily in all suites, starting from maximum observed values of 0.9–1.2 wt% in the most mafic members (basalts or basaltic andesites). In contrast, many of the tholeiitic centers in the thin-crust segment south of 37° S have suites that fractionate to peak TiO_2 values of 1.3–1.6 wt% at 55–57% SiO_2 before assuming a negative trend with further SiO_2 enrichment (e.g., Lopez-Escobar et al. 1981; Déruelle 1979, 1982; Gerlach et al. 1987). Because ilmenite does not crystallize until 58–60% SiO_2, nor amphibole until 57–60% SiO_2, the progressive TiO_2 decline at northerly centers is probably caused by greater assimilation of Ti-poor crustal melts and/or earlier onset of titanomagnetite fractionation.

The low TiO_2 (and Nb and Ta) contents of arc basalts, relative to alkalic basalts and most intraplate tholeiitic basalts, have been widely attributed to buffering by a hypothetical Ti-rich residual phase uniquely stabilized in the hydrous environment of the slab or mantle wedge (Saunders et al. 1980). However, Arculus and Powell (1986) pointed out several chemical and petrologic problems with such a model, and Green and Pearson (1986) have demonstrated experimentally that the high solubility of Ti in basaltic magma essentially precludes saturation in a Ti-rich phase or survival of such a phase in its mantle residuum. According to their data, at P and T values characteristic of the mantle wedge, arc-basaltic liquids, hydrous or not, would require more than 5 times the observed TiO_2 contents in order to attain saturation with a Ti-rich phase; and basaltic andesite having 1.0–1.3% TiO_2 would not saturate until it had cooled to 900°–950° C, an unreasonably low temperature for such magma in the mantle. Green and Pearson (1986) therefore ruled out models that postulate a Ti-rich mantle phase residual to generation of arc basalts and called instead upon prior Ti-depletion of (unspecified) source regions to account for the characteristically low TiO_2 contents of arc suites.

A refractory Ti-rich accessory phase has also been widely postulated as a sink for Nb and Ta, and even for Zr and Hf by some investigators, as each of these HFS elements is depleted in arc basalts relative to most ocean-island and intracontinental basalts. If a residual Ti-rich phase can survive generation of basaltic magma in neither slab nor mantle wedge, however, then either (1) the HFSE are retained in arc-magma sources by phases not particularly rich in TiO_2; or (2) the slab contribution is large, HFSE-poor, and nonbasaltic; or (3) the mantle-wedge source is intrinsically HFSE-depleted; and/or (4) the HFSE-poor component is in part crustal.

(1) In the first case, titaniferous amphibole, phlogopite, or garnet might retain HFSE in wedge peridotite that need not actually be deficient in these elements relative to other mantle reservoirs. Several authors, following Morris and Hart (1983), have proposed a major role in arc-magma genesis for mantle sources similar to those of ocean-island basalt (OIB) – although the proposition has hardly gone unchallenged (Perfit and Kay 1986). OIB-like volcanic rocks are fairly scarce in unrifted arcs, however, especially so on volcanic fronts. Where xenolithic mantle fragments containing titaniferous amphibole, mica, and/or garnet are brought to the surface in near-arc rifts or in other tectonic settings (e.g., Stern et al. 1986; Menzies and Hawkesworth 1987), the host magmas are generally far richer in HFSE than are those characteristic of convergent margins; i.e., such minerals are not so much associated with Ti–Nb–Ta depletion as with their enrichment. Indeed, if Ti-rich accessory phases (ilmenite, rutile, crichtonite, sphene) cannot survive basaltic magma generation in the sub-arc mantle, then the low HFSE content of most arc basalt is itself an important piece of evidence against major contributions from OIB-source peridotite during the main episodes of magma generation beneath volcanic fronts.

(2) Gill (1981) summarized compelling evidence against direct derivation of arc magmas by slab melting, but slab derived HFSE-poor fluids or silicic-alkalic melts could nonetheless contribute significantly toward depletion of wedge-derived magmas in HFSE, either indirectly by wedge metasomatism (Wyllie 1982) or directly by fluid-melt mix-

ing in the wedge. Basaltic melts are not expected to leave behind a HFSE-rich residual phase, but rhyodacitic melts or solute-rich fluids derived from the slab probably would. Even though such source mixing may contribute to HFSE underabundance in arcs, the mass requirements of wholesale dilution of OIB-like wedge melts by HFSE-poor slab contributions seem too great for such mixing to be the main HFSE-depleting process. If a large mass proportion (tens of percent) were truly derived from subducted sources (which are expected to be rich in sediments, seawater Sr, and quartz eclogite), control of REE patterns and Sr-, Pb-, and O-isotopic signatures of arc magmas by such sources should be unequivocal. It certainly isn't.

If, on the other hand, wedge peridotite were intrinsically depleted (MORB-source or MORB-residue), this could account for much of the apparent HFSE-underabundance of arc basalts, both oceanic and continental. Although arc basalts are clearly impoverished in HFSE relative to intraplate basalts, it is a commonly repeated misconception that they are also generally HFSE-deficient relative to MORB. Abundant published data actually indicate extensive overlap of Ti, Zr, Hf, Nb, and Ta concentrations for N-MORB and arc basalts worldwide; it is the superimposed enrichment of the arc basalts in LILE and LREE from slab and crustal sources that creates the strikingly negative HFSE anomalies on normalized abundance diagrams. Low-K intraoceanic-arc basalts, however, characteristically overlap only the more depleted halves of the HFSE arrays exhibited by N-MORB data. This relationship can be accounted for by (a) the slight dilution caused by persistent flux of low-HFSE slab-derived contributions; (b) extensive wedge melting sustained by this flux; (c) smaller intracrustal HFSE contributions compared to crustally more mature arcs (as is Chile where the HFSE overlap between arc basalts and N-MORB is complete); and (d) in special cases, by extreme wedge depletion resulting from recent prior magma extraction – as in northern Tonga (Ewart and Hawkesworth 1987).

The observation that HFSE-richer OIB-type basalts sometimes do erupt in extensional zones within or behind active arcs, or along segment boundaries, or soon after cessation of subduction (Gill 1981, 1984; Luhr and Carmichael 1981) signifies that OIB-source peridotite can be locally available beneath arcs, whether as asthenospheric streaks and blobs or as veins and pods in subcrustal lithosphere. Because such material seldom contributes recognizable HFSE enhancement of *volcanic-front* magmas but may do so for certain arc magmas that erupt behind the front (Hickey et al. 1986; Kay and Rapela 1986), the causes of HFSE suppression are evidently most effective beneath the front itself. This spatial and tectonic restriction points not to wedge-wide HFSE depletion but to more localized phenomena involving the fluid flux from the slab, the higher degree of wedge melting locally induced thereby, and/or the concentrated basaltic flux focussed upon a narrow strip of the lower crust.

(4) The deep arc crust is another potential source reservoir capable of yielding Ti–Nb–Ta-depleted partial-melt contributions. Indeed, the results of Green and Pearson (1986) confirm the expectation that most crustal melting would be buffered at low TiO_2 contents by refractory Ti-rich phases, producing partial melts having $\sim 1\%$ TiO_2 at 60% SiO_2, or perhaps more important, $<0.5\%$ TiO_2 in rhyolitic extracts. Rutile, ilmenite, sphene, titanomagnetite, and Ti-bearing amphibole and garnet could all provide Ti–Nb–Ta sinks during partial melting of heterogeneous lower-crustal rocks.

General resolution of the low Ti–Nb–Ta abundances in arc magmas thus requires consideration of the degree of prior depletion of wedge peridotite and of at least three superimposed processes, all fundamentally focussed by slab dehydration: (1) the flux of HFSE-poor slab fluid or silicic-alkalic melt; (2) extensive sub-arc melting of wedge peridotite persistently fluxed; and (3) mixing of wedge-derived basalt with low-HFSE partial melts of the lowermost crust.

HFSE in the SVZ. Because the Chilean SVZ has virtually no primitive basalts, the contributions of various source reservoirs to the HFSE contents and ratios observed here are difficult to distinguish from superimposed effects of fractionation and assimilation. Nonetheless, Figs. 13–16 highlight some large differences in Ta, Nb, Hf, and Zr patterns among the suites studied and illustrate several points suggestive of major crustal influence. These four HFSE, as well as Th and U, are enriched with increasing SiO_2 in all suites, Nb concentration consistently being 15–19 times that of Ta and Zr 35–55 times that of Hf. Modest regional differences in the low TiO_2 contents of these suites were mentioned earlier.

An important generalization, that Zr, Hf, Ta, Nb, U, and Th contents are much greater in these continental-margin arc suites than in intraoceanic island arcs (Gill 1981), suggests that there are large crustal HFSE contributions and that their source is dominantly intracrustal rather than subduction-derived. For mafic andesites (53–57% SiO_2) at centers under study, the abundances (in ppm) of Zr (125–240), Hf (3–5), Ta (0.3–0.6), Th (3–12), and U (0.7–3.3) are generally 3 to 10 times as great as those of comparable rocks (at equivalent SiO_2) in the Tonga-Kermadec, Mariana, or South Sandwich arcs.

On the other hand, compared to ocean-island and intracontinental basalts, the SiO_2-variation trends for HFSE on the SVZ volcanic front project back toward *low* concentrations of Ta (<0.2 ppm), Hf (<3 ppm), and Zr (<125 ppm) for the basaltic (50–53% SiO_2) ranges of all suites (Fig. 13). There is therefore no compelling basis for calling upon a major contribution from relatively HFSE-enriched (OIB-type) mantle sources at any of the volcanic-front centers.

Ba/Ta values. Such OIB-like contributions are significant, even dominant, however, at centers well behind the front in Argentina (Llambias 1966; Skewes and Stern 1979; Llambias et al. 1982; Stern et al. 1986) and are evidently important in establishing across-arc trends toward more alkaline magmatism (Saunders et al. 1980; Kay and Rapela 1986). Addition of an OIB-like component was invoked by Hickey et al. (1986) to explain some of the variability among arc basalts in the SVZ itself; they pointed out that mafic lavas with *higher* overall abundances of incompatible elements (LREE, HFSE, Th, K, Rb, Ba, P) tend to have *lower* ratios of Ba/Nb (and of La/Nb, Zr/Nb, Ba/La, and Ba/Th) and vice versa. Greater relative abundances of LREE and HFSE were attributed to (1) larger contributions from enriched lithosphere or, alternatively, (2) lower degrees of melting of enriched wedge asthenosphere – both models involving an enriched OIB-type source. Because Ba/Nb (and Ba/Ta) values are exceptionally high in ordinary

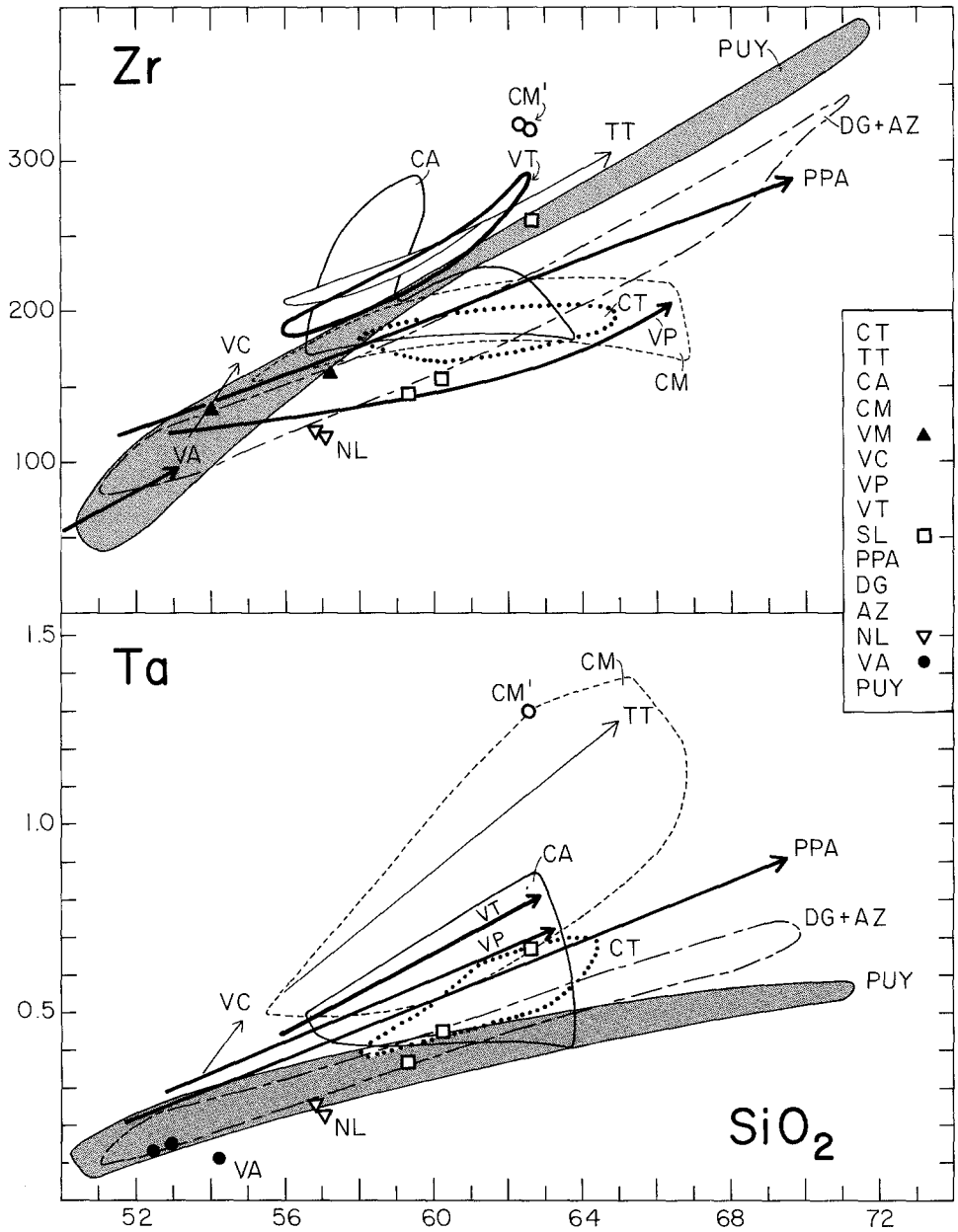

Fig. 13. Ranges of Zr and Ta concentrations (ppm) vs SiO_2 (wt%) for volcanic-front centers; abbreviations from *Table 1* are listed in order from north to south. CM' is subordinate high-K andesite at Marmolejo

arc magmas but are much lower in OIB, these ratios were used by Hickey et al. (1986) as key indicators of relative contributions from the slab vis-à-vis the OIB-source mantle domains. All of their high-Ba/Nb magmas erupted on the volcanic front, whereas the low-Ba/Nb magmas were sampled at only three centers, two of which are clearly behind the front (Quetrupillan and Laguna del Maule); the third (Casimiro), a satellite of Volcan Maipo, is at least arguably behind the front (Fig. 1).

Fields for the "high- and low-abundance magmas" of Hickey et al. (1986), along with our data for the 33°–36°S centers on the volcanic front, are shown in Figure 14, wherein Ba/Ta is set equal to 15 (Ba/Nb). The diagram shows that several centers, both north and south along the front, have wide Ba/Ta (and thus Ba/Nb) ranges that overlap both fields of Hickey et al. (1986). Only the Marmolejo (CM) and Planchon (PPA) suites exhibit significant correlations among fractionation indices and Ba/Ta and $^{87}Sr/^{86}Sr$ ratios. Because the Sr-isotopic trends of both suites are readily interpretable in terms of mid-to-upper-crustal AFC (Fig. 6), the correlations between Ba/Ta and $^{87}Sr/^{86}Sr$ evident in Figure 14 are also likely to reflect crustal assimilation. Moreover, the likelihood that crustal contributions more widely influence Ba/Ta (and Ba/Nb) values is supported by the low ratios of the Tupungatito suite (TT), which contains an abundance of partially melted, relatively Ta-rich granitoid xenoliths and exhibits Ba/Ta values similar to those of the few nearby rhyolites (Fig. 14). The very extensive Ba/Ta ranges of Cerro Alto (CA), Marmolejo (CM), and Cerro Azul (AZ) in Figure 14 probably reflect complex crustal reservoirs beneath each of these long-lived multi-vent centers.

That the wide ranges in Ba/Ta are not simply products of crystal fractionation in evolved suites is illustrated by relations among the four northernmost suites (CT, TT, CA, and CM in Figs. 10 and 14), which have similar andesite-

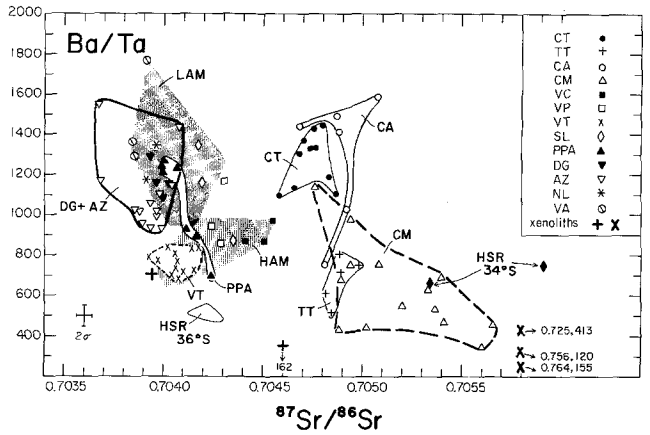

Fig. 14. Ba/Ta vs $^{87}Sr/^{86}Sr$ values for volcanic-front centers 33°–37°S. *HAM* and *LAM* are fields of "high and low-abundance magmas" given by Hickey et al. (1986), where their Ba/Nb data (including VC and VA) have been plotted by assuming Nb = 15 Ta. Abbreviations of volcano names as in *Table 1*, listed in order from north to south. Partially melted granitoid xenolithic ejecta are from Tupungatito (X) and Cerro Azul (+). HSR indicates data for high-silica rhyolites at given latitudes (Hildreth and Moorbath, unpubl. data; Stern et al. 1984). Fields for MORB and OIB would plot well below the diagram, generally at Ba/Ta values <75 and <250 respectively

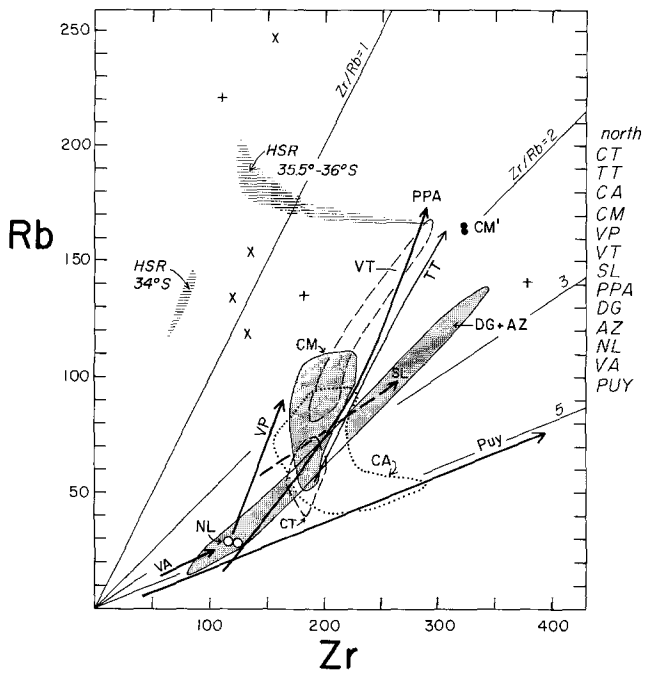

Fig. 15. Rb vs Zr concentrations (ppm) for volcanic-front centers 33°–36°S. Abbreviations listed north to south as in *Table 1*. Also given are trends for Antuco (VA; 37.4°S) and Puyehue (PUY; 40.5°S) in the next arc segment south (Hickey et al. 1986; Déruelle 1979; Gerlach et al. 1987); and fields of high-silica rhyolites (HSR) on or behind the volcanic front at indicated latitudes (Hildreth, unpubl. data). Partially melted granitoid xenolithic ejecta: (+) from Cerro Azul; (x) from Tupungatito. CM' indicates subordinate high-K samples from Marmolejo

dacite compositional ranges and plagioclase-pyroxene-magnetite phenocryst assemblages; three of the suites additionally crystallized hornblende at 57% SiO_2, and one high-Ba/Ta suite (Tupungato) and one low-Ba/Ta suite (Marmolejo) also crystallized biotite at 60–61% SiO_2 (Table 1). That the fractionation of hornblende and/or biotite is unlikely to be the main cause of low Ba/Ta values, however, is illustrated by the low-Ba/Ta Tupungatito and Tinguiririca suites, which lack such phases. Although crystal fractionation and differences arising from mantle sources may each contribute some of the variability, the wide ranges and marked *local* variability displayed in Figures 10 and 14 point to a major role for crustal assimilants representing broad spectra of Ba, HFSE, and LREE concentrations and mutual ratios – as expected for a variety of rhyolitic and dacitic partial melts generated at various levels of the crust.

It is sometimes assumed that crustal assimilation can only *raise* the Ba/Nb (and Ba/Ta) ratios of basalts, because most crustal rocks have Ba/Nb values 2 to 10 times those of N-MORB (~4) and OIB (6–15). The assumption is invalid, however, in an arc setting, where Ba/Nb values of wedge-derived basalts little modified by intracrustal additions (intraoceanic-arc tholeiites) are characteristically in the range 50–>200, owing to the slab-derived Ba contribution. By comparison, the Ba/Nb ratio of the bulk continental crust is ~23 and of the average shale ~34 (Taylor and McLennan 1985); ratios for continental rhyolites range down to <1, and our (unpublished) Ba/Ta data (95–725) for 20 SVZ rhyolites suggest a Ba/Nb range of ~6 to ~48. As is implicit in Fig. 14, intracrustal contributions can clearly lower the Ba/Nb and Ba/Ta values of most arc basalts.

Zr and Hf. Although Zr and Hf abundances increase with SiO_2 in all suites (Fig. 13), their enrichment is relatively retarded at four of the northernmost centers (CT, CA, CM, VP), despite the absence of zircon in eruptive products other than rhyolite. Most suites appear to originate at roughly similar values of Zr/Rb and Hf/Ta in their mafic members (Figs. 15, 16), but with further differentiation the northerly suites trend toward much lower values of both ratios than do southerly ones. In marked contrast, volcanic-front centers in the thin-crust segment south of 37°S maintain nearly constant ratios throughout their evolution (e.g., PUY, VA in Figs. 15, 16). The large shifts in Zr/Rb and Hf/Ta in part reflect greater crustal contributions of alkalies and Ta to magmas that evolved in the thick crust beneath the northerly volcanoes, but most of these volcanoes also display real retardation of Zr and Hf enrichment (Fig. 13). Because all suites (north and south) are zircon-free, this retardation almost surely results from crustal addition of Zr-Hf-poor silicic-alkalic partial melts extracted from residues in which zircon remained stable.

The Hf–Zr retardation exhibited by most of the northerly centers (Figs. 13, 15, 16) shows, moreover, that the northward regional increase in Hf/Lu (Fig. 9) does not result from relative Hf enrichment but from the northward suppression of HREE enrichment (Fig. 12), attributed above to deep-crustal garnet stability. Because of the regional systematics, it seems clear that crustal zircon and garnet are the main influences on Hf and HREE behavior during differentiation. Thus, there is no need to appeal to a northward-increasing role for subducted zirconiferous terrigenous sediments as a control on the regional Hf/Lu trend; in any event, within this segment there is no evidence for nor reason to expect a significant along-trench change in the nature of the predominantly terrigenous sediment being subducted.

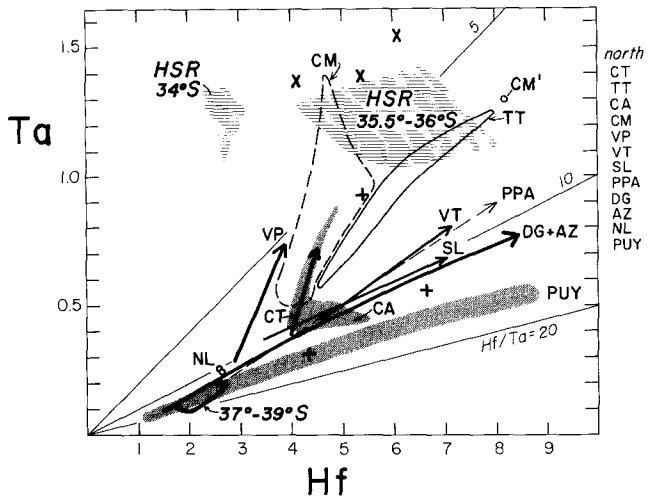

Fig. 16. Ranges of Ta and Hf concentration (ppm) for volcanic-front centers 33°–36°S. Abbreviations listed north to south as in *Table 1*. In addition, Puyehue (PUY 40.5°S) field from Gerlach et al. 1987; field of mafic lavas from Antuco, Llaima, and Villarrica (37°–39°S) from Hickey et al. 1986 (converting their Nb values to 15 Ta. CM' is a high-K sample from Marmolejo as in *Figs. 13, 15*. Fields of high-silica rhyolites (HSR) from indicated latitudes as in *Fig. 15*. Partially melted granitoid xenolithic ejecta: (+) from Cerro Azul; (×) from Tupungatito

The double trends in HFSE shown by the Cerro Alto (CA) suite and the lesser retardation of Zr and Hf in the very northerly Tupungatito (TT) suite (Figs. 13–16) further illustrate the surprisingly wide geochemical variability among neighboring andesite-dacite volcanoes; such contrasts are more likely to reflect variable contributions from thick heterogeneous crust (variably rich in accessory minerals) than drastic variations in mantle or slab contributions on so local a scale. Marmolejo (CM) and nearby Tupungatito (TT) are both relatively enriched in Ta, but in Zr and Hf Marmolejo is retarded and Tupungatito is not (Figs. 13, 16). Relative to the southerly Puyehue suite (Fig. 13), nearly all centers on thick northern crust are Ta-enriched, but in Hf and Zr only Tinguiririca and Tupungatito are unequivocally so. Absence of any clear linkage between Zr–Hf and Nb–Ta behavior weighs heavily in favor of crustal processes rather than HFSE control by OIB-style mantle enrichments.

Additional geochemical evidence favoring major crustal influence is given by the array of Zr/Hf values, which along the SVZ volcanic front range from 35 to 55, exhibiting no latitudinal systematics. Some centers individually show wide ranges, 35–46 at both Marmolejo and Puyehue, 38–55 at Cerro Azul, and 35–43 at Tinguiririca, compared to 39 ± 5 for both MORB and OIB (Gill 1981). Since zircon has higher Zr/Hf than coexisting liquid, its fractionation or its survival in crustal residues would lower magmatic Zr/Hf values (e.g., commonly 25–35 in rhyolites), whereas its dissolution or entrainment from a crustal assimilant would normally raise the ratio of the assimilating magma. Therefore, mixing with low-Zr rhyolitic melts extracted from zircon-retaining crustal material and, alternatively, bulk assimilation of zircon-rich plutonic rocks together bracket a spectrum of crustal interactions that could either reduce or elevate the Zr/Hf ratio (and Zr and Hf contents) of a basalt or andesite that had never itself crystallized zircon. The wide ranges in Zr/Hf within and among volcanoes in the SVZ apparently require such zircon controls and, because zircon is very unlikely to be present in wedge peridotite or in basaltic magma (Watson and Harrison 1983), those controls must be dominantly intracrustal.

K/Hf and Rb/Zr. Both of these ratios are larger at northern centers than in the south (Fig. 15), reflecting the lower rates of Hf and Zr enrichment in the north as well as the greater rates of alkali enrichment. K/Hf is generally 2500–3500 at Llaima (38.7°S) and Puyehue (40.5°S) (Hickey et al. 1986; Gerlach et al. 1987), 3000–4500 at Cerro Azul (35.5°S) and Tinguiririca (34.8°S), and 4000–5500 at the four northernmost centers. Comparable latitudinal shifts in Rb/Zr are shown in Figure 15. In most suites north of 36°S, both ratios increase with differentiation, but the general along-arc shift in trends is unequivocal (Fig. 15). Tatsumi and Nakano (1984) explained an across-arc increase of K/Hf in northeastern Japan in terms of lesser degrees of wedge melting behind the front, release of a K-richer fluid from deeper parts of the slab, and to Hf buffering by zircon or Ti-rich accessory minerals residual to wedge melting. In central Chile, however, we see even larger variations in K/Hf, K/Zr, and Rb/Zr *along* the volcanic front at essentially constant slab depth, with no evidence or need to evoke large subcrustal variations in the LIL or HFSE contents of primitive basalts.

Th and U. Concentrations of Th and U are much higher in these continental arc suites than in intraoceanic island arcs (Gill 1981). Values of $Th_{57.5}$ range from 3 to 14 (Fig. 9) and are clearly greater north of 36°S than farther south along the front. There is great local variability, even along the volcanic front, with adjacent volcanoes showing two-fold differences in contents of both U and Th. Th/U ratios of analyzed samples range between 2.9 and 4.9 and average values of suites from 3.3 to 4.2, showing no systematic correlation with latitude, alkali contents, or SiO_2. The Tinguiririca center at 34.8°S represents the volcanic-front suite richest in alkalies (Figs. 2, 3, 9) and in Zr and Hf (Fig. 13), as well as in U and Th (Fig. 9); its low Nb–Ta abundances and high Th/Ta ratios, however, weigh against those enrichments resulting from a large OIB-type contribution and in favor of the suite reflecting especially strong crustal influence.

Nb/U ratios. The ratio Nb/U is 47 ± 10 in both MORB and OIB as well as in their sources (Hofmann et al. 1986), whereas the continental crustal average is estimated to be near 12 (Taylor and McLennan 1985). Values for Chilean volcanic-front lavas (including $15 \times$ Ta/U ratios) fall in the range 2–10, the most mafic rocks giving 6–10. There is no latitudinally systematic pattern, but even the most magnesian basalts (6–7% MgO) exhibit crustal Nb/U values. Although far outside the range of mantle values, the low Nb/U ratios do not in themselves distinguish between control by subducted vis-à-vis intracrustal contributions. They do, however, weigh heavily against a major OIB-like mantle-derived contribution having high values of Nb and Nb/U.

As intraoceanic-arc suites have similarly low Nb/U ranges (3–10), the low ratios are apparently linked to subduction-related processes, and the question becomes whether a low-Nb/U slab contribution is proximate or is scavenged from an arc-crustal reservoir secularly accumulated. The regional distribution of Rb/Cs, Ba/La, Hf/Lu,

$^{87}Sr/^{86}Sr$, and $^{143}Nd/^{144}Nd$ values already presented, and the much higher Nb and U (and Ta and Th) abundances here, relative to intraoceanic island arcs, all weigh in favor of intracrustal control of the exceptionally low Nb/U and (Ta/Th) ratios.

Summary and discussion

The evidence presented suggests that much of the geochemical and isotopic variation along the Quaternary volcanic front of the SVZ results from extensive blending of subcrustal and deep-crustal magmas at or near the mantle-crust transition. Higher-level AFC processes can subsequently modify ascending magmas, but the base-level geochemical signature of each center is established within zones of melting, assimilation, storage, and homogenization (MASH) near the base of the crust. Each base-level signature is controlled principally by the mixing proportions of deep-crustal and subcrustal components, the average age and composition of the lower-crustal source rocks, and the depth at which the MASH process takes place. The evidence and lines of reasoning leading to such a model can be summarized as follows.

Lower plate

Although we affirm the importance of a slab component, there is no justification for attributing the chemical and isotopic *differences* along the volcanic front to variation in proximate slab-derived contributions or to variation in processes and $P-T$ conditions in the subducting plate. Plate convergence rate, arc-trench separation, dip of the inclined seismic zone, its depth beneath the volcanic front, age of subducting lithosphere, seafloor topography, trench-axis depth, thickness and proportions of pelagic sediments and axial turbidites, and the lack of an accretionary prism at the continental margin are factors that are virtually constant along the segment under study. The linearity and trench-parallelism of the volcanic front itself provide the best evidence that plate convergence somehow initiates arc magmatism, possibly by depth-influenced dehydration of the slab and/or by systematic convection induced in the mantle wedge. Constant subduction geometry and lower-plate composition, however, require that the large, latitudinally systematic changes in magmatic chemistry along the front originate in the overriding plate. A water-rich slab contribution may well initiate mantle melting, but its mass must be overwhelmed by basaltic magma production in the peridotite wedge and the geochemical signature of that magma (probably similar to intraoceanic arc tholeiite) must be overprinted in MASH zones at the mantle-crust transition.

Subducted sediments

There is no doubt that sediments have been subducted in enormous volumes beneath the entire arc segment, but there is no indication that they possess either the isotopic leverage or the latitudinal variability to control the large chemical and isotopic differences along the volcanic front. The along-arc variations of Ba, Cs, and $^{207}Pb/^{204}Pb$ (Figs. 7, 9), which are widely cited as key indicators of a subducted sedimentary component in arc magmas, instead favor intracrustal control. Many of the centers studied have higher $^{207}Pb/^{204}Pb$ than the known range of Nazca plate sediments (Fig. 7); the northward decline of Ba/La and rise of Rb/Cs are specifically antithetic to trends that would be predicted for control of the along-arc isotopic and alkalinity variations by slab-derived contributions. It is geologically unreasonable to attribute latitudinally systematic Sr- and Pb-isotopic leverage to subducted sediments that show little ostensible variation along the segment; moreover, the along-arc gradient in $^{143}Nd/^{144}Nd$ (Fig. 5) provides strong support for intracrustal control of the isotopic variations in all three elements. The best evidence for a large sedimentary contribution may be the low Rb/Cs values of several centers south of 36°S (Hickey et al. 1986), where the intracrustal overprint is apparently smaller or includes alkalies remobilized from post-Triassic Andean arc-plutonic rocks.

Mantle contribution

The along-arc isotopic and chemical changes cannot reasonably be attributed to the mantle wedge, no matter how materially dominant wedge contributions may be in the total arc-magmatic budget. The *convecting* mantle is expected to be sufficiently well mixed on a regional scale (Hoffman and McKenzie 1985) that it is unlikely to yield magmas having so wide a range of Sr and Nd isotopic ratios, let alone to distribute such magmas systematically along a volcanic front. On the other hand, there is no justification for postulating an along-arc regional contrast in degree of enrichment of the *lithospheric* mantle. Since *some* Paleozoic crust (thick or thin) is thought to underlie the entire segment (Fig. 1), there is no reason to expect older or more enriched lithosphere beneath the part of that crust compressively thickened in Neogene time. Moreover, because the crust and mantle beneath the modern arc have undergone many episodes of magmatism during Cenozoic, Mesozoic, and Permian time, sustained integrity of mantle lithosphere isotopically "aged" enough to yield the large spread of Nd and Sr isotope values is beyond all expectation. Any post-Paleozoic fluid or magmatic enrichment of the sub-arc mantle is likely to have been related to Andean arc magmatism itself, thus providing neither latitudinal variation nor any special isotopic leverage. Indeed, the persistence of Andean magmatism throughout much of Cenozoic time here casts doubt on the very existence of mantle lithosphere beneath the front; it could be that much of the sub-arc wedge has become incipiently molten and is now entirely convective. Finally, complementary to the thicker crust, the mantle wedge thins northward along the segment, from 50–60 km in the south to only ~30 km beneath the northerly volcanoes having the most "enriched" eruptive products. Attributing the more "crustal" compositions northward to the thinner mantle instead of the thicker crust calls for very special pleading indeed.

"OIB" has become a catchword loosely applied to a wide spectrum of relatively HFSE-rich mafic lavas ranging from E-MORB to nephelinite and variously attributed to enriched mantle sources either deep and primitive, or convectively scattered, or lithospherically stabilized beneath continents. The evidence is insufficient to know if convecting sub-arc mantle beneath Chile contains a patchwork of enriched streaks and blobs similar to the postulated sources of some OIB. Existence of variably enriched lithosphere east of the front is indeed suggested by marked west-to-east decreases in the Ba/Nb and Ba/La values of lavas (Hickey

et al. 1986; Kay and Rapela 1986) and by the co-eruption of depleted, fertile, and veined ultramafic xenoliths in Patagonian alkali basalts (Stern et al. 1986). The lack of any similarly convincing eruptive or compositional evidence for enriched reservoirs beneath the volcanic front of the SVZ suggests that contributions from enriched material (if present there at all) are overwhelmed by extensive wedge melting of more depleted host peridotite, by the large flux of slab-derived material, and by mixing with crustal components in MASH zones. Specifically, the consistently low Ti–Nb–Ta contents, the very low Nb/U and Ta/Th values, the restricted range of Pb-isotope ratios, and the lack of latitudinal coherence in LIL, Zr–Hf, and Nb–Ta enrichments weigh heavily against OIB-like contributions having a significant influence on the large compositional variations seen along the Chilean volcanic front.

Continental crust

In contrast to the difficulties with subcrustal scenarios, the latitudinal chemical and isotopic changes along the arc can readily be explained if the magmas contain significant contributions derived from the continental crust. The elevated K, Rb, Cs, Ba, Th, and LREE values of the northerly centers are just what one would predict for a northward increase in crustal components. Although complicated by plagioclase fractionation, the high Sr content (600–900 ppm) of andesites at northern centers (Table 2) probably also reflects partial melting of plagioclase-rich crustal rocks; many unusually Sr-rich andesitic suites elsewhere are likewise associated with thick continental crust. The more radiogenic Sr and less radiogenic Nd (Fig. 5) reflect not only larger crustal contributions but also the greater *average* age of the thicker northern crust. The increasing SiO_2 mode, decreasing representation of basalt and mafic andesite, and the greater "calc-alkalinity" (Fig. 4) of centers northward along the volcanic front are all consistent with crustal interception of mantle-derived basalts and addition of crustal components. Relative to the more tholeiitic volcanoes farther south, the smaller degrees and rates of Fe enrichment of all centers constructed on the thick northern crust can be explained by early large-scale assimilation of silicic-alkalic partial melts, mostly in the deep crust. If such assimilants were also relatively oxidized and hydrous, they would promote early precipitation of titanomagnetite or amphibole, thereby reconciling assimilation and fractionation hypotheses for suppression of Fe enrichment in calcalkaline suites.

Additionally indicative of crustal contributions are the surprisingly large compositional contrasts among suites from neighboring northerly volcanoes and the wide compositional ranges within some of them – e.g., in silica-normalized concentrations of alkalies, Ba, and HFSE, in Sr-isotope ratios, and in the values of K/Rb, Rb/Cs, Ba/La, Ba/Ta, Hf/Ta, and Zr/Rb (Figs. 2, 5, 9–16). Extensive variability among and within nearby centers (pronounced on thick crust but minimal on thin crust) is much more likely to reflect variable interactions of subcrustal magmas with heterogeneous continental crust than any markedly different mantle or slab contributions on so local a scale.

Relative to the compositionally rather similar volcanic-front suites farther south (Figs. 2, 5, 7, 8, 9; Déruelle 1982; Lopez-Escobar 1984), most of the isotopic and chemical changes we have documented start near 36°S (Figs. 2, 5, 9), but many of them become pronounced only north of 34.5°S (Figs. 5, 6, 10, 12). These two latitudes are the apparent limits of the transition in crustal thickness, as suggested by the elevation and gravity gradients in Fig. 2; northward across this transition is just where HREE suppression (Fig. 12) becomes conspicuous, evidently reflecting melt contributions from lower-crustal rocks at depths great enough for garnet to be an important residual phase. At the geophysically inferred segment boundary near 37°S, on the other hand, there is little geochemical change along the front except in SiO_2 mode and no significant change in basement geology or crustal thickness. Regional relationships thus independently support the geochemical evidence that the continental crust does, and the subducted plate does not, strongly influence along-arc magmatic variability.

Lower crust vs upper crust

Assimilation of crustal components is expected anywhere that basaltic magma is stalled or stored in the crust, but for most systems studied here the data suggest that little of the crustal contribution comes from the *upper* crust. The $^{87}Sr/^{86}Sr$ ratios of the Quaternary magmas (mostly <0.705) contrast sharply with the high ratios of Paleozoic sedimentary and igneous rocks (0.725–0.77; Table 2) that strike under the northern volcanoes, suggesting that shallow assimilation was limited, except perhaps at Marmolejo (Fig. 6). Similarly, reconnaissance $\delta^{18}O$ determinations for plagioclase separates from a selection of basaltic to rhyodacitic rocks representing nine of the volcanic-front centers (including the four northernmost) fall within the range +5.5 to +7.0 (Hildreth, unpubl. data), suggesting little assimilation of ^{18}O-rich upper-crustal rocks. Large northward increases in Ce/Yb, Rb/Cs, and Hf/Lu (Fig. 9) suggest that much of the crustal contribution at northern centers originates at great depth in the thick crust, where garnet is stable, where average composition is mafic to intermediate, and where Cs had been depleted relative to other alkalies during previous episodes of magma or fluid extraction. In the flat-slab segment just north of the study area (Fig. 1), progressive shifts toward lower HREE contents, steeper REE patterns, and increased deep-crustal melting and assimilation are key aspects of successive episodes of Miocene magmatism associated with compressive thickening of the crust during the shallowing of subduction (Kay et al. 1987); the increasing influence of garnetiferous deep crust seen there as a trend in time (28 to 6 m.y. ago) is analogous to that in space seen today in the SVZ.

The high Sr and Ba contents of mafic and intermediate rocks at several northerly centers (Figs. 6, 9) also favor large contributions from the lower crust, many gabbroic, anorthositic, and mafic granulitic components of which are rich in these elements (Arculus and Johnson 1981). It is sometimes asserted that crustal assimilation cannot enrich mantle-derived magmas in Sr, an overgeneralized inference presumably based on typical *upper*-crustal contamination relationships (as in Fig. 6). Many lower-crustal mafic granulites, however, are greatly enriched in Sr (and in Ba), values of 700–1800 ppm Sr being fairly common (Tarney and Windley 1977; Rogers and Hawkesworth 1982; McCulloch et al. 1987). It is easy to illustrate generation of high-Sr crustal melts by assuming modal batch melting of such rocks, here assigned modal ranges of 40–60% plagioclase, 25–35% cpx, and 15–25% phases in which Sr is

more incompatible (opx, garnet, oxides, or olivine). If extracted melts are broadly andesitic, then partition coefficients tabulated by Arth (1976) and Gill (1981) yield bulk D_{Sr} values in the range of 0.75 to 1.1, which in turn give ratios of Sr concentration in the liquid to that in the initial rock (Sr^{liq}/Sr_o) in the range 0.9–1.3 for 10–50% melting. If extracted batches are more silicic and D_{Sr} data for dacitic to rhyodacitic liquids apply ($D_{Sr}^{plag} \sim 2.8$–3.5), then bulk D_{Sr} values of 1.2–2.1 yield Sr^{liq}/Sr_o ratios of 0.5–0.85 for 10% melts and 0.65–0.95 for 50% melts. Partial melting of rocks poorer (than 40–60%) in plagioclase or melting of plagioclase in greater than its modal proportion would further increase Sr^{liq}/Sr_o. Accordingly, it is quite reasonable for Sr-rich lower-crustal rocks to yield melt contributions having 600–1000 ppm Sr, well above the abundance range of most arc basalts.

The tendency for northern SVZ suites to have elevated values of *both* Sr and $^{87}Sr/^{86}Sr$ almost certainly reflects such deep-crustal contributions. This can be contrasted with the negative correlations between Sr and $^{87}Sr/^{86}Sr$ that reflect AFC processes involving more radiogenic mid- and upper-crustal wall rocks (CM in Fig. 6; Francis et al. 1980). Such processes are especially characteristic of large-volume systems having complex intracrustal reservoirs or large magma chambers. On the other hand, intrasuite trends that show little or no systematic increase of $^{87}Sr/^{86}Sr$ with rising SiO_2 and declining Sr can signify various processes: (1) closed-system fractionation, which is probably rare for mafic magma in the crust; (2) deep-crustal MASH *prior* to intrasuite fractionation, entailing little or no (or unsystematic) upper-crustal assimilation during subsequent ascent of small batches – typical of andesite-dacite volcanoes (e.g., Hawkesworth et al. 1982); (3) AFC processes that involve assimilants having little isotopic contrast with the magma, rendering ambiguous the distinction between upper- and lower-crustal contributions (e.g., AZ in Fig. 6; Davidson et al. 1987).

Prior to the Miocene crustal thickening, olivine-pyroxene-oxide fractionation of arc basalt near the base of a 35-km crust would have concentrated Sr (and Ba and Pb) in gabbroic, anorthositic, dioritic, and tonalitic differentiates, but after the thickening many such rocks would transform into garnet-granulite and pyroxene-granulite. Later partial melting at 50–60 km depth would probably leave plagioclase-diminished residues of pyroxenes + garnet + plagioclase + oxides ± zircon, promoting in the extracted magmas (1) elevated values of Sr, Ba, and Pb, (2) lowered TiO_2 contents, and (3) steepened REE patterns. Whether Zr, Hf, Nb, or Ta are enriched or depleted by any particular instance of lower (or upper) crustal melting and/or assimilation is likely to depend sensitively upon the accessory mineralogy of wall-rock residues.

If *upper*-crustal AFC processes subsequently become important (as at Marmolejo), Sr contents drop (Fig. 6), negative Eu anomalies develop, and Ba enrichment can be variably retarded (Figs. 9, 10). Additional contributions of alkalies, Th, U, and Pb from middle- and upper-crustal rocks and fluids are likely during magma ascent, especially if ascent takes place by dike propagation in slightly molten percolation columns beneath long-lived eruptive centers (Hildreth 1981). The regional Rb/Cs relationship (Fig. 9), however, favors predominantly deep-crustal alkali control. The scarcity of rhyolites, ring-fracture calderas, well-defined AFC trends, or stable-isotope evidence for shallow assimilation suggests a corresponding scarcity of large upper-crustal magma chambers beneath the volcanic front. Finally, if contamination by heterogeneous granitoid-rich upper crust were the dominant mechanism of introducing crustal components into the magmas, we should expect much wider ranges in $^{87}Sr/^{86}Sr$ and $^{143}Nd/^{144}Nd$ and less coherent incompatible-element variation trends at each volcano; Marmolejo and (on many plots) Cerro Alto illustrate the scattered exceptions that prove the lower-crustal rule.

Arc crust as a slab-signature repository

Abundances of K, Rb, Cs, Sr, Ba, Pb, U, Th, LREE and HFSE are all *much* greater (at equivalent SiO_2) in the Andean suites studied here than in most rocks from intraoceanic island arcs. In spite of this, the Andean and island-arc suites show partial or extensive overlap in many key *ratios* of these elements, including Ba/La, Ba/Ta, and La/Ta, which provide the clearest geochemical discrimination of subduction-related igneous suites vis-à-vis MORB and OIB. A comprehensive explanation of these differences and similarities requires evaluation of at least three contributing factors: (1) the extent of original (pre-arc) depletion of the mantle wedge, probably MORB-source or MORB-residue peridotite beneath most arcs; (2) the nature of the subducted component added to the wedge, both as the proximate slab contribution to magma genesis on the 10^3-to-10^6-year time scales of individual magmatic centers and as a longer-term secularly stored additive; and (3) secular storage of wedge-derived magma in the arc crust. The last factor may be crucial for the geochemistry of mature arcs, as relative volumes of arc-volcanic, arc-plutonic, and deep-crustal metaigneous rocks point to (very uncertain) intrusive/extrusive ratios in the range 3–15; in general, the intrusive fraction is expected to increase with crustal thickness, intracrustal differentiation, and arc longevity.

Crustal maturation is important not only because the total intracrustal intrusive mass grows with time but because repeated intracrustal partial melting augments the primary fractionation of each new basaltic batch in yielding a plexus of differentiated plutons, pods, dikes, and veins that inevitably dominate subsequent assimilation. Although the subcrustal (wedge + slab) input to the arc crust may always be basaltic, its thermal contribution persistently induces extraction of deep-crustal intermediate-to-silicic melt segregations, which can either mix directly with fractionating basalts or temporarily resolidify within the deep (or shallower) crust. Such segregations will generally retain an arc signature (unless a non-arc basement terrane is also an important contributor), and with time that signature can evolve and influence arc compositions in the following ways.

(1) LREE are preferentially partitioned into the intermediate-to-felsic differentiates, progressively raising La/Yb in the rocks most susceptible to assimilation by subsequent basalts. In unusually thick crust, deep-crustal garnet further enhances the relative HREE retention. Few intraoceanic arcs have yet accumulated a crustal repository adequate to overprint the characteristically flat (or even positive) REE patterns of basalts generated in a depleted mantle wedge. Furthermore, the extremely low REE contents and flat patterns of some island-arc lavas indicate that the slab contribution of REE is trivial, and that the original degree of wedge depletion remains the main control until the arc-

crustal reservoir has matured sufficiently to dominate the REE budget.

(2) The low Zr, Hf, Nb, and Ta contents of intraoceanic-arc basalts suggest that slab contributions of these elements are trivial as well. Moreover, the *high* La/Ta ratios of many island-arc basalts having very low LREE abundances points to strongly depleted (MORB-residue?) peridotite as the wedge source. Secular subduction-related re-enrichment of wedge peridotite is not likely to raise La/Ta (LREE/HFSE) substantially in derivative basalts, but contributions from a mature arc-crustal repository would surely do so. As nearly all crustal differentiates have elevated HFSE *and* LREE abundances relative to wedge-derived basalts, their assimilation would normally enrich the hybrids in *both* groups of elements, as observed for continental arc suites in general. The crustal contributions, however, would tend to have diverse LREE/HFSE ratios owing to variable retention of residual zircon, ilmenite, and rutile. Accordingly, values of La/Ta (25–85) in the Chilean basalts and andesites show not only a wide range but wholesale overlap with values for island arcs (20–110).

(3) Because of the intracrustal retention of zircon and oxide minerals, HFSE are expected to be partitioned less efficiently than alkalies into the repository fractions most susceptible to assimilation, thereby raising ratios such as Rb/Zr in affected magmas. This would account for the generally high values of Rb/Zr in the Chilean suites (0.2–0.55; Fig. 15), especially at northern centers, compared to most intraoceanic-arc lavas (mostly 0.05–0.35).

(4) Although Zr, Hf, Nb, and Ta are all greatly enriched in the Chilean suites relative to island-arc lavas, ratios such as Zr/Nb (20–60) and Hf/Ta (4–20) overlap extensively, providing yet another indication that there is no need to evoke a low-Zr/Nb (3–15) OIB-type contribution. The tendency toward lower Zr/Nb and Hf/Ta (Fig. 16) at northerly SVZ centers probably reflects greater effectiveness of intracrustal zircon retention in the thick crust. Quite variable HFSE behavior can reasonably be expected during different intracrustal assimilation and/or mixing episodes, depending upon the extent to which zircon and oxide minerals were entrained, dissolved, or left behind in various residues of heterogeneous crustal rocks.

(5) Values of $\delta^{18}O$ would show only small increases (generally <0.5 permil) owing to deep-crustal igneous fractionation and would seldom exceed $+7.0$ unless metasedimentary or upper-crustal granitic rocks were assimilated.

(6) Radiogenic isotope ratios are expected to change only modestly in the lower-crustal repository, owing to the limited lifespans of arcs and to the much shorter residence times of the successive generations of fractionated segregations susceptible to assimilation by incoming basalts. Both secular accumulation of slab-derived Sr in the arc crust and intracrustal ^{87}Rb decay, however, are likely to contribute to the general contrast between $^{87}Sr/^{86}Sr$ ranges of intraoceanic arcs (mostly 0.7030–0.7040, overlapping MORB) and of crustally mature arcs like the SVZ, where ratios are commonly 0.7037 to >0.705. Of course, in the special cases where arcs overlie ancient crust (e.g., southern Peru) or are influenced by shield-derived sediments (e.g., southern Antilles, Banda), the modest isotopic signature of a self-generated arc repository can itself be overprinted.

(7) High LILE contents (relative to HFSE and LREE) most clearly distinguish the geochemical signature of arc basalts from that of MORB. Among arc suites, however, island arcs typically show higher ranges of LILE/HFSE and LILE/LREE than continental arcs like the SVZ. Ba/La ratios, for example, are 17–35 in the SVZ but range from 20 to >90 in island-arc suites; and Ba/Ta is 400–2000 in the SVZ but commonly 1500 to >3000 in island arcs. Similarly, the respective ranges for Ba/Th are 30–190 and 120–650. The differences are readily explained in terms of a secular evolution from (a) an early arc stage when the arc signature is controlled by a high-LILE/(LREE + HFSE) slab contribution, a MORB-like wedge contribution depleted in all three groups, and little or no arc-crustal repository, toward (b) a mature arc stage when the main influence is no longer the proximate slab-derived flux but rather the partial remobilization of the secularly accumulated arc-intrusive repository, from which larger HFSE, Th, and LREE contributions are available.

MASH hypothesis

The data lead us to envisage deep beneath each large magmatic center a zone of melting, assimilation, storage, and homogenization (MASH), in the lowermost crust or mantle-crust transition, where basaltic magmas that ascend from the mantle wedge become neutrally buoyant, induce local melting, assimilate and mix extensively, and either crystallize completely or fractionate to the degree necessary to re-establish buoyant ascent. Magmas ascending from such zones may range from evolved basalts to dacites, but all will have acquired a base-level isotopic and trace-element signature characteristic of that particular MASH domain. The values defining such a signature usually remain fairly restricted throughout the lifetime of an eruptive center, and they constitute starting points for subsequent fractionation and AFC arrays for each system. Real constancy in base-level values would require consistent homogenization prior to resumed ascent and would suggest that the mixing proportions of crustal and mantle melts, the mineral assemblages residual to crustal melting, and probably therefore the depth of the MASH zone all remain more or less fixed. Beneath a large long-lived center, however, one can imagine gradual depletion of the crustal material available (leading, for example, to a decline in base-level $^{87}Sr/^{86}Sr$ values); or just the opposite in the case of an expanding MASH zone.

By the MASH process we mean not simple contamination of basalts in the lower crust but true magma generation there (thermally induced by intrusion and crystallization of basalt) on a scale large enough that *tens* of percent of subsequently ascending mixtures can be of deep-crustal derivation. We imagine a variety of basaltic magmas arising from the mantle wedge, stalling at the crust-mantle transition, and mixing with each other as well as with the array of magmas derived from the induced partial melting of heterogeneous deep-crustal rocks.

Physically, the MASH zone is likely to be a plexus of dikes, sills, pods, small chambers, and mushy differentiated intrusions. The distinction between mixing of magmas and ductile mixing of partially molten rocks may blur, as thermal pulses associated with recurrent injections of basalt promote partial remelting of crystallizing intrusions and as deformation promotes extraction and aggregation of interstitial melts, blending them with batches of variably fractionated basalt. The distinction between crust and mantle can also blur in such a zone, as differentiating intrusions

crystallize within peridotitic wall rocks, ultramafic cumulates amass in lower-crustal magma chambers, and granulite-facies recrystallization and ductile deformation lead to complex interlayering. A crust-mantle transition zone many km thick may develop, veined, dike-ridden, and heterogeneous on a small scale (e.g., Griffin and O'Reilly 1986).

During periods of constant subduction geometry and long-term stability of the volcanic front, as in the Quaternary SVZ, impenetrable MASH zones beneath the major centers apparently operate continuously as effective interceptors, heat exchangers, and blenders. Where intra-arc, arc-adjacent, or back-arc upper-plate extension is superimposed on the convergence regime, however, a wide range of alkalic to low-K-tholeiitic basalts can rise from various mantle sources uninterruptedly enough to avoid modification by the MASH processes. Such evasion is unknown beneath the volcanic front of the SVZ, but it evidently takes place not far behind the front in Argentina (Muñoz and Stern 1985; Llambias et al. 1982). Moreover, eruptions of such "non-arc" basalts have been closely associated with normal arc volcanism in parts of the Mexican, Central American, Indonesian, and Cascades arcs tectonically more complex than the SVZ. If this widespread evidence for heterogeneous sub-arc mantle sources can be generalized, then the lack of both "non-arc" basalts and primitive arc basalts on the volcanic front could be invoked as evidence for suppression of the mantle-derived diversity by MASH-zone modulation. Not a single primitive basalt (having high enough Mg, Ni, and Cr for equilibration with peridotite) is known to us in Chile, and their remarkable scarcity in arc settings worldwide has been emphasized by Nye and Reid (1986). It might be that intrinsically lower basalt diversity results in part from high supply rates and associated large degrees of wedge melting beneath volcanic fronts, but the absence of primitive compositions favors MASH as an overriding influence. Lower-crustal MASH zones are thought to form beneath large centers elsewhere, wherever the basaltic flux is persistent and focussed, but they may be the norm below volcanic fronts because of the long-lived subduction-controlled concentration of the basaltic flux upon a relatively narrow linear strip of the sub-arc crust. Persistent focussing promotes thermal and mechanical feedback between entrapment of basalt, enhancement of lower-crustal ductility and melting, and maintenance of a buoyancy barrier (Hildreth 1981).

MASH in the SVZ: North vs south. We know of no evidence that the integrated slab-plus-mantle contribution to the MASH process differs significantly in composition along the segment. Because the constant depth of the Benioff zone implies that the mantle wedge thins northward beneath the thickening crust, it is conceivable that the subcrustal magma supply rate also diminishes northward, but no systematic change in either eruption rate or edifice size is evident along the volcanic front. The isotopic and chemical changes along the front must therefore largely reflect different MASH-zone contributions from the lower continental crust, which changes latitudinally in depth, average age, presumably in mineralogy, and less certainly in bulk composition.

Identification of the deep-crustal rocks contributing to MASH processes in the northern SVZ is constrained as follows. (1) Ancient U-depleted granulitic crust comparable to the exposed Proterozoic basement of southern Peru (Tilton and Barreiro 1980) is clearly not involved, because of the limited variability in Pb-isotope ratios (Figs. 7, 8) and lack of evidence for significant involvement of a low-$^{206}Pb/^{204}Pb$ component. (2) Deep-crustal contributions cannot come directly from partial melting of ultramafic rocks or little-fractionated gabbros, as their low Sr contents would fail to provide sufficient leverage to attain the high Sr and moderate $^{87}Sr/^{86}Sr$ values of the Quaternary volcanic rocks. Since high Sr contents are required (Fig. 6), the observed $^{87}Sr/^{86}Sr$ values indicate that the lower-crustal rocks were not strongly depleted in Rb. (3) They are unlikely to be granitic (s.s.), again owing to the high Sr requirements and because high-Rb/Sr contributors would tend to raise $^{87}Sr/^{86}Sr$ well above the base-level values observed (as in the case of the Marmolejo array in Fig. 6). (4) On average, they must be LREE-enriched (low Sm/Nd) and must include some rocks old enough to have evolved ranges of $^{143}Nd/^{144}Nd$ and $^{87}Sr/^{86}Sr$ capable of levering in basaltic and andesitic magmas the regional isotopic shifts illustrated in Fig. 5. This is consistent with geologic evidence for Paleozoic (but not older) crust in this part of South America (Caminos et al. 1982). (5) $\delta^{18}O$ values between +5.5 and +7.0 imply that metasedimentary contributions are limited or absent. (6) Consistently low HREE and high Ce/Yb in northerly suites (Fig. 12) apparently require abundant residual garnet, supporting other inferences for fairly mafic average compositions and extraordinary crustal depths.

The deep-crustal picture that emerges for the SVZ is one of Paleozoic and Triassic mafic to intermediate metaplutonic rocks (permissibly including remnants of older oceanic lithosphere and metagreywacke), partially remelted, migmatized, and pervasively intruded by 200 Ma worth of Andean arc-plutonic rocks. The latter are basaltic in bulk composition but fractionated to suites of contaminated gabbro-diorite-tonalite (with ultramafic and anorthositic cumulates) that have themselves subsequently undergone repeated remelting, migmatization, and granulite-facies recrystallization. Although such intrusion and basal magmatic accretion are intrinsically crust-thickening processes, in the northern 200 km of the SVZ (and in much of the Andes farther north) the crust has additionally undergone drastic tectonic thickening during late Cenozoic time by some combination of upper-crustal overthrusting, mega-underthrusting of the (Paleozoic) Argentine basement, and presumably ductile deep-crustal compression. In the north, therefore, during and since the Miocene, the lower-crustal suites just mentioned have been depressed from depths of ~30 km to 50–60 km and presumably tectonized and recrystallized in the garnet-granulite facies. The relative recency of this depression is consistent with the apparent lack of severe Rb and U depletion in lower-crustal rocks now at great depth and temperature.

The deep-crustal magma contribution in the northern SVZ is thus likely to be derived in unknown but variable proportions from (1) late Cenozoic arc-intrusive rocks emplaced at 50–60 km, (2) Jurassic-to-Paleogene arc-intrusive rocks originally emplaced at 30–40 km, and (3) heterogeneous pre-Andean continental basement of late Paleozoic and Triassic age. Partial assimilation of such rocks and mixing of silicic partial melts extracted from them into new batches of basalt stalled and stored in MASH zones at 50–60 km (and itself fractionating garnet and clinopyroxene) are thought to be the main processes yielding the base-level magmas of the northern SVZ (and CVZ), which are characteristically rich in Sr and Ba, poor in HREE, and

have moderately crustal (but not upper-crustal) ratios of Sr and Nd isotopes. During subsequent crustal ascent and higher-level storage, magmas may assimilate additional alkalies, Pb, U, Th, and LREE, as well as more radiogenic Sr and less radiogenic Nd, and they may mix with rhyolitic liquids poor in Sr, Ba, Zr, and Hf that were extracted as partial melts of upper-crustal granitoid rocks. With respect to these variable overprints the length of the percolation column (crustal thickness) is significant, but the fundamental crustal geochemical signature reflects not thickness itself but the depth and average age of the lowermost crust.

The SVZ crust south of 36°S has, in contrast, not undergone such neotectonic thickening and is thought to be only 30–35 km thick, at least as far south as 41°S. Moreover, its Paleozoic crystalline basement may have been thinned during Mesozoic back-arc extension (Coira et al. 1982); also because the Quaternary arc angles obliquely SSW onto the main belt of Cenozoic and Mesozoic plutonic rocks (Drake et al. 1982), Paleozoic remnants may today comprise only a limited proportion of the sub-arc crust south of 36°S. Accordingly, most of the deep crust is likely to consist of Andean (Jurassic to Quaternary) igneous and metaigneous rocks of basaltic bulk composition. At 30–35 km, these would crystallize mostly as hornblende-bearing gabbro, ultramafic cumulates, and dioritic-to-tonalitic differentiates; depending on local H_2O concentration, they would recrystallize as amphibolite and 2-pyroxene-plagioclase granulite ($\pm$ hornblende), having little or no garnet until depths greater than about 35 km.

MASH zones formed at the base of such crust would entail partial assimilation of mafic-to-intermediate rocks having only limited contrast in isotopic or trace-element ratios with the intruding batches of new basalt. Even mid-to-upper-crustal granitoids, being relatively young and rarely very evolved, would provide little isotopic leverage; the principal evidence for crustal contamination thus lies in incompatible trace-element ratios modified by assimilation of silicic-alkalic partial melts (Davidson et al. 1987). Stressing the role of slab-originated hydration of the lower crust, Takahashi (1986) invoked a MASH-like process, involving partial remelting of hornblende-rich gabbroic and amphibolitic deep-crustal rocks by intrusion and mixing of wedge-derived basalt, to generate calc-alkaline suites of northeastern Japan (where the crust is similarly $\sim$30 km thick).

No firm evidence is available concerning the compositions of primitive basalts arriving at deep-crustal MASH zones along the SVZ, but by analogy with other arcs (Tatsumi et al. 1983; Conrad and Kay 1984; Kay and Kay 1985, 1986; Nye and Reid 1986) we believe that a range of olivine tholeiites through picrites (10–18% MgO) could be represented. MASH-zone assimilation of partial melts of the hornblende-rich lower-crustal rocks, accompanied by clinopyroxene + olivine fractionation, would yield the array of high-alumina basalts, the Mg-richest magmas erupted in the southern SVZ. MASH processes in mafic crust as young (on average) as that predicted for the southern SVZ should shift originally MORB-like isotope ratios of Sr and Nd to base-level values no more "crustal" than about 0.7037 and 0.5129, as observed.

High contents of alkalies, Ba, and H_2O, low Rb/Cs and HFSE, and elevated $^{207}Pb/^{204}Pb$ (all relative to oceanic basalts) are sufficiently general features of arc basalts to make the importance of a long-term slab contribution a compelling hypothesis. The along-arc geochemical differences documented here indicate, however, that the slab contribution need not be proximate but can be persistently reclaimed from secular storage in the arc crust.

Although the ideas expressed here developed in the course of an experiment on a single (very special) arc segment, we suspect that they have some applicability for a wider understanding of arc magmatism (and perhaps for continental flood-basalt genesis as well). Production of relatively homogeneous parental magma by hybridization of mantle-derived and crust-derived magmas, at or near the mantle-crust transition, may be a much more general phenomenon than previously recognized – above subduction zones, in continental rift zones, and beneath long-lived intraplate volcanoes. We do not dismiss mantle heterogeneity as trivial nor do we reject suggestions of a contribution from subcontinental lithosphere where evidence is compelling, but the deep-crustal MASH hypothesis accounts so well for the chemical and isotopic data in both arc and intracontinental settings that it reduces the need to postulate major contributions from grossly enriched mantle lithosphere. Quantification of the MASH process is a fundamental aim of future research, but a difficult one in view of the heterogeneous nature of the inaccessible lower continental crust.

Acknowledgements. Bob Drake and Judy Fierstein took part in most of the field studies upon which this work is based, and at various times George Cagwin, Estanislao Godoy, Anita Grunder, and Dan Tormey also contributed substantially to the remote back-country fieldwork. Reynaldo Charrier, José Corvalan, Moyra Gardeweg, Alfredo Lahsen, Leopoldo Lopez, Hugo Moreno, Francisco Munizaga, and Mario Vergara provided valuable perspectives and logistical assistance. David Gerlach generously sent us a preprint of his superbly detailed study of Puyehue, which helped focus our north-south comparisons. We are grateful to Paul Taylor for much help and discussion, to Ardith Bartel, Peggy Bruggman, Douglas Foster, Roy Goodwin, Clive Johnson, Louis Schwarz, and Joseph Taggart for skilled analytical support, and to Dorothy Johnson for meticulous manuscript preparation. Thoughtful reviews by Richard Arculus, Charles Bacon, Fred Frey, Chris Hawkesworth, Rosemary Hickey, Gail Mahood, and George Plafker improved the manuscript in form and substance. Hildreth was supported by a Grove Karl Gilbert Fellowship, granted in 1984–85 by the U.S. Geological Survey.

References

Aldrich LT, Tatel HE, Tuve MA, Wetherill GW (1958) The Earth's crust: Carnegie Inst Wash Yearbook 57:104–111

Arculus RJ, Johnson RW (1978) Criticism of generalized models for the magmatic evolution of arc-trench systems. Earth Planet Sci Lett 39:118–126

Arculus RJ, Johnson RW (1981) Island-arc magma sources: A geochemical assessment of the roles of slab-derived components and crustal contamination. Geochem J 15:109–133

Arculus RJ, Powell R (1986) Source component mixing in the regions of arc magma generation. J Geophys Res 91:5913–5926

Arth JG (1976) Behavior of trace elements during magmatic processes – A summary of theoretical models and their applications. J Research US Geol Survey 4:41–47

Bacon CR, Druitt TH (1988) Compositional evolution of the zoned calcalkaline magma chamber of Mount Mazama, Crater Lake, Oregon. Contrib Mineral Petrol 98:224–256

Barazangi M, Isacks BL (1976) Spatial distribution of earthquakes and subduction of the Nazca plate beneath South America. Geology 4:686–692

Barreiro B (1983) Pb isotopic compositions of South Sandwich Island volcanic rocks and their bearing on magma genesis in

intra-oceanic island arcs. Geochim Cosmochim Acta 47:817–822
Barreiro B, Cameron M, Cameron K, Grunder A (1982) A lead isotope study of silicic and intermediate volcanic rocks from south-central Chile and the Sierra Madre Occidental, Mexico. Carnegie Inst Wash Yearbook 81:494–498
Bevis M, Isacks BL (1984) Hypocentral trend surface analysis: Probing the geometry of Benioff zones. J Geophys Res 89:6153–6170
Caminos R (1979) Cordillera Frontal. In: Segundo Simposio de Geología Regional Argentina. Córdoba, Academia Nacional de Ciencias 1:397–453
Caminos R, Cingolani CA, Hervé F, Linares E (1982) Geochronology of the pre-Andean metamorphism and magmatism in the Andean Cordillera between latitudes 30° and 36°S. Earth-Science Reviews 18:333–352
Charrier R (1981) Geologie der Chilenischen Hauptkordillere zwischen 34° and 34°30′ südlicher Breite und ihre tektonische, magmatische, und paläogeographische Entwicklung. Berliner Geowiss Abh (A) 36:270 pp Berlin
Chase CG (1978) Plate kinematics: The Americas, East Africa, and the rest of the world. Earth Planet Sci Lett 37:355–368
Coira B, Davidson J, Mpodozis C, Ramos V (1982) Tectonic and magmatic evolution of the Andes of northern Argentina and Chile. Earth-Science Reviews 18:303–332
Conrad WK, Kay RW (1984) Ultramafic and mafic inclusions from Adak Island: Crystallization history and implications for the nature of primary magmas and crustal evolution in the Aleutian arc. J Petrology 25:88–125
Coulon C, Thorpe RS (1981) Role of continental crust in petrogenesis of orogenic volcanic associations. Tectonophysics 77:79–93
Dasch EJ (1981) Lead isotopic composition of metalliferous sediments from the Nazca plate. Geol Soc Amer Memoir 154:199–209
Davidson JP, Dungan MA, Ferguson KM, Colucci MT (1987) Crust-magma interactions and the evolution of arc magmas: The San Pedro-Pellado volcanic complex, southern Chilean Andes. Geology 15:443–446
Delpino DH, Bermudez AM (1985) Volcan Plateado. Actas del IV Congreso Geol Chileno 3:4–108 to 4–119
DePaolo DJ (1981) Trace element and isotopic effects of combined wall rock assimilation and fractional crystallization. Earth Planet Sci Lett 53:189–202
Déruelle B (1979) Pétrologie d'un volcanisme de marge active: Atacama et Andes Méridionales. Orsay, Université de Paris, XI, These, 403 p
Déruelle B (1982) Petrology of the Plio-Quaternary volcanism of the south-central and meridional Andes. J Volcanol Geotherm Res 14:77–124
Déruelle B, Harmon RS, Moorbath S (1983) Combined Sr-O isotope relationships and petrogenesis of Andean volcanics of South America. Nature 302:814–816
Diez Rodriguez A, Introcaso A (1986) Perfil transcontinental sudamericano en el paralelo 39°S. Geoacta (Buenos Aires) 13:179–201
Dragícevic M (1970) Carta Gravimétrica de los Andes meridionales e intertretación de las anomalias de gravedad de Chile central. Departamento de Geofísica y Geodesía, Universidad de Chile, Publicación No. 93
Dragícevic M, Kausel E, Lomnitz C, Meinardus H, Silva L (1961) Levantamiento gravimétrico de Chile: Anales de la Facultad de Ciencias Físicas y Matemáticas. Universidad de Chile 18:221–242
Drake RE (1976) Chronology of Cenozoic igneous and tectonic events in the central Chilean Andes – latitudes 35°30′ to 36°S. J Volcanol Geothermal Res 1:265–284
Drake RE, Vergara M, Munizaga F, Vicente JC (1982) Geochronology of Mesozoic-Cenozoic magmatism in central Chile, Lat. 31°–36°S. Earth Sci Rev 18:353–363
Ewart A, Hawkesworth CJ (1987) The Pleistocene-Recent Tonga-Kermadec arc lavas: Interpretation of new isotopic and rare earth data in terms of a depleted mantle source model. J Petrology 28:495–530
Francis PW, Thorpe RS, Moorbath S, Kretzschmar GA, Hammill M (1980) Strontium isotope evidence for crustal contamination of calc-alkaline volcanic rocks from Cerro Galan, northwest Argentina. Earth Planet Sci Lett 48:257–267
Frey FA, Gerlach DC, Hickey RL, Lopez-Escobar L, Munizaga F (1984) Petrogenesis of the Laguna del Maule volcanic complex, Chile (36°S). Contrib Mineral Petrol 88:133–149
Gardeweg M (1981) El volcanismo cenozoico superior del área del Nevado de Longaví: Una zona de transición en los Andes de Chile central. VIII Congreso Geológico Argentino, San Luis, Actas III:221–240
Gerlach DC, Frey FA, Moreno H, López-Escobar L (1987) Recent volcanics of the Puyehue-Cordon Caulle region, southern Andes, Chile (40.5°S), I. Petrogenesis of evolved lavas. J Petrology, in press
Gill JB (1981) Orogenic Andesites and Plate Tectonics. Springer, Berlin Heidelberg New York, 390 p
Gill JB (1984) Sr–Pb–Nd isotopic evidence that both MORB and OIB sources contribute to oceanic island-arc magmas in Fiji: Earth and Planetary Science Letters 68:443–458
González-Bonorino F (1971) Metamorphism of the crystalline basement of central Chile. J Petrol 12:149–176
Green TH, Pearson NJ (1986) Ti-rich accessory phase saturation in hydrous mafic-felsic compositions at high P, T. Chem Geol 54:185–201
Griffin WL, O'Reilly SY (1986) The lower crust in eastern Australia: xenolith evidence. In: Dawson JB et al. (eds) The Nature of the Lower Continental Crust. Geol Soc Spec Publ 24:363–374
Hamilton W (1979) Tectonics of the Indonesian Region. US Geol Surv Prof Paper 1078, 345 p
Harmon RS, Barreiro BA, Moorbath S, Hoefs J, Francis PW, Thorpe RS, Déruelle B, McHugh J, Viglino JA (1984) Regional O-, Sr-, and Pb-isotope relationships in late Cenozoic calc-alkaline lavas of the Andean Cordillera. J Geol Soc London 141:803–822
Hart SR (1984) A large-scale isotopic anomaly in the Southern hemisphere mantle. Nature 309:753–757
Hawkesworth CJ, Hammill M, Gledhill AR, van Calsteren P, Rogers NW (1982) Isotope and trace element evidence for late-stage intracrustal melting in the High Andes. Earth Planet Sci Lett 58:240–254
Herron EM (1981) Chile margin near lat 38°S Evidence for a genetic relationship between continental and marine geologic features or a case of curious coincidences? In: L.D. Kulm et al. (eds) Nazca Plate: Crustal Formation and Andean Convergence. Geol Soc Amer Memoir 154:755–760
Hickey RL, Frey FA, Gerlach DC, López-Escobar L (1986) Multiple sources for basaltic arc rocks from central south Chile: Trace element and isotopic evidence for contributions from subducted oceanic crust, mantle, and continental crust. J Geophys Res 91:5963–5983
Hildreth W (1981) Gradients in silicic magma chambers: Implications for lithospheric magmatism. J Geophys Res 86:10153–10192
Hildreth W, Grunder AL, Drake RE (1984) The Loma Seca Tuff and the Calabozos caldera: A major ash-flow and caldera complex in the southern Andes of central Chile. Geol Soc Amer Bull 95:45–54
Hoffman NRA, McKenzie DP (1985) The destruction of geochemical heterogeneities by differential fluid motions during mantle convection. Geophys J (RAS) 82:163–206
Hofmann AW, Jochum KP, Seufert M, White WM (1986) Nb and Pb in oceanic basalts: new constraints on mantle evolution. Earth Planet Sci Lett 79:33–45
Huang W-L, Wyllie PJ (1986) Phase relationships of gabbro–tonalite–granite–water at 15 kb with applications to differentiation and anatexis. Amer Mineral 71:301–316
Hussong DM and others (1976) Crustal structure of the Peru-Chile

trench: 8°S–12°S latitude. In: Sutton GH et al. (eds) The Geophysics of the Pacific Ocean Basin and its Margin. Amer Geophys Union, Geophysical Monograph 19:71–85
Introcaso A (1976) Modelo gravimétrico provisorio de corteza andina en el paralelo 36°S. Geoacta (Buenos Aires) 8:107–115
Introcaso A, Huerta E (1972) Perfil gravimétrico transcontinental sudamericano (paralelo 32°S). Instituto Panamericano de Geografía e Historia (Buenos Aires), Revista Cartográfica 22:133–159
Irvine TN, Baragar WRA (1981) A guide to the chemical classification of the common volcanic rocks. Can J Earth Sci 8:523–548
James DE (1971) Andean crustal and upper mantle structure. J Geophys Res 76:3264–3271
Jordan TE, Isacks BL, Allmendinger RW, Brewer JA, Ramos VA, Ando CJ (1983) Andean tectonics related to geometry of subducted Nazca plate. Geo Soc Amer Bull 94:341–361
Kausel E, Lomnitz C (1968) Tectonics of Chile: Pan-American symposium on the upper mantle, Proceedings, v. 2, p. 47–67. International Upper Mantle Symposia, No. 22-B, Mexico
Kay RW (1977) Geochemical constraints on the origin of Aleutian magmas. In Talwani M, Pittman III WC (eds) Island Arcs, Back-arc Basins, and Deep-sea Trenches. Amer Geophys Union, Maurice Ewing Series 1:229–242
Kay RW (1980) Volcanic arc magmas: Implications of a melting-mixing model for element recycling in the crust-upper mantle system. J Geol 88:497–522
Kay RW, Kay SM (1986) Petrology and chemistry of the lower continental crust: an overview. In: Dawson JB et al. (eds) The Nature of the Lower Continental Crust. Geol Soc Spec Publ 24:147–159
Kay RW, Sun SS, Lee-Hu C-N (1978) Pb and Sr isotopes in volcanic rocks from the Aleutian Islands and the Pribilof Islands, Alaska. Geochim Cosmochim Acta 42:263–273
Kay SM, Kay RW (1985) Role of crystal cumulates and the oceanic crust in the formation of the lower crust of the Aleutian arc. Geology 13:462–464
Kay SM, Maksaev V, Moscoso R, Mpodozis C, Nasi C (1987) Probing the evolving Andean lithosphere: Mid-late Tertiary Magmatism in Chile (29°–30.5°S) over the modern zone of subhorizontal subduction. J Geophys Res, in press
Kay SM, Rapela CW (1986) Mixing of arc and continental alkaline sources in the southern Andes: Geochemistry of Lower-Mid Tertiary Andean volcanic rocks (40°–42°S). Eos 67:1281
Kulm LD, Schweller WJ, Masias A (1977) A preliminary analysis of the subduction processes along the Andean continental margin, 6° to 45°S, *in* M. Talwani and W.C. Pitman III (eds) Island Arcs, Deep Sea Trenches, and Back-Arc Basins. Amer Geophys Union, Maurice Ewing Series 1:285–301
Levi B, Aguirre L (1981) Ensialic spreading-subsidence in the Mesozoic and Paleogene Andes of central Chile. J Geol Soc London 138:75–81
Llambías EJ (1966) Geología y petrografía del volcan Payún Matrú. Acta Geológica Lilloana 8:265–310
Llambías EJ, Danderfer JC, Palacios M, Brogioni N (1978) Las rocas igneas cenozóicas del Volcán Domuyo y áreas adyacentes. VII Congreso Geologico Argentino, Neuquén, Actas 2:569–584
Llambías EJ, Palacios M, Danderfer JC (1982) Las erupciones Holocenas del Volcan Tromen (Provincia del Neuquen) y su significado en un perfil transversal E–O a la latitud de 37°S. Quinto Congreso Latinoamericano de Geología, Argentina, 1982, Actas, 3:537–545
Lomnitz C (1962) On Andean structure. J Geophys Res 67:351–363
López-Escobar L (1984) Petrology and chemistry of volcanic rocks of the southern Andes. In: RS Harmon, BA Barreiro (eds) Andean Magmatism, chemical and isotopic constraints. Shiva Publ Co, Cheshire (UK) 47–71
López-Escobar L, Frey FA, Vergara M (1977) Andesites and high-alumina basalts from the central-south Chile High Andes: Geochemical evidence bearing on their petrogenesis. Contrib Mineral Petrol 63:199–228
López-Escobar L, Moreno RH, Tagiri M, Notsu K, Onuma N (1985) Geochemistry of lavas from San José volcano, Southern Andes (33°45′S). Geochem J 19:209–222
López-Escobar L, Vergara M, Frey FA (1981) Petrology and geochemistry of lavas from Antuco volcano, a basaltic volcano of the southern Andes (37°25′S). J Volcanol Geotherm Res 11:329–352
Luhr JF, Carmichael ISE (1981) The Colima Volcanic Complex, Mexico: II. Late Quaternary cinder cones. Contrib Mineral Petrol 76:127–147
Marangunic C, Moreno H, Varela J (1979) Observaciones sobre los depósitos de relleno de la depresión longitudinal de Chile entre los rios Tinguiririca y Maule. Segundo Congreso Geologicó Chileno (Arica) 3:I29–I39
McCulloch MT, Bradshaw JY, Taylor SR (1987) Sm–Nd and Rb–Sr isotopic and geochemical systematics in Phanerozoic granulites from Fiordland, southwest New Zealand. Contrib Mineral Petrol 97:183–195
McLennan SM, Taylor SR (1981) Role of subducted sediments in island-arc magmatism: Constraints from REE patterns. Earth Planet Sci Lett 54:423–430
Meijer A (1976) Pb and Sr isotopic data bearing on the origin of volcanic rocks from the Mariana island-arc system. Geol Soc Amer Bull 87:1358–1369
Menzies M, Hawkesworth CJ (1987) Mantle Metasomatism. Academic Press, London, 410 p
Minster JB, Jordan TH (1978) Present-day plate motions: J Geophys Res 83:5331–5354
Miyashiro A (1974) Volcanic rock series in island arcs and active continental margins. Amer J Science, v. 274, p. 321–355
Mordojovich KC (1974) Geology of a part of the Pacific margin of Chile. In: Burk CA, Drake CL (eds) The Geology of Continental Margins. New York, Springer-Verlag, 591–598
Moreno H (1974) Airplane flight over active volcanoes of central south Chile: Santiago, International Symposium on Volcanology, International Association of Volcanology and Chemistry of the Earth's Interior. Guidebook Excursion D-3, 56 p
Moreno H (1975) Características petrológicas del volcanismo Cenozóico Superior en los Andes del Sur de Chile (39°00′–41°30′S). VI Congreso Geológico Argentino, Bahía Blanca, Actas 2:131–147
Moreno H, Naranjo JA, López L (1979) Geología y petrología de la cadena volcanica Osorno-Puntiagudo, Andes del Sur, latitud 41°10′S. Segundo Congreso Geologico Chileno E:109–131
Morris JD, Hart SR (1983) Isotopic and incompatible element constraints on the genesis of island arc volcanics, Cold Bay and Amak Island, Aleutians. Geochim Cosmochim Acta 47:2015–2030
Muñoz J, Stern C (1985) El complejo volcanico Pino Hachado. IV Congreso Geol Chileno, Actas 3:4–380 to 4–412
Nicholls IA, Harris KL (1980) Experimental rare earth element partition coefficients for garnet, clinopyroxene, and amphibole coexisting with andesitic and basaltic liquids. Geochim Cosmochim Acta 44:287–308
Nye CJ, Reid MR (1986) Geochemistry of primary and least fractionated lavas from Okmok volcano, central Aleutians: Implications for arc magmagenesis. J Geophys Res 91:10271–10287
Pankhurst RJ, O'Nions RK (1973) Determination of Rb/Sr and $^{87}Sr/^{86}Sr$ ratios of some standard rocks and evaluation of X-ray fluorescence spectrometry in Rb–Sr geochemistry. Chem Geol 12:127–136
Peacock MA (1931) Classification of igneous rock series. J Geol 39:54–67
Perfit MR, Kay RW (1986) Comment on "Isotopic and incompatible element constraints on the genesis of island arc volcanics from Cold Bay and Amak Island, Aleutians, and implications for mantle structure" by J.D. Morris and S.R. Hart. Geochim Cosmochim Acta 50:477–481
Plafker G (1972) Alaskan earthquake of 1964 and Chilean earthquake of 1960: Implications for arc tectonics. J Geophys Res 77:901–925

Ramos VA, Jordan TE, Almendinger RW, Mpodozis C, Kay SM, Cortes JM, Palma M (1986) Paleozoic terranes of the central Argentine-Chilean Andes. Tectonics 5:855–880

Richard P, Shimizu N, Allegre CJ (1976) $^{143}Nd/^{144}Nd$, a natural tracer: an application to oceanic basalts. Earth Planet Sci Lett 31:269–278

Rogers NW, Hawkesworth CJ (1982) Proterozoic age and cumulate origin for granulite xenoliths, Lesotho. Nature 299:409–413

Saunders AD, Tarney J, Weaver SD (1980) Transverse geochemical variations across the Antarctic Peninsula: Implications for the genesis of calc-alkaline magmas. Earth Planet Sci Lett 46:344–360

Scholl DW, Christensen MH, Von Huene R, Marlow MS (1970) Peru-Chile trench sediments and sea-floor spreading. Geol Soc Am Bull 81:1339–1360

Scholl DW, Marlow MS (1974) Sedimentary sequence in modern Pacific trenches and the deformed circum-Pacific eugeosyncline. In: Dott RH Jr, Shaver RH, eds, Modern and Ancient Geosynclinal Sedimentation. Society of Economic Paleontologists and Mineralogists Special Publication 19:193–211

Scholl DW, Marlow MS, Cooper AK (1977) Sediment subduction and offscraping at Pacific margins. In: Talwani M, Pitman WC III, eds, Island Arcs, Deep Sea Trenches, and Back-Arc Basins. Am Geophys U, Maurice Ewing Series 1:199–210

Schweller WJ, Kulm LD, Prince RA (1981) Tectonics, structure, and sedimentary framework of the Peru-Chile Trench. Geol Soc Am Mem 154:323–349

Shaw HR (1980) The fracture mechanisms of magma transport from the mantle to the surface. In: RB Hargraves, ed, Physics of Magmatic Processes. Princeton Univ Press, 201–264

Skewes MA, Stern CR (1979) Petrology and geochemistry of alkali basalts and ultramafic inclusions from the Pali-Aike volcanic field in southern Chile and the origin of the Patagonian plateau basalts. J Volcanol Geotherm Res 6:3–25

Stacey JS, Kramers JD (1975) Approximation of terrestrial lead isotope evolution by a two-stage model. Earth Planet Sci Lett 26:207–221

Stauder W (1973) Mechanism and spatial distribution of Chilean earthquakes with relation to subduction of the oceanic plate. J Geophys Res 78:5033–5061

Stern CR, Futa K, Muehlenbachs K, Dobbs FM, Munoz J, Godoy E, Charrier R (1984) Sr, Nd, Pb, and O isotope composition of late Cenozoic volcanics, northernmost SVZ (33–34°S). In: Harmon RS, Barreiro BA, eds, Andean Magmatism, Chemical and Isotopic Constraints. Shiva Publ Co, Cheshire (U.K.), 96–105

Stern CR, Futa K, Saul S, Skewes MA (1986) Nature and evolution of the subcontinental mantle lithosphere below southern South America and implication for Andean magma genesis. Revista Geol Chile 27:41–53

Stern CR, Skewes MA, Duran M (1976) Volcanismo orogénico en Chile Austral. Primero Congreso Geológico Chileno, Actas 2:F195–F212

Swift SA, Carr MJ (1974) The segmented nature of the Chilean seismic zone. Phys Earth Planet Interiors 9:183–191

Takahashi E (1986) Genesis of calc-alkali andesite magma in a hydrous mantle-crust boundary: Petrology of lherzolite xenoliths from the Ichinomegata crater, Oga Peninsula, northeast Japan, Part II. J Volc Geoth Res 29:355–395

Tarney J, Windley BF (1977) Chemistry, thermal gradients, and evolution of the lower continental crust. J Geol Soc 134:153–172

Tatsumi Y, Nakano S (1984) Lateral variation of K/Hf ratios in Quaternary volcanic rocks of northeastern Japan. Geochem J 18:305–314

Tatsumi Y, Sakuyama M, Fukuyama H, Kushiro I (1983) Generation of arc basalt magmas and thermal structure of the mantle wedge in subduction zones. J Geophys Res 88:5815–5825

Taylor SR, McLennan SM (1985) The Continental Crust: its Composition and Evolution. Oxford, Blackwell Sci Publ, 312 p

Thiele R (1980) Hoja Santiago, Carta Geológica de Chile, escala 1:250000. Instituto de Investigaciones Geológicas, No. 39. (Map and 51-page pamphlet)

Thiele R, Katsui Y (1969) Contribucion al conocimiento del volcanismo post-Miocenico de los Andes en la provincia de Santiago, Chile. Departamento de Geología, Universidad de Chile, Publicación 35, 23 p

Thornburg TM, Kulm LD (1987a) Sedimentation in the Chile Trench: Depositional morphologies, lithofacies, and stratigraphy. Geol Soc Amer Bull 98:33–52

Thornburg TM, Kulm LD (1987b) Sedimentation in the Chile Trench: Petrofacies and provenance. J Sed Petrol 57:55–74

Thorpe R, Francis PW, Hammill M, Baker MCW (1982) The Andes. In: Thorpe RS (ed) Andesites. John Wiley and Sons, London, p. 187–205

Tilton GR (1979) Isotopic studies of Cenozoic Andean calc-alkaline rocks. Carnegie Inst Wash Yearbook 78:298–304

Tilton GR (1983) Evolution of depleted mantle: The lead perspective. Geochim Cosmochim Acta 47:1191–1197

Tilton GR, Barreiro BA (1980) Origin of lead in Andean calc-alkaline lavas, southern Peru. Science 210:1245–1247

Unruh DM, Tatsumoto M (1976) Lead isotopic composition and U, Th, and Pb concentrations in sediments and basalts from the Nazca plate. In Yeats RS, Hart SR, eds, Initial Reports of the Deep Sea Drilling Project 34:341–347

Vergara M, Muñoz J (1982) La Formacion Cola de Zorro en la alta cordillera andina Chilena (36°–39° Lat. S), sus caracteristicas petrográficas y petrológicas: Una revisión. Revista Geológica de Chile 17:31–46

Watson EB (1982) Basalt contamination by continental crust: Some experiments and models. Contrib Mineral Petrol 80:73–87

Watson EB, Harrison TM (1983) Zircon saturation revisited: Temperature and composition effects in a variety of crustal magma types. Earth Planet Sci Lett 64:295–304

White WM, Dupré B (1986) Sediment subduction and magma genesis in the Lesser Antilles: Isotopic and trace element constraints. J Geophys Res 91:5927–5941

White WM, Patchett J (1984) Hf–Nd–Sr isotopes and incompatible element abundances in island arcs: Implications for magma origins and crust-mantle evolution. Earth Planet Sci Lett 67:167–185

Wortel MJR, Vlaar NJ (1978) Age-dependent subduction of oceanic lithosphere beneath western South America. Phys Earth Planet Inter 17:201–208

Wyllie PJ (1977) Crustal anatexis: an experimental review. Tectonophysics 43:41–71

Wyllie PJ (1982) Subduction products according to experimental prediction. Geol Soc Amer Bull 93:468–476

Wyllie PJ, Huang W-L, Stern CR, Maaloe S (1976) Granitic magmas: possible and impossible sources, water contents, and crystallization sequences. Can J Earth Sci 13:1007–1019

Yrigoyen MR (1979) Cordillera Principal. In: Segundo Simposio de Geología Regional Argentina. Córdoba, Academia Nacional de Ciencias 1:651–694

Zartman RE, Doe BR (1981) Plumbotectonics – the model. Tectonophysics 75:135–162

Received June 5, 1987 / Accepted December 7, 1987

Editorial responsibility: I.S.E. Carmichael

Appendix

Analytical methods

All samples were pulverized by shatterbox, in alumina for INAA and in WC for other determinations. Major elements were determined by XRF at USGS Laboratories in Lakewood, Colorado, and Rb, Sr, Y, Zr, and Ba by energy-dispersive XRF at the USGS,

Menlo Park, California. Sc, Cr, Co, Zn, Sb, Cs, La, Ce, Nd, Sm, Eu, Tb, Yb, Lu, Hf, Ta, Th, and U were measured by INAA at the USGS, Reston, Virginia. Precision of the three methods is measured by repeated analysis of internal standards, as tabulated and discussed by Bacon and Druitt (1988). Determinations for USGS standards generally agree with accepted values within measured precision.

Isotopic determinations were made at Oxford. Sr was separated by a conventional ion exchange technique (Pankhurst and O'Nions 1973) and isotopically analyzed on single Ta filaments on a VG-Micromass 30 spectrometer. $^{87}Sr/^{86}Sr$ ratios were corrected for mass-fractionation by normalizing to $^{88}Sr/^{86}Sr = 8.37521$. Repeated measurements of the Eimer and Amend $SrCO_3$ standard yielded an average $^{87}Sr/^{86}Sr$ ratio of 0.70776, indicating a systematic deviation of -0.00024 from the accepted value of 0.70800. Appropriate correction has been made to all ratios. 2σ errors on $^{87}Sr/^{86}Sr$ ratios are better than 0.01% (Table 2). Rb/Sr ratios were determined on pressed powder pellets by XRF (Pankhurst and O'Nions 1973). Precision of Rb/Sr ratios is $\pm 1\%$. Rb and Sr contents, computed with mass absorption coefficients obtained from Compton scatter peak intensities, are precise to better than $\pm 5\%$.

Pb was separated using HBr on an anion exchange resin, and isotopically analysed on single Re filaments with a fully automated VG Isomass 54E mass spectrometer. Mass fractionation corrections were made by references to repeated analyses of Pb isotope standard NBS 981. 2σ errors on Pb isotopic ratios average $\sim 0.1\%$.

Sm and Nd were separated by a method based on that of Richard et al. (1976), using cation exchange for separation of the REE as a group, followed by reversed phase chromatography, using di-(2 ethylhexyl) phosphoric acid supported on PTFE powder. Sm and Nd concentrations and Nd isotopic compositions (for CM samples only) were measured using a mixed ^{150}Nd and $^{149}/Sm$ spike. For the other samples, $^{143}Nd/^{144}Nd$ ratios were measured directly on unspiked aliquots. Sm and Nd were isotopically analyzed on the Ta side filaments of a triple filament assembly on the VG Isomass 54E. 2σ errors on $^{143}Nd/^{144}Nd$ ratios are shown in Table 3. Measurements of the standard BCR-1 yield a composite value of 0.512636 ± 0.000012, which is within error of the accepted value.